STUDIES OF NONCOVALENT PROTEIN-PROTEIN AND PROTEIN-SMALL-MOLECULE COMPLEXES BY ELECTROSPRAY IONIZATION MASS SPECTROMETRY

by

Yang Kang

B.Sc., Peking University, 2008

A THESIS SUBMITTED IN PARTIAL FULFILLMENT OF
THE REQUIREMENTS FOR THE DEGREE OF

DOCTOR OF PHILOSOPHY

in

THE FACULTY OF GRADUATE STUDIES

(Chemistry)

THE UNIVERSITY OF BRITISH COLUMBIA

(Vancouver)

March 2012

Abstract

Gas-phase ions of tetrameric protein−protein complexes, hemoglobins, and protein−small-molecule complexes, cellulasexylanase (Cex) binding with aza-sugar inhibitors, have been studied by electrospray ionization mass spectrometry with measurements of collision cross sections, hydrogen/deuterium exchange (H/Dx), and tandem mass spectrometry (MS/MS), with the goal of investigating their gas-phase conformations and binding strengths and any relation to the solution properties.

Adult hemoglobin (Hb A, $\alpha_2\beta_2$) prepared from fresh erythrocytes and commercial lyophilizate showed similar collision cross sections, but different mass spectra. Heme-deficient dimers found in commercial Hb are attributed to oxidative modifications on the β chains. Both oxidation and lyophilization in commercial proteins produce higher levels of monomer and dimer ions in mass spectra.

Gas-phase properties of ions of Hb A, sickle hemoglobin (Hb S, E6V[β]) and fetal hemoglobin (Hb F, $\alpha_2\gamma_2$) have been compared. Tetramer ions of Hb S have greater collision cross sections and higher gas-phase H/Dx levels than Hb A tetramers. In MS/MS, dimer and tetramer ions of Hb F show different dissociation pathways and energies from the same species of Hb A and S. Thus the single mutation in the β chain of Hb S and the 39 residue alterations of the γ chain of Hb F change the gas-phase properties of Hb complexes. No consistent correlation is found between gas-phase stability and solution binding constants.

With a home-built "time-resolved" ESI source, millisecond-H/Dx in solution is studied with these three hemoglobins. No conformational differences are found. Interestingly, H/Dx kinetics show good correlations with tetramer-dimer (ca. 1 s) and dimer-monomer (minutes) inter-conversions in solution.

In gas-phase ions of three Cex−inhibitor complexes, Cex−xylobiosyl deoxynojirimycin (X_2DNJ), Cex−xylobiosyl isofagomine lactam (X_2IL), and Cex−xylobiosyl isofagomine (X_2IF), the relative binding strengths measured by MS/MS follow the order in solution. In solution complexes have less flexibility and therefore exchange fewer hydrogens than free proteins. In the gas phase, complexes have lower collision cross sections than free proteins, indicating a more compact structure, but interestingly complexes show greater H/Dx levels. Detailed studies suggest that ions can "remember" their original solution conformations for milliseconds in the gas phase, but may fold or unfold on a time scale of seconds.

Preface

A version of chapter 2 has been published as, Kang, Y., Terrier, P., Douglas, D. J.: Mass Spectra and Ion Collision Cross Sections of Hemoglobin, *J. Am. Soc. Mass Spectrom*. **22**, 290-299 (2011). The project was initiated by Dr. Douglas. Also Dr. Douglas contributed greatly to the design of the project and editing of the manuscript. Dr. Terrier gave valuable suggestions on protein extraction and instrumental setup. My major contributions are: literature survey, design of the research project, data acquisition, interpretation of the observations, and preparing the manuscript.

A version of chapter 3 has been published as, Kang, Y., Douglas, D. J.: Gas-Phase Ions of Human Hemoglobin A, F, and S, *J. Am. Soc. Mass Spectrom*. **22**, 1187-1196 (2011). The project was initiated by Dr. Douglas. My major contributions are: literature survey, design of the research project, data acquisition, interpretation of the observations, and preparing the manuscript.

A version of chapter 4 has been submitted for publication, as Kang, Y., Douglas, D. J.: Solution Hydrogen/Deuterium Exchange of Human Hemoglobin A, F, and S Monitored by Electrospray Mass Spectrometry. The project was initiated by Dr. Douglas. My major contributions are: literature survey, design of the research project, data acquisition, interpretation of the observations, and preparing the manuscript.

A version of chapter 5 has been published as, Kang Y., Terrier, P., Ding, C. F., Douglas, D. J.: Solution and Gas-Phase H/D Exchange of Protein-Small-Molecule Complexes: Cex and Its Inhibitors, *J. Am. Soc. Mass Spectrom*. **23**, 57-67 (2012). The project was initiated by Dr. Douglas. Dr. Terrier and Dr. Ding acquired data on solution and gas-phase H/Dx respectively. My major contributions are: literature survey, data acquisition, interpretation of the observations, and preparing the manuscript.

Table of Contents

List of Tables

List of Figures

List of Schemes

List of Symbols and Abbreviations

ACN	Acetonitrile
A_g	Area calculated from radius of gyration
apo-, a	Heme-free
A_s	Area calculated from Stokes radius
BIRD	Blackbody infrared radiative dissociation
Cex	Cellulasexylanase
C	Cex ion formed from solution of a complex
C_D	Drag coefficient
C_{Dd}	Drag coefficient with diffuse scattering
CEM	Channel electron multiplier
CID	Collision-induced dissociation
^{CN}Hb	Cyanide-bound hemoglobin
CSD	Charge state distribution
Cur	Curtain plate
CX	Cex−inhibitor complex
Da	Dalton (atomic mass unit)
DC	Direct current
DEF	Deflector
^{deoxy}Hb	Oxygen-free hemoglobin (Fe^{2+} in heme)
DPG	2,3-Diphosphoglycerate
E^0	Ion kinetic energy at entrance of collision cell
E	Ion kinetic energy at exit of collision cell
E_a	Arrhenius activation energy
E_{CM}	Center-of-mass energy
eV	Electron volt
EDTA	Ethylenediaminetetraacetic acid
ESI	Electrospray ionization
FWHM	Full width at half maximum
Hb	Hemoglobin
Hb A	Adult hemoglobin
Hb S	Sickle hemoglobin
Hb F	Fetal hemoglobin
H/Dx	Hydrogen/deuterium exchange
HPLC	High-performance liquid chromatography
holo-, h	Heme-bound
i	Ion charge
ICR	Ion cyclotron resonance

i. d.	Inside diameter
IM	Ion mobility
IR	Infrared
k	Rate constant
k_a	Association rate constant
K_d	Dissociation equilibrium constant
K_i	Inhibition constant
l	Length of collision cell
$l\,'$	Distance over which dissociation occurs in collision cell
LDT	Linear drift tube
LIT	Linear quadrupole ion trap
m_1	Mass of the protein
m_2	Mass of collision gas
MCP	Microchannel plate
MeOH	Methanol
^{met}Hb	Oxygen-free hemoglobin (Fe^{3+} in heme)
MS	Mass spectrometry
MW	Molecular weight
MWCO	Molecular weight cut off
m/z	Mass to charge ratio
n	Gas number density
NH_4Ac	Ammonium acetate
NMR	Nuclear magnetic resonance
oa-TOF	Orthogonal acceleration TOF
o.d.	Outside diameter
ori	Orifice
^{oxy}Hb	Oxygen-bound hemoglobin (Fe^{2+} in heme)
ppm	Parts-per-million
Q	Mass-resolving quadrupole
q	Radio frequency only quadrupole
QqQ	Triple quadrupole
Q0	Ion guide in triple quadrupole MS
Q1	First mass analyzer in triple quadrupole MS
Q2	Collision cell in triple quadrupole MS
Q3	Second mass analyzer in triple quadrupole MS
Q0/Q1, Q1/Q2, Q2/Q3	Interquadrupole lens
RF	Radio frequency
r_g	Radius of gyration
r_s	Stokes radius
s	Ratio of object's speed to the thermal speed of the gas
ski	Skimmer

t	Reaction time
T	Gas temperature
Th	Unit of mass-to-charge ratio
tris	Tris(hydroxymethyl)aminomethane
TOF	Time-of-flight
TWIG	Travelling wave ion guide
UV-Vis	Ultraviolet-visible
X_2DNJ	Xylobiosyl deoxynojirimycin
X_2IF	Xylobiosyl isofagomine lactam
X_2IL	Xylobiosyl isofagomine
v	Ion speed
v/v	Volume/volume
w/v	Weight/volume
3D	Three-dimensional
%H/Dx	Relative exchange level
$\alpha_2\beta_2$	Tetramer of adult or sickle hemoglobin
$\alpha_2\gamma_2$	Tetramer of fetal hemoglobin
$\alpha\beta$	Dimer of adult or sickle hemoglobin
$\alpha\gamma$	Dimer of fetal hemoglobin
λ	Free mean path
μ	Reduced mass
σ	Collision cross section
Φ	Average fraction of center-of-mass kinetic energy transferred to internal energy in a collision
Ω	Angular frequency of RF applied to a quadrupole
ΔG^0_{sol}	Free energy change in solution
ΔE_{int}	Total internal energy transferred into ions in collision cell
ΔV	Dissociation voltage
ΔV_{os}	Voltage difference between the orifice and skimmer
ΔV_{Q0-Q2}	Offset voltage difference between Q0 and Q2 quadrupole

Acknowledgements

First and foremost, I want to thank my supervisor, Dr. Don Douglas, for opening the door of mass spectrometry to me and being the best teacher and advisor I could have wished for. I am deeply grateful for your thoughtful, wise, and patient guidance during every step in my PhD studies, and giving me every opportunity to develop and succeed in both research and beyond. I have learned so much from your profound knowledge and enthusiasm in research. Your kind encouragement and trust have always pushed me to be a better researcher. This thesis certainly would not have been possible without your help.

I would also like to thank my supervisory committee members, especially Dr. Michael Blades for his help throughout my studies and for review of this thesis. Thanks to all members of chemistry mechanical and electronic engineering services for their help to our machines, especially Pritesh Padhiar for his great assistance in making ESI source. Thanks also to Elena Polishchuk and Jessie Chen of biological services laboratory, for providing facilities for protein extraction.

This research is supported by the Natural Sciences and Engineering Research Council of Canada (NSERC) through a Discovery Grant. I would also like to acknowledge Dr. Maria Gyongyossy-Issa of the UBC Centre for Blood Research and Dr. Jason Ford of Vancouver Children's Hospital for the human blood samples.

Thanks to all my former and current group members, for sharing their knowledge and giving me support and help: Peran, Chuanfan, Winnie, Xianzhen, Ori, Hui, Dunmin, Negar, Cong and Kim. Particularly I would like to thank Peran and Chuanfan, who have taught me a lot about biology and mass spectrometry, and conducted part of the experiments presented in this thesis.

I would like to express my sincere gratitude to my parents, who made me who and what I am today. Your unconditional love is the sweetest thing in my life. Thanks for your understanding and support on my choice in chemistry. I pray deeply our whole family have a healthy and enjoyable life.

In the end, a big "thank you" goes to Chang, my Mr. Right and my best friend, who always stays by my side and loves me more than himself. Thanks to all my friends, in Vancouver, Beijing and all over the world: life would have much less fun without you!

To my parents

Chapter 1 Introduction

1.1 Noncovalent Protein Complexes

Most proteins, under physiological conditions, have tightly folded structures [1, 2], which are assembled in four levels. The first, the primary structure, refers to the sequence of amino acids in peptide chains. The secondary, tertiary, and quaternary structures are characterized to be higher orders, corresponding to formations of α-helices and β-sheets, interactions between amino acid chains and the spatial arrangements of polypeptides, respectively, all of which contribute to a final protein global three-dimensional conformation [2]. Interactions in these higher-order structures are noncovalent in nature, including hydrophobic effects, hydrogen bonding, van der Waals forces and electrostatic interactions.

Proteins also frequently interact noncovalently with each other or other molecules, termed ligands, to form complexes. Examples are protein−protein or protein multimers [3, 4], protein−DNA [5, 6], protein−metal [7, 8], and protein−carbohydrate [9] complexes. A variety of modular protein domains have specific binding sites, with examples in antibody−antigen, protein−cofactor, and enzyme−substrate complexes [6]. Ligands may also bind to other sites on a protein, called non-specific binding [10, 11].

In living organisms, noncovalent protein assemblies form numerous different biological functional models [12], involved in biochemical regulation, signaling pathways, transport, energy conversion and many other cellular processes. Thus the studies of these non-covalent protein interactions in large complexes are of increasing interest, with the potential for developments in molecular recognition, drug discovery, and biosensors design [4]. To understand the biological mode of action, characteristic

determination of the structure and dynamics of a noncovalent complex is highly relevant. For such analysis, it is necessary to define how the features of the complex as a whole differ from those of its individual components, and then determine the contribution of each subunit to the subunit−subunit interactions, based on the identity, stoichiometry, structure, and binding strength of the complex. A challenge of studying three-dimensional noncovalent protein assemblies comes from their large size, heterogeneous composition, flexibility and asymmetric structures [13].

Currently a variety of biophysical tools are available to determine the structure, dynamics and noncovalent specific or nonspecific interactions of protein complexes [2, 14]. Nuclear magnetic resonance (NMR) [15] and X-ray crystallography [16-18] are two standard methods to provide three-dimensional structures with atomic scale resolution. Optical methods, such as circular dichroism (CD) [19], UV-Vis [20], IR [21], and light scattering spectroscopy [22], are often employed for studying global structural aspects. Other methods, such as surface plasmon resonance [23], analytical ultracentrifugation [24] and isothermal titration calorimetry [25], are used as well. In addition to these traditional techniques, mass spectrometry which is the focus in this thesis is another extensively used structural biological approach, and will be discussed below.

1.2 Electrospray Ionization Mass Spectrometry

1.2.1 General

Mass spectrometry (MS) is an analytical method of charactering compounds by their "mass to charge ratios" (m/z). The first mass spectrum was measured by J. J. Thomson in 1910 [26]. Nowadays, mass spectrometry has become a widespread technique in a variety of fields with key functions in identifying and quantifying compounds, studying molecular structures, and probing the fundamentals of chemical or physical properties of compounds [27].

A typical mass spectrometer consists of a sample introduction device, ion source region, mass analyzer, ion detector, data process system, and a vacuum system. The ion source and mass analyzer are two key parts of a mass spectrometer. In an ion source, gaseous ions with positive or negative charges are produced and transferred into a mass analyzer. Two "soft" ionization techniques, electrospray ionization (ESI) and matrix assisted laser desorption ionization (MALDI), are able to transfer large biomolecules into the gas phase as intact ions with little dissociation, and this has brought an explosive growth of MS in molecular-level biological research [4, 28].

In a mass analyzer, ions are separated based on their motion in electric fields (quadrupole, time-of-flight, 3D ion trap), or magnetic fields (magnetic sectors, ion cyclotron resonance), or both fields (double-focusing magnetic and electric sectors). The ion motion is related to an ion's "mass to charge ratio" (m/z). Different mass analyzers vary in their mass spectral resolution, mass assignment accuracy, detectable mass range,

speed of data acquisition, and cost, and the selection depends on the needs of a specific

application. The IUPAC definition for resolution in mass spectrometry is $\frac{M}{\Delta M}$, where M

is the m/z of an ion and ΔM is the resolving power. In peak width definition, the value of

ΔM is the width of a peak measured at a specified fraction of the peak height. At half

height, ΔM is called the full width at half maximum (FWHM).

"Hybridization" of conventional mass analyzers has been commonly used in

modern MS to allow additional instrument functionality, for example, for ion focusing or

conducting gas-phase reactions, often with significant performance enhancements. In

combining two or three mass analyzers in tandem, "ion processing" steps are separated

from the final mass analysis, to improve both sensitivity and resolution [29]. Examples

include magnetic sector- time-of-flight (TOF), triple quadrupole (QqQ), and quadrupole-

TOF instruments.

1.2.2 Electrospray Ionization

Electrospray ionization (ESI) is an ion source in which gas-phase ions are generated from

charged droplets by progressive solvent evaporation under a high electric field at

atmospheric pressure. In principle, the ionization process consists of three stages, droplet

formation, droplet shrinkage and gaseous ion formation [30]. An analyte solution is

introduced through a capillary with a high voltage of several kilovolts at atmospheric

pressure. At the tip of the capillary, charged ions are formed from a "Taylor cone" [30],

then move towards a vacuum system attracted by the voltage difference between ESI

capillary and a counter electrode. In this process a fine spray of charged droplets formed

from the solution leave the capillary. As the solvent evaporates, often facilitated by a

nebulizer gas, the droplet shrinks and the charge density on the surface of the droplet

increases. The droplet finally reaches a point where the Coulomb repulsion from the

electric charge is greater than the surface tension holding it together. This causes the

droplet to break down and produces charged analyte ions. The formation of a single ion

has been proposed in two different mechanisms. In the "charge residue" model,

continuous shrinkage and fission of droplets results in only single ion left in a droplet

[31]. This mechanism is thought to apply in the ionization of large molecules [6, 32],

such as proteins and their complexes. In the "ion evaporation" mechanism, a single ion is

ejected from the small highly charged droplets under strong electrostatic repulsion that is

greater than the surface tension [33]. This mechanism is thought to apply to small organic

or inorganic ions [6]. The ESI apparatus used in this research will be discussed in detail

in chapter 2 and chapter 4.

1.2.3 ESI Coupled to Different Mass Analyzers

1.2.3.1 Quadrupole

A linear quadrupole is a set of four parallel hyperbolic rods with the two opposite rods

electrically connected to produce a two-dimensional electric field, as shown in Figure 1.1.

A combination of direct current (DC) and radio frequency (RF) voltages is applied

between electrode pairs. Due to the difficulty of manufacturing hyperbolic rods to high

precision, circular rods are commonly used with the proper selection of rod radius [34].

The operation principles have been reviewed in the literature [35, 36]. Ion motion is calculated by the Mathieu equation, and the solutions of this equation are expressed in a stability diagram [37]. With fixed RF (V_0) and DC (U_0) voltages, ions with certain m/z ratios are stable and can pass through the quadrupole. Scanning the RF and DC voltages with a fixed ratio allows ions with different masses to be transmitted in sequence of m/z and mass analyzed in order to produce a mass spectrum. Increasing the DC/RF ratio enhances the resolution but decreases the sensitivity. Typically the mass range of quadrupole is 10 m/z to 6500 m/z, but it can be extended by reducing the operating frequency (Ω) [38].
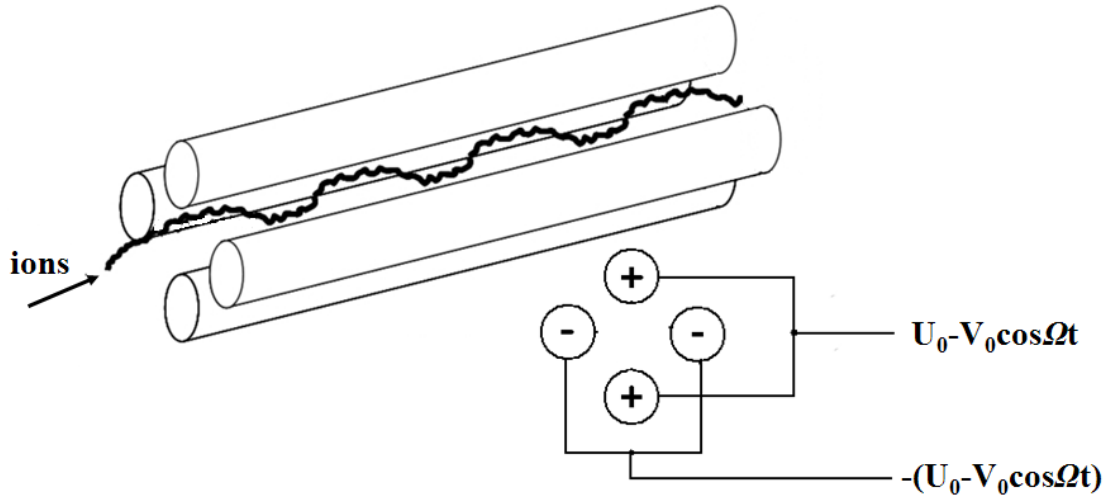
Figure 1.1. Schematic representation of the quadruple and its connections. U_0, DC voltage; V_0, amplitude of the RF voltage; Ω, angular frequency of the RF voltage.

In RF-only operation mode, ions of a broad range of m/z can be transmitted. The quadrupole then can serve as an "ion guide" to transport ions to increase transmission efficiency, or a "collision cell" where ions with sufficient energy collide with a buffer gas leading to fragmentation. Adding timed stopping potentials at the entrance and exit of an RF-only quadrupole creates a linear ion trap (LIT), in which gas-phase reactions can be conducted. Linear ion traps can also be used as mass analyzers, with radial or axial ejection of ions [36].

The first studies of ESI coupled to MS used quadrupole mass spectrometers [39, 40]. A quadrupole is a continuous analyzer, and thus is highly compatible with a continuous infusion source. Currently quadrupoles have been extensively used in tandem mass spectrometers. In a triple quadrupole (QqQ) MS, a collision cell (q, RF-only quadrupole) for ion fragmentation is located between two quadrupole mass filters (Q, mass-resolving quadrupole). As an alternative, the collision cell can also contain another multipole such as a hexapole or octopole [36, 41]. A triple quadrupole MS system can be programmed for a variety of scan modes, such as precursor ion scans, fragment ion scans, neutral loss scans, and selected/multiple reaction monitoring, making it widely used in peptide identification experiments. A standard ESI triple quadrupole MS is capable of unit resolution and mass accuracy of 0.01% or better. Recent instrumental improvements have been reported for enhanced resolution with FWHM of 0.2 Dalton (Da) [42, 43]. Considering their compact configurations, relatively low cost, modest resolution and mass range, and ease of operation, quadrupoles have become one of most commonly used mass analyzers. A detailed description of the ESI triple quadrupole MS used in this study is given in chapter 2.

1.2.3.2 TOF

The general concept of time-of-flight (TOF) MS is that a mixture of ions accelerated through a pulse of potential *U*, is separated based on the m/z-dependent flight times (*t*) of ions in a field-free region. The resolution of a TOF mass analyzer corresponds to $\frac{t}{2\Delta t}$, where Δt is the FWHM of the peak arising from the recorded ion arrival times. Ideally the spectral resolution is infinite. However, the initial spatial and energy spreads of ions lower the resolving power. Innovative developments to compensate for these problems include mass reflectron for energy focusing [44] and two- or multiple-stage accelerating regions for space focusing [45, 46]. Orthogonal acceleration TOF (oa-TOF) is another notable improvement, in which ions are accelerated in a direction (TOF axis) perpendicular to their initial direction of movement (source axis). This geometry decouples the ion velocity in the source ion beam from the TOF axis, giving rise to reduced initial velocity and energy spreads along the TOF axis, and resulting in excellent resolution. The coupling of continuous ESI source to oa-TOF has been an attractive technique for mass spectrometry [47, 48].

In a hybrid tandem MS, TOF provides a valuable final stage for mass analysis, with the benefits of relatively high mass resolution ($\frac{M}{\Delta M}$ of 5000-20,000) [29], good mass accuracy (<5 ppm) [41], potentially high sensitivity and unlimited mass range. Examples of hybrid instruments include QqTOF, LIT TOF and 3D-trap TOF MS. A detailed description of the ESI LIT-oa-reflectron TOF MS used in this research is given in chapter 3.

1.3 Applications of ESI MS in the Study of Noncovalent Protein Complexes

1.3.1 General

With the gentle conditions of ESI, the tertiary and quaternary structures, and even thermally labile noncovalent interactions of protein complexes can be preserved in a highly non-physiological environment free of solution [6]. Multiply charged ions generated by ESI give lower mass to charge ratios, making it easier for MS to determine the molecular weights of high-mass compounds. As proposed by de la Mora [32], the maximum charge of a folded protein ion produced from ESI can be estimated using Rayleigh charge, z_R, given by,

$$z_R = \frac{8\pi}{e}\left(\gamma \varepsilon_0 R^3\right)^{1/2} \tag{1.1}$$

where γ is the surface tension of solvent, R is the radius of ion, ε_0 is the electrical permittivity of vaccum, and e is the electron charge. Currently it is possible to transfer large protein complexes with masses of several mega-Daltons into the gas phase [49]. Although from MS data alone it is not yet possible to determine the high-resolution 3D protein structures that can be achieved with NMR or X-ray crystallography, ESI MS has complemented these conventional methods to give valuable information on structures of protein noncovalent complexes, with advantages of speed, sensitivity and selectivity, and relatively low sample consumption (10^{-12} to 10^{-15} mol [50]) is needed. Targeted species and specific interactions can be studied, even in the presence of other compounds. Since

1991 when ESI MS was first applied for the analysis of receptor-ligand complexes [51] and native myoglobin interactions [52], a wide range of noncovalent protein complexes have been studied: intact multimeric proteins [53-55], protein−carbohydrate [11, 56-58], protein-metal [7, 14], and protein−DNA [5, 14] complexes. Several reviews focusing on the application of ESI MS in the study of noncovalent interactions and macromolecular biological complexes have already been published [4, 6, 14, 49, 59, 60].

In general, the performance of ESI MS in detecting noncovalent complexes is dependent on the conditions of the ion source interface and the MS instrument, the complex of interest, and the composition of buffered solutions. The conditions in the ESI interface have to be sufficiently gentle to preserve noncovalent interactions, but sufficient energy is required for complete desolvation and removal of adducts. In some cases, auxiliary approaches are needed to remove solvent, such as increasing the temperature in the source region [61, 62]. The study of noncovalent complexes has been facilitated by the use of collisional cooling of ions by elevating the pressure in the first vacuum stage of the MS [6, 63]. To be compatible with ESI, protein solutions need to be free of nonvolatile additives such as detergents and salts ($<10^{-4}$ M) [50]. In most cases protein purification is required, accomplished by a series of separation steps, such as centrifugation, dialysis, and gel filtration [64]. A buffered solution with low-percentage organic solvents and at neutral pH is frequently used to preserve native conditions and to prevent denaturation of noncovalent complexes. The reagents also have an impact on the stability of complexes in ESI droplets [65] and the extent of multiple charging of ions [66, 67].

In measurements of noncovalent complexes, multiple ESI MS-based methods can be combined to provide insights into composition, structural and dynamic properties in term of mass, size and stability. In detail, information can be obtained about the stoichiometry and heterogeneity, conformational characteristics upon binding a ligand, thermodynamic parameters such as binding constants and binding energies, as well as the folding and unfolding kinetics. Several approaches to the study of conformations and binding strengths of noncovalent complexes are discussed below.

1.3.2 Approaches to Conformational Studies

The investigation of protein ion conformation in solution or *in vacuo* has led to the development of several MS-based analytical methods, including direct analysis with positive-ion charge state distributions, and measurements of collision cross sections and hydrogen/deuterium exchange levels.

1.3.2.1 Charge State Distributions

In positive ESI, multiply protonated protein ions are generated. Direct observation of the ion charge state distributions (CSD) reveals the overall compactness of a protein in solution. Tightly folded protein molecules have smaller surface areas compared to less folded protein molecules, and thus accommodate fewer charges on the protein surface. This effect makes MS an attractive method to simultaneously detect multiple coexisting conformations of a protein complex in solution based on their different charge state

distributions. These coexisting conformations cannot be observed with other conventional methods such as NMR and UV-Vis spectroscopy.

Analysis of positive ion CSD has been used to monitor the conformational changes of proteins in unfolding or refolding processes. Multiple-state transitions have been found in acid-induced [68, 69] or methanol-induced [19] unfolding process of myoglobin in equilibrium studies. In combination with time-resolved (millisecond) measurements, refolding of cytochrome *c* with increasing pH [70] and refolding of acid or methanol-denatured ubiquitin by changing to a physiologically active environment [71] have been monitored in "on-line" kinetic studies. Negative ion CSD was insensitive to conformational changes. Protein unfolding that causes pronounced shifts in the positive ion CSD only leads to marginal changes in the negative ion CSD [72].

1.3.2.2 Collision Cross Sections

Collision cross sections are a measure of an ion's size averaged over all orientations, which is directly related to the quaternary conformation of protein assemblies [7, 53, 61, 73]. Measurements of ion mobility as well as ion kinetic energy loss have been employed to determine collision cross sections of gas-phase ions of noncovalent protein complexes.

In ion mobility (IM) MS, ions migrate in a buffer gas under the influence of an electric field. In principle, larger protein ions with more open structures experience greater resistance to the motion in the gas, and thus travel more slowly than those with more compact conformations. Two types of ion mobility devices that are frequently used to measure collision cross sections are linear drift tube (LDT) and travelling wave ion

guide (TWIG). Only in LDT IM MS, can absolute collision cross sections be determined by measuring ion drift time [74]. In TWIG IM MS, the ion mobility of protein ions cannot be directly related to the collision cross sections, so calibration against cross sections measured by LDT IM MS with the same biomolecular class and using the same type of ionization is required, and only relative cross sections can be estimated [61, 74]. Most studies with LDT at a pressure of 0.75 Torr to 11.25 Torr focus on relatively small noncovalent protein complexes [75]. In a recent study, Faull et al. have demonstrated the application of LDT IM MS in measuring collision cross sections of large protein−protein complexes, cytochrome c multimers and hemoglobin [7]. The TWIG IM MS allows lower cell pressures in a range of 10^{-2} Torr to 10^{-1} Torr [54, 61, 75, 76], and currently has been applied to measure collision cross sections of large protein−protein complexes of up to several mega-Daltons, such as virus capsids [76, 77].

Measurements of ion kinetic energy loss are done in a triple quadrupole mass spectrometer at a pressure of 10^{-3} Torr [78, 79]. In principle, when passing through a low-density inert gas in a collision cell, larger ions have a greater number of collisions and lose more kinetic energy than smaller ions of the same mass. Ion axial kinetic energy losses have been interpreted with a collision model [80] or a drag model [78, 81] to give absolute cross sections. Collision cross sections of various heme-containing proteins, cytochrome c, myoglobin and hemoglobin, have been measured with this method [78, 80, 82-84]. Chen et al. have compared the cross sections of myoglobin and cytochrome c measured with LDT ion mobility and energy loss, and found a good correlation with these two methods when using a diffuse scattering model [78]. Energy losses calculated

14

in a diffuse scattering drag model are used in this study and the calculation is presented in detail below.

1.3.2.3 Hydrogen/Deuterium Exchange

Hydrogen/deuterium exchange (H/Dx) is combined with MS to detect different protein conformations or to monitor protein conformational changes over time. The isotope labeling can occur either in solution with a D_2O-based reagent prior to injection of ions into an MS or in the gas phase by trapping ions with deuterium-based vapor. The mechanism of solution H/Dx is well characterized [1, 85, 86]. In general, isotopic exchange rates and the exchange extents of backbone amide hydrogens and labile hydrogens on side chains of a protein are related to a protein's higher-level structure [1]. In contrast the mechanism of gas-phase H/Dx is more complex and less well understood [87].

1.3.2.3.1 Solution H/Dx

In solution H/Dx, the exchangeable hydrogens are backbone amides, polypeptide termini and side-chain O-H, N-H, and S-H groups of a protein. For the same protein, labile and more accessible hydrogens on a protein's surface exchange much more rapidly than hydrogens protected in interior regions or involved in hydrogen bonding. Thus at a given pH and temperature [88], and with a given exchange time, greater exchange levels show a protein has a more unfolded or more flexible conformation. With mass spectrometry, the

mass increase from deuterium incorporation in an aqueous environment can be easily monitored to provide structural information, either on an entire protein or on localized regions, particularly in ligand-binding regions [1, 85, 89].

The mechanism of solution H/Dx has been well described [1, 85, 86]. The H/Dx of an amide hydrogen, N-H → N-D, can only occur in a short-lived "open" (unfolding) conformation in which the hydrogen becomes unprotected. Two exchange mechanisms, EX1 and EX2, are considered in two limiting situations. When the unfolding rate is small compared to the intrinsic exchange rate, all amides exposed in the unfolded state become exchanged, referred to as the EX1. When the unfolding rate constants sufficiently exceed the intrinsic exchange rates, exchange of the exposed residues is complete only after several unfolding/refolding cycles, referred to as the EX2. Almost all native proteins follow EX2 mechanism, whereas denatured proteins favor EX1 exchange [1]. Intermediate cases under mixed EX1/EX2 conditions have been discussed as well [86].

Two fundamentally different strategies, "continuous" H/Dx and "pulsed" H/Dx, are used in monitoring protein conformational dynamics. In "continuous labeling" experiments, a protein is incubated in a deuterium-based reagent for minutes to hours before analysis. This method is suitable for studying relatively slow-exchange (>1 min) processes [89, 90], and provides information on conformations averaged over the relatively long time scale of the exchange [21, 91]. For systems which fluctuate rapidly between distinct conformations, or in which a protein's conformation changes with time, the "continuous labeling" method is less effective and an alternative approach is "pulse labeling", in which a protein is exposed to a deuterating reagent for a brief time (e.g. milliseconds) prior to analysis. Literature exchange rate constants, k (min^{-1}) ≈ 10^3 (pH= 7,

20 ℃) [92], show that 99% of unprotected backbone amide and side chain hydrogens can exchange with D_2O within 300 ms. With millisecond-pulse labeling at neutral pH, unfolded regions can exchange extensively, while folded domains do not. In this way folded and unfolded states in equilibrium can be distinguished [24, 93]. Pulsed H/Dx is also useful in kinetic studies, for characterizing rapid conformational changes [71], or detecting short-lived folding intermediates [85, 94].

1.3.2.3.2 Gas-Phase H/Dx

In comparison to solution H/Dx, the mechanism of gas-phase H/Dx is less well established and more difficult to interpret [87, 95-97]. For exchange, gas-phase ions can be trapped in a variety of reagents, such as D_2O [96, 98], CD_3OD [97], or ND_3 [95], at a pressure of 10^{-1} Torr in an ion mobility drift tube [99], 10^{-3} Torr in a quadrupole ion trap [100] or 10^{-7} Torr in an ICR cell [95, 98, 101].

For a reagent with a low proton affinity such as D_2O, a relay mechanism has been proposed for the exchange reaction [87, 96, 101]. Because of a high energy barrier (E_a >10 kcal/mole) for direct reaction, D_2O cannot exchange with a neutral amide alone and must attack at a protonated charged site (B) such as a lysine side chain or the N-terminus, as shown in Figure 1.2. The D_2O forms a hydrogen bond to the charged site, then can exchange with a nearby amide hydrogen, as proposed in a "relay" mechanism. Thus to exchange in the gas phase, a hydrogen must be not only accessible on the surface of the protein, but also near a charged site. This complicates relating H/Dx levels to protein conformations. In unfolded conformations, an exchangeable site and charged site

may be too widely separated to allow exchange, leading to lower exchange levels than the same protein in a more folded conformation.
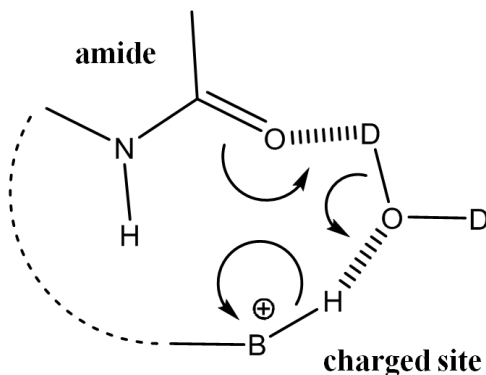
Figure 1.2. Schematic representation of the "relay" mechanism.

In this mechanism, the exchange rate is determined by the chemistry of the individual protein and a conclusive description is still missing. For example, Evans et al. [97] found that +15 cytochrome *c* ions confined in a 3D trap with CD_3OD vapor exchange more hydrogens than +8 ions, while +10 ubiquitin ions exchange fewer hydrogens than +7 ions. Collision cross section measurements show that with both proteins the more highly charged ions generally have more unfolded conformations [82, 99]. Freitas et al. using Fourier transform (FTICR) MS also found that +7 and +9 ubiquitin ions exchange hydrogens more rapidly with D_2O than +8 or +10 ions [98]. In a study combining ion mobility measurements of cross sections with H/Dx, Valentine and Clemmer [99] found that with +8, +9 and +10 cytochrome *c* ions, compact conformations exchanged fewer hydrogens than more diffuse ions of the same charge with larger cross sections, but the more highly charged ions +11 to +18, which have substantially greater

18

cross sections, all exchanged about the same number of hydrogens as the diffuse ions in the lower charge states. These studies indicate that ions with different cross sections may not show different exchange levels. Thus gas-phase H/Dx does not necessarily reveal the folding state of an ion. However different H/Dx levels can reveal different conformations of a given ion.

1.3.3 Approaches to Studies of Noncovalent Binding Energies

Gas-phase dissociation of intact noncovalent interactions in a controlled way is an effective approach to quantitatively determine gas-phase noncovalent binding strengths and stabilities, and to provide information on each subunit of a complex. Frequently cited MS-based methods come from thermal dissociation [10, 11, 56, 57, 102-104] and collision-induced dissociation (CID) or collisionally activated dissociation (CAD) [54, 79, 105-108]. In thermal dissociation, blackbody infrared radiative dissociation (BIRD), combined with ICR MS, has been used to study dissociation rate constants of gas-phase complexes to give insights into absolute binding energies (Arrhenius activation energies, E_a) (see for example [10, 11, 56, 57, 103, 104]).

In CID, noncovalent complexes dissociate either in the ion-sampling region without precursor ion mass selection [62] or in a tandem mass spectrometer. In a tandem-in-space MS, such as triple quadrupole MS [79], QqTOF MS [107] or Qq IM MS [54], an ion of interest is mass selected in a first mass analyzer and subjected to collisions with a buffer gas in a collision cell. The resultant fragment ions are then mass analyzed in the final stage. This process is called MS/MS. In a tandem-in-time MS, such as an ion trap

MS [108] or an ICR MS [106], the various stages, mass selection, ion activation and fragmentation, and fragment ion mass analysis, are conducted within the same physical trapping volume but at different times. Tandem MS in traps is capable of multiple sequential mass selection and ion storage/fragmentation steps (MS^n). In tandem MS experiments, the collision energy of precursor ions is systematically increased, and the point at which the relative intensity is reduced to some fraction of the initial intensity is often taken as a measure of the additional energy required to cause dissociation. By comparing this energy, the relative binding strengths among different interactions can be compared. The higher the energy needed for a certain extent of dissociation, the more stable the ions are. Dissociation in a triple quadrupole MS is studied in this research and the energy calculation in a collision model is discussed in detail below.

1.4 Relation of Gas-Phase Properties to Solution Properties

Attempts to elucidate fundamental biological properties or processes of complexes based on MS analysis raise a long-standing question: how closely are gas-phase and solution structures and binding related? Although some evidence has shown that at least some partial noncovalent interactions and folded conformations are preserved after transferring proteins into the gas phase [109, 110], the general relationship of conformations and noncovalent binding strengths between the solution and gas phase is still inconclusive. If conditions can be found where gas-phase properties are related to those in solution, mass spectrometry would be more useful in determining properties of protein complexes with a greater biological significance.

In some cases, how gas-phase binding compares to that in solution depends on the nature of the specific interactions. Recent observations include specific intermolecular hydrogen bonding preserved in several protein−oligosaccharide complexes [11, 56-58], and hydrophobic interactions retained in beta-lactoglobulin binding to a series of fatty acids [103]. Detailed studies have demonstrated that either strong van der Waals attractions between binding partners [111], or hydrogen bonding and salt bridges [110], can compensate for the loss of hydrophobic bonding in the gas phase and stabilize the native structures of complex ions. Ionic interactions may not be well preserved in the gas phase. In some cases, ionic interactions are strengthened in the gas phase, and thus binding strength is enhanced [112]. In contrast there are other protein−ligand complexes stabilized by strong ionic interactions in solution that turn out to be thermodynamically unstable in the gas phase [79, 104].

1.4.1 Gas-Phase Conformations

A challenge in structural determination with ESI MS is the possible conformational alterations of protein ions *in vacuo* free of solvent. If water is preferentially involved in noncovalent interactions in a folded state [113, 114], destabilization or unfolding may occur after removal of solvent [49]. Recent studies have indicated that many elements of solution structure of large protein complexes are preserved in ESI MS upon desolvation [55, 109, 115]. In some cases, protein complexes collapse in the absence of water but the overall compact structures are preserved [3].

There is now substantial evidence from collision cross section measurements to support the view that the gas-phase complex ions can reflect, under controlled conditions, the native or native-like structures [7, 53, 55, 61, 73]. Collision cross sections of ions with lower charge states measured in several proteins, including cytochrome c [7, 73], myoglobin [73], and hemoglobin [7, 61], compare well with those calculated from X-ray crystal structures. As the charge state is enhanced, an increase in overall cross sections of the complexes is observed in these proteins [7, 61, 73, 78], indicating a gradual unfolding which is thought to be due to the effects of Coulomb repulsion. However, in a recent study in a 12-mer protein−protein complex, it was shown that an increase in charge state lowers the energies required for dissociation of protein ions in MS/MS but does not influence their collision cross sections [54].

Another issue that has been often overlooked is the time scale of gas-phase experiments in relation to a protein conformation. Protein ions can be kinetically trapped in their native state in the gas phase. The exact amount of time for protein ions to undergo structural transitions depends on the protein chemistry and the experimental conditions. Recent studies indicate that proteins can retain their folded structure for a limited time during ESI MS analysis [110, 116, 117]. Badman et al. [116] compared the drift times of cytochrome c ions with IM MS after a trapping time of 10 ms to 10 s. With trapping up to 60 ms, cytochrome c keeps its compact conformation, with cross sections similar to that calculated for the native cytochrome c structure. At trapping times longer than 60 ms, proteins appear to be elongated and partially unfolded. Thus in experiments where ions are stored for times of seconds, protein folding/unfolding events should be considered.

1.4.2 Noncovalent Binding Strengths

Noncovalent binding constants can be obtained directly from mass spectra by comparing the relative intensity of the complex to that of each subunit. In some cases, protein noncovalent complexes partially dissociate in the ion-source region [10, 83, 111, 118], which lowers the yield of complex ions observed in mass spectra and results in an underestimate in solution binding constant. In other cases, nonspecific adducts or clusters are artificially formed during ESI MS analysis [10, 11, 93]. These do not represent solution species, leading to errors in determining solution binding characteristics. Thus the abundances of gas-phase noncovalent complexes do not always reflect the solution binding. However, with low collision energies of ions, it is possible to find a reasonable correlation of the proportions of free protein and complex in mass spectra to solution dissociation constants (K_d), particularly in protein−small-molecule complex systems [23, 114, 119].

For protein−ligand complexes, a good correlation between gas-phase stability and solution binding constants indicates specific intermolecular interactions of the solution complex are preserved in the gas-phase ions. Such correlations have been reported for several protein complexes including heme-binding proteins [120] and antibody-sugar complexes [58, 121]. A few studies have shown that with the same dissociation pathway, gas-phase binding energies determined from ESI-MS experiments parallel binding energies in solution [105, 120, 122]. In heme loss from myoglobin ions, the activation energies (E_a) measured in ion trapping experiments range from 0.7 to 1.0 eV [122], similar to the heme-binding energies in solution (1.1 eV) [120].

1.5 Theoretical Calculations

1.5.1 Collision Cross Sections

The collision cross sections are measured with axial kinetic energy loss experiments
using a drag coefficient model [81]. An ion moving through a collision gas experiences
some resistance to its movement. The force exerted by the gas on a moving object is
called the aerodynamic force. The drag coefficient, C_D, relates this aerodynamic force, F,
to the projection area or cross section, σ, of an object moving with speed, v, by,

$$F = m_1 \frac{dv}{dt} = -C_D \frac{\sigma n m_2 v^2}{2}$$

(1.2)

where n is the gas number density, m_1 is the mass of the object, m_2 is the mass of the
collision gas. Equation (1.2) can be written as,

$$\frac{dv}{v} = -\frac{C_D \sigma n m_2}{2} dx$$

(1.3)

Integrating equation (1.3) over a distance, l, gives,

$$\left(\frac{v}{v_0} \right)^2 = \frac{E}{E^0} = \exp\left(-\frac{C_D \sigma n m_2 l}{m_1} \right)$$

(1.4)

In equation (1.4), the kinetic energy is proportional to the square of the velocity of the
particle, E^0 is the initial ion kinetic energy, and E is the ion kinetic energy after moving a
distance l. The drag coefficient for diffuse scattering, C_{Dd}, which in general provides a

best description of collisions between protein ions and rare gases [78], is used, as calculated in equation (1.5) [123],

$$C_{Dd} = \frac{2}{\sqrt{\pi}} \frac{e^{-s^2}}{s} \left(1 + \frac{1}{2s^2} \right) + 2 \left(1 + \frac{1}{s^2} - \frac{1}{4s^4} \right) erf(s) + \frac{2\sqrt{\pi}}{3s}$$

(1.5)

where Erf(s) is the error function, and s is the ratio of the object's speed to the thermal speed of the gas, given by,

$$s = \frac{v}{\sqrt{\frac{2k_B T}{m_2}}},$$

(1.6)

where k_B is Boltzmann's constant and T is the gas temperature. Experimental drag coefficients include the effects of inelastic collisions, the thermal speed of the target and scattering through a range of angles from a rough surface. With the drag coefficient included in equation (1.4), the kinetic energy loss can be directly related to the collision cross section.

1.5.2 Internal Energies

The total internal energy transferred into ions after multiple collisions, ΔE_{int}, is calculated in a collision model [105] as follows. Based on equation (1.4), the laboratory (LAB) kinetic energy of an ion after moving a distance z from the cell entrance is,

$$E_z = E^0 \exp\left(-\frac{C_{Dd} n \sigma m_2 z}{m_1} \right)$$

(1.7)

25

Only the center-of-mass kinetic energy, E_{CM}, can be transferred to internal energy for ion activation. The maximum internal energy ions can acquire in a single collision is given by,

$$E_{CM} = \frac{1}{2} \mu v_{rel}^2 = \frac{m_2}{M} E^0 \exp\left(-\frac{C_{Dd} n \sigma m_2 z}{m_1}\right)$$

(1.8)

Where v_{rel} is the relative velocity of the object to collision gas, μ is the reduced mass

$(\frac{m_1 m_2}{m_1 + m_2})$, and $M = m_1 + m_2$.

The total number of collisions in a finite distance Δz is determined by $\frac{\Delta z}{\lambda}$, where λ is the free mean path, given by

$$\lambda = \frac{1}{n\sigma}$$

(1.9)

Let Φ be the average fraction of E_{CM} transferred to internal energy in a single collision. Then the total internal energy gained in traveling a distance, dz, is determined by E_{CM} in one collision, multiplied by the number of collision times, described as,

$$dE_{int} = \Phi \frac{m_2}{M} E^0 \exp\left(-\frac{C_{Dd} n m_2 \sigma z}{m_1}\right) \times n\sigma dz$$

(1.10)

Integrating over a distance l gives the total internal energy added to an ion, as,

$$\Delta E_{int} = \Phi \frac{m_2}{M} E^0 \frac{m_1}{m_2} \frac{1}{C_{Dd}} \left[1 - \exp\left(-\frac{C_{Dd} n m_2 \sigma l}{m_1}\right)\right]$$

(1.11)

1.6 Two Protein Systems

1.6.1 Protein−Protein Complex: Hemoglobin

Hemoglobin (Hb) serves as a model to study noncovalent interactions in a multimeric globular protein system. All hemoglobins are heterotetrameric proteins. In normal adult human erythrocytes, the predominant Hb, hemoglobin A (Hb A), is assembled from four polypeptide chains (Figure 1.3a), two alpha and two beta chains, with 141 and 146 amino acid residues respectively. The total molecular weight (MW) is approximately 60 kDa. Each chain is formed by eight α-helices, folded similarly to myoglobin [17, 124]. A prosthetic group, heme, which is a large organic ring (protoporphyrin IX) with a central iron (Figure 1.3b), is inserted in a cleft between the E and F helices of each globin. The whole heme is oriented and stabilized by a large number of noncovalent contacts with the globin [124]. Each subunit can be in the heme-bound form (holo-, α^h and β^h) or heme-free form (apo-, α^a and β^a).

The four globins bind noncovalently to form a tetrameric structure ($\alpha_2\beta_2$) [124]. Two distinct types of interfaces exist in solution Hb tetramers. The first, between the dimer ($\alpha\beta$) pairs that form the tetramers is referred to as the $\alpha_1\beta_2$ or $\alpha_2\beta_1$ interface; the second, between the two individual α- and β- subunits to form dimers is referred to as the $\alpha_1\beta_1$ or $\alpha_2\beta_2$ interface [125]. Noncovalent contacts are located along the interfaces, including hydrophobic and van der Waals interactions, hydrogen bonding, and salt bridges. Tetrameric Hb exists in solution in equilibrium with low-abundance dimers and monomers [126-129].

27

(a)   **(b)**
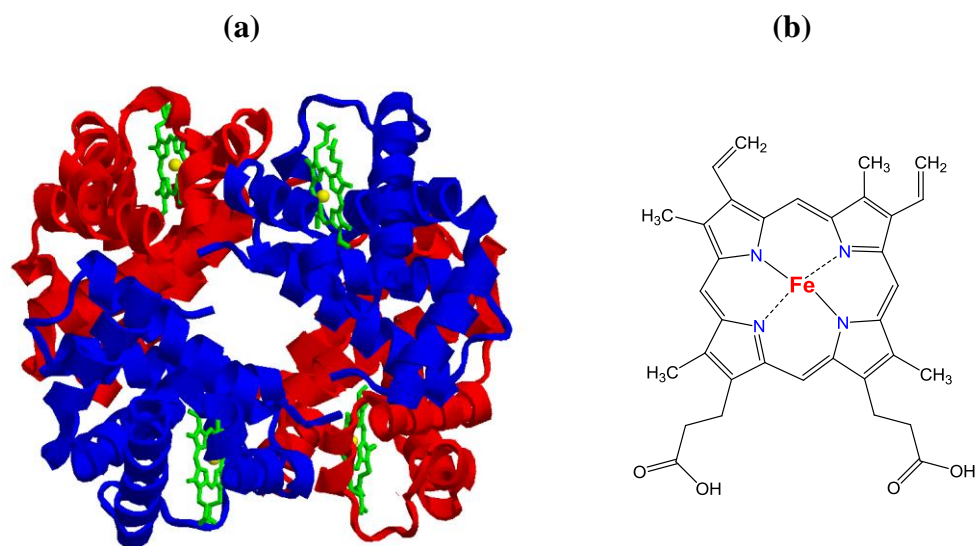
Figure 1.3. (a) Ribbon diagram of the three-dimensional structure of deoxy human hemoglobin. In red and blue are α chains and β chains, respectively. PDB code: 1A3N. (b) Structure of heme.

Hemoglobin transports oxygen in mammalian red blood cells [124, 130]. Oxygen binding is triggered by an iron-oxygen linkage and proceeds in a cooperative manner [124]. Ferrous Hb (Fe^{2+} in heme, also referred to as [deoxy]Hb) can bind oxygen to form [oxy]Hb (oxygen-bound state with Fe^{2+} in heme), while physiologically inactive ferric Hb (Fe^{3+} in heme, also referred to as [met]Hb) does not bind oxygen. Other than oxygen, hemoglobin ligands also include carbon monoxide ([CO]Hb), nitric oxide ([NO]Hb) and cyanide ([CN]Hb).

In addition to Hb A that composes about 97% of total Hb in normal human erythrocytes, the other minor components are also of interest, such as Hb A_2 ($\alpha_2\delta_2$) and Hb F ($\alpha_2\gamma_2$) [124]. Fetal hemoglobin, Hb F, takes up less than 1% of Hb in adult red blood cells, but is the predominant Hb form (80%) throughout fetal life and at birth. The

28

Hb F concentration decreases after birth to less than ca. 10% after 20 weeks [124]. It is formed from two pairs of heme-containing alpha chains and gamma chains through noncovalent interactions. The normal γ chains are of two types, γ^G and γ^A, which differ only in one amino acid residue at position 136 (glycine in γ^G and alanine in γ^A). The ratio of γ^G to γ^A is 3:1. The α chains of Hb F and Hb A are identical, while the γ chains differ from the β chains in 39 amino acid residues, with 22 on the exterior and 3 at the $\alpha_1\gamma_1$ or $\alpha_1\beta_1$ interface [124]. This difference in sequence results in several significant functional differences between Hb A and Hb F. For example, Hb F shows lower responses to 2,3-diphosphoglycerate (DPG) binding and thus increased oxygen affinity in the presence of DPG [124], and, in solution, Hb F dimers and tetramers are more strongly bound than the same species of Hb A [125, 128, 131, 132].

Approximately 1000 Hb variants have been discovered and characterized at the molecular level [133, 134]. Studies of abnormal hemoglobins are of considerable interest not only for better understanding of globin-gene expression but also in the diagnosis of a variety of disorders. One example of a Hb that causes serious health problems is sickle hemoglobin, Hb S ($\alpha_2\beta_2$, E6V[β]). In fully or partially deoxygenated blood, the substitution of valine for glutamic acid at the $\beta6$ position changes the conformation of Hb to allow tetramers to pack into polymers [135]. This molecular stacking alters the shape of red blood cells, decreases the solubility of the protein and consequently impairs oxygen delivery to tissues [136], leading to sickle cell anemia. However, *in vitro*, Hb S has entirely normal functional properties in dilute solution [137]. In contrast, fetal Hb has been tested to treat sickle cell anemia [138] because it has an anti-sickling effect due to unfavorable contacts for polymerization [125].

1.6.2. Protein−Small-Molecule Complex: Cex-Inhibitor

In this study, binding of the catalytic domain of the enzyme exo-1,4-β-D-glycanase (cellulasexylanase or "Cex") with aza-sugar inhibitors, serves as a model to study solution and gas-phase conformations of protein−small-molecule noncovalent complexes. Cex (from the microorganism *Cellulomonas fimi*) is a family 10 glycosyl hydrolase. It consists of a C-terminal cellulose binding domain, and an N-terminal catalytic domain which is involved in substrate and inhibitor binding. The catalytic domain of Cex folds as a $(\alpha/\beta)_8$-barrel with a MW of approximately 30 kDa (Figure1.4). It catalyses hydrolytic cleavage of β-1,4 linked polymers of D-xylose [139].

A series of small-molecule xylobiosyl inhibitors that noncovalently bind at the active site of the catalytic domain of Cex (Cex-cd) with high affinity have been described [139]: imidazole, lactam oxime, deoxynojirimycin (X_2DNJ), isofagomine lactam (X_2IL), and isofagomine (X_2IF), three of which are used in this work and are shown in Figure 1.5. These xylobiose-derived nitrogen-containing inhibitors consist of two sugars, a common distal xylose that binds to the -2 sub-site of Cex and a distinct proximal aza-sugar that binds to the -1 sub-site [16, 139]. Cex binds to inhibitors mainly through hydrogen bonding but also through van der Waals forces and electrostatic interactions [140]. Changing the inhibitors affects the binding of Cex to the proximal sugar while the binding to the distal xylose is largely preserved [16].
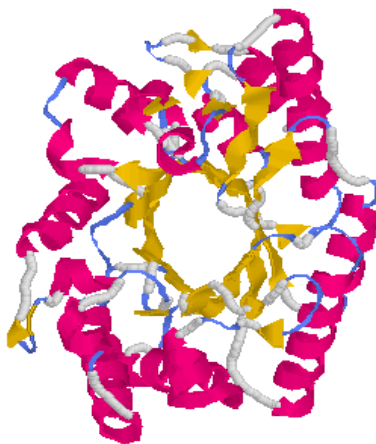
Figure 1.4. Ribbon diagram of the three-dimensional $(\alpha/\beta)_8$-barrel fold of the catalytic domain of Cex. PDB Code: 2EXO.

Xylobiosyl Deoxynojirimycin (X_2DNJ)
MW = 265 Da

Xylobiosyl Isofagomine Lactam (X_2IL)
MW = 263 Da

Xylobiosyl Isofagomine (X_2IF)
MW = 249 Da
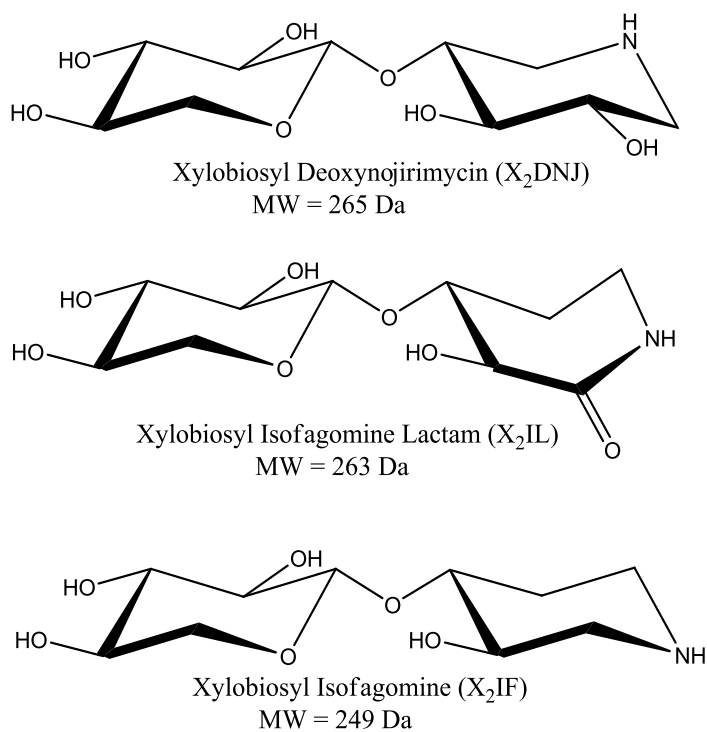
Figure 1.5. Structures and MW of the three inhibitors, X_2DNJ, X_2IL and X_2IF. The distal xylose is on the left and the proximal aza-sugar is on the right.

1.7 Research Objectives

In this thesis, physical properties of gas-phase ions of variant hemoglobins and Cex−inhibitor complexes have been investigated with ESI MS. Studies of gas-phase conformations come from measurements of collision cross sections and gas-phase H/Dx. Gas-phase noncovalent binding strengths are measured in MS/MS experiments. Solution H/Dx has also been employed to study protein conformations in solution.

In previous studies of Hb A with ESI MS, commercial lyophilizate of hemoglobin has been frequently used as an established model in protein−protein complexes because it is readily available. However, the commercial proteins have shown different mass spectra [20, 83], and different properties from hemoglobins freshly extracted from human red blood cells in measurements of collision cross sections [61, 83] and acid-induced dissociation [20, 69]. In work described in chapter 2, hemoglobins from different sources and prepared in different ways have been studied with ESI MS, to further investigate the differences of gas-phase properties between commercial and fresh proteins in mass spectra and collision cross sections. Possible factors that contribute to these differences are discussed.

The physical properties of gas-phase Hb ions and any relation of these properties to the solution characteristics of Hb are potentially informative. The well-characterized properties of Hb A in solution provide good references for comparison to properties of gas-phase Hb ions. The availability of natural Hb variants allows studying the effects of changing the individual chains on the properties of this model protein−protein complex. Although the gas-phase structures and dissociation of Hb A have been studied with ESI

MS in a few studies [7, 61, 62, 107], another two hemoglobins, Hb S and Hb F, have been studied much less. In chapter 3, a study of gas-phase conformations and binding strengths of Hb A, Hb F and Hb S is described. The relation of properties measured in the gas-phase ions to the well-studied characteristics in sizes and binding constants in solution is discussed as well.

Previously hydrogen/deuterium exchange of Hb A in solution has been studied either on the entire protein [21, 91, 141-144] or on localized regions [91, 93, 142, 145, 146]. However, "continuous-labeling" from minutes to hours was employed in most of the studies, with an exchange time much longer than the tetramer-dimer interconversion time in solution [147, 148]. Solution H/Dx of the other two hemoglobins, Hb F and Hb S, has not been reported. In work described in chapter 4, a home-made flow mix and sprayer system has been used to probe the "pulsed-labeling" solution H/Dx for milliseconds in Hb A, Hb F and Hb S, to investigate the possible conformational differences in these three hemoglobins and to monitor their H/Dx kinetics. Exchange at longer times has also been studied with a commercial sprayer.

Cex binds to a series of inhibitors with different binding strengths in solution [9]. It is of interest to investigate the potential of MS to distinguish these small binding differences as well as the conformational changes in Cex upon binding in the gas phase. In work described in chapter 5, the gas-phase conformations and binding strengths of Cex binding with three aza-sugar inhibitors, X_2DNJ, X_2IL, and X_2IF, have been studied. Conformations of the protein after in-source dissociation have been measured as well. In addition, solution H/Dx has also been employed and compared with gas-phase H/Dx.

Chapter 2 Mass Spectra and Ion Collision Cross Sections of

Hemoglobin A

2.1 Introduction

Electrospray ionization (ESI) mass spectrometry (MS) has been widely used to study hemoglobins [133, 134]. In ESI MS, ions of monomers (α, β), dimers ($\alpha\beta$) and tetramers ($\alpha_2\beta_2$) of Hb A are observed [7, 20, 61, 69, 83, 149]. The conformations of these gas-phase ions, and the relation of these conformations to solution conformations of the same species are of interest [3, 150]. Collision cross sections of ions formed from Hb have come from measurements of migration time with ion mobility mass spectrometry (IM MS) [7, 61] and from measurements of ion axial kinetic energy losses with a triple quadrupole MS system [83].

The mass spectra and properties of Hb ions formed from commercial lyophilized Hb [69, 83, 93, 133, 151], differ significantly from the spectra and properties of Hb freshly prepared from mammalian red blood cells [20, 61]. Boys et al. found, heme-deficient dimer and apo-monomer ions were formed from commercial bovine Hb, but not from fresh bovine Hb [20]. The acid-induced dissociation of freshly prepared bovine ^{met}Hb, showed a highly symmetric unfolding mechanism, $(\alpha^h\beta^h)_2 \rightarrow 2\alpha^h\beta^h$ [20], while the commercial protein produced a heme-deficient dimer ($\alpha^h\beta^a$) as an intermediate in the disassembly process [69]. With commercially obtained bovine ^{met}Hb, Wright and Douglas reported, surprisingly, that gas-phase dimer ions ($\alpha^h\beta^h$) (+11, +12) had smaller cross sections than monomer ions (α^h) in low charge states (+7, +8) [83]. However, with freshly extracted human Hb, Scarff et al. found that cross sections of gas-phase dimer ions ($\alpha^h\beta^h$) (+12 to +14) were greater than those of monomer ions (α^h) (+6 to +10) [61]. It had been noted earlier that in commercial ^{met}Hb there can be oxidative modifications [20, 93, 151], mainly sulfoxide formation on methionine residues [20]. It was proposed that

35

this oxidation might be responsible for the unusual properties of commercial Hb. This led us to ask whether the unusually low cross sections of dimer ions reported by Wright and Douglas could also be attributed to oxidation or some other chemical change in commercial Hb, or possibly to the sequence difference between bovine and human Hb.

The work in this chapter, therefore, was undertaken to further elucidate the differences between hemoglobins from different sources and hemoglobins prepared in different ways, and to determine if there are differences in the cross sections of ions from these various hemoglobins. Physiologically inactive ^{met}Hb was used to allow comparison with previous studies. We have recorded ESI mass spectra of fresh human Hb, commercial human Hb, commercial bovine Hb, fresh human Hb chemically oxidized with H_2O_2, lyophilized fresh human Hb, fresh human Hb both lyophilized and chemically oxidized, and commercial human Hb chemically oxidized. With the same solution and mass spectrometer conditions, commercial human Hb and fresh human Hb give significantly different spectra, with commercial human Hb forming higher levels of dimers and monomers. Oxidation, lyophilization, and lyophilization followed by oxidation, of human Hb all give higher levels of monomer and dimer ions in the mass spectrum. Oxidation of fresh Hb also produces heme-deficient dimers in the mass spectrum. Both the commercial human Hb and commercial bovine Hb give α-chain monomer masses within 3 Da or better of the masses expected from the sequences, and thus do not show evidence of oxidation. However the β chains do show evidence of oxidation. Heme-deficient dimers with the commercial hemoglobins show masses 32 Da higher than expected, indicating that the commercial proteins were partially oxidized. Further oxidation of commercial human Hb did not produce major changes to the

spectrum. Thus differences in the spectra between fresh and commercial human Hb are partially due to oxidation, as proposed by Boys et al. [20], but also due to lyophilization of the proteins. Cross sections of monomer, dimer and tetramer ions of fresh human Hb, commercial human Hb, commercial bovine Hb, and commercial human Hb further oxidized with H_2O_2 have been measured. With all four hemoglobins, cross sections of dimer ions were similar, and greater than cross sections of monomer ions. Thus we cannot reproduce the result of Wright and Douglas [83]. However it appears that neither oxidation of the protein, nor the difference in sequence between bovine and human Hb make substantial differences to the collision cross sections.

2.2 Experimental Methods

2.2.1 ESI Triple Quadrupole Mass Spectrometer System

A pneumatically-assisted ESI source was used, as shown in Figure 2.1. A solution is pumped through a fused silica capillary (75.0±0.4 μm i.d., Polymicro Technologies, Phoenix, AZ, USA) with a syringe pump (Harvard Apparatus, St. Laurent, QC, Canada Havard) at 1 μL/min, into a stainless steel capillary (i.d. 250 μm and o.d. 380 μm). A second stainless steel capillary (i.d. 500 μm, o.d. 760 μm) is concentric with the other two capillaries. Air flows between the two stainless steel capillaries to assist nebulization. The end of the capillary is flush with the end of the stainless steel tube with a high voltage applied (4 kV), which provides the actual electrospray outlet.
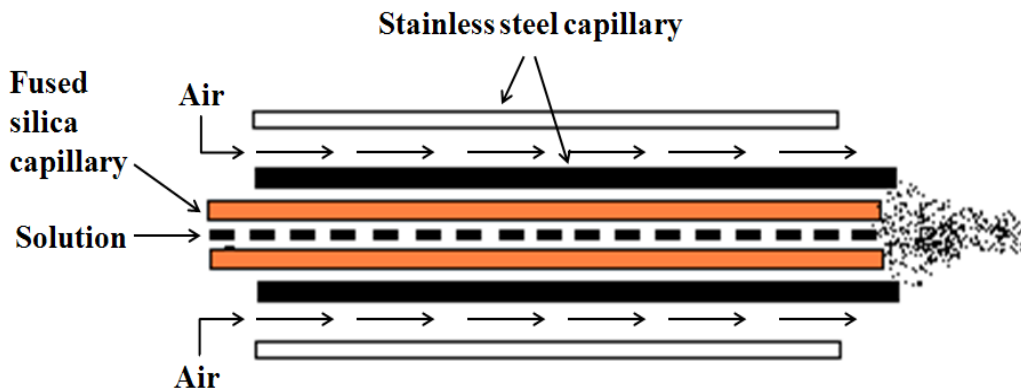
Figure 2.1. Pneumatically-assisted ESI source.

A home-built ESI triple quadrupole mass spectrometer described previously [78, 79, 120], but modified to increase sensitivity, was used, as shown in Figure 2.2. Protonated ions, formed by pneumatically-assisted electrospray, pass through a 2.4 mm diameter aperture in a curtain plate (1150 V), a dry nitrogen curtain gas (~ 2 L/min), an ion sampling orifice (250 V) into a region with a background pressure of ca. 0.7 Torr. Ions then pass through a skimmer (150 V), into a quadrupole ion guide Q0 (~ 9×10^{-3} Torr, DC offset = 120 V). In Q0, ions are cooled to translational energies and energy spreads of about 1-2 eV per charge [152]. After passing through a short RF-only quadrupole (DC offset = 108 V), ions enter a quadrupole, Q1, (DC offset = 95 V), a collision cell with a quadrupole ion guide, Q2, (DC offset = 105 V), and a quadrupole, Q3, (DC offset = 90 V). After mass analysis ions of selected m/z ratios pass through the exit lens (EXIT) and are deflected (DEF, 50 V) into a channel electron multiplier (CEM, −4 kV) for ion detection. Noise is rejected by a discriminator and the ion signal is recorded in ion counting mode. The vacuum of this apparatus is maintained by a three-stage differential pumping system, including a mechanical (rotary) pump for the interface region and two

turbo molecular pumps for Q0 and the main chamber respectively. The pressure in Q1 and Q3 is roughly 1×10^{-5} Torr measured with a hot-filament ionization gauge. The pressures in Q2 vary in the range of 10^{-5} to 10^{-3} Torr, and are measured with a precision capacitance manometer (model 120AA; MKS Instruments, Boulder, CO, USA).

To increase the sensitivity, the sampling orifice diameter was increased to 0.25 mm, and the skimmer aperture diameter to 2.90 mm. The 50 L s^{-1} turbo pump on the Q0 region was replaced with a 360 L s^{-1} pump. These changes increased the gas flow into Q0 by a factor of about 7, and the sensitivity by about the same amount. The ion optics from Q0 through to the detector were not changed.
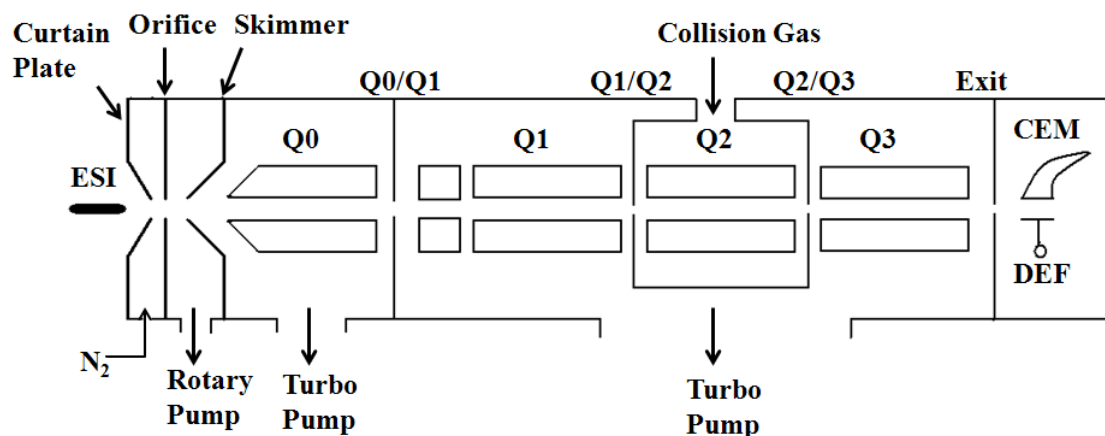
Figure 2.2. Schematic of the ESI triple quadrupole mass spectrometer system. Q0/Q1, Q1/Q2, Q2/Q3, interquadrupole lens; EXIT, exit aperture plate; CEM, channel electron multiplier; DEF, deflector.

2.2.2 Collision Cross Section Measurements

Collision cross sections were measured with axial kinetic energy loss experiments, as described in chapter 1 [78, 80, 153]. In Q2, ions lose kinetic energy through multiple collisions with a low-density gas (Ar). The energy losses can be related to the collision cross sections with an aerodynamic drag model [81] through equation (1.4)

$$\frac{E}{E^0} = \exp\left(-\frac{C_{Dd}nm_2l\sigma}{m_1}\right)$$

(1.4)

where E is the ion kinetic energy at the exit of Q2, E^0 is the ion kinetic energy at the entrance of Q2, C_{Dd} is a drag coefficient for diffuse scattering [78], n is the gas number density, m_1 is the mass of the protein ion, m_2 is the mass of the collision gas, l is the length of Q2 and σ is the collision cross section.

The initial kinetic energy of ions at the entrance of collision cell, E^0, is determined by the DC rod offset voltage difference between Q0 and Q2, multiplied by the ion charge. To determine the ion energy at the exit of the cell, the DC rod offset of Q3 is increased step by step to give a stopping curve (ion intensity vs. Q3 rod offset). The Q3 rod offset is arbitrarily taken as the "stopping potential" when the ion signal decreases to one-tenth of the initial signal. The kinetic energy of ions at the exit of Q2, E, is determined by the difference of the stopping potential and Q2 rod offset, multiplied by the ion charge. The pressure of Ar in the collision cell was varied between 0.0 and 1.2 mTorr, and the stopping potential as well as value of E/E^0 was obtained at each pressure. Cross sections were then calculated by plotting $-\ln\frac{E}{E^0}$ versus $\frac{C_{Dd}nm_2l}{m_1}$.

To record mass spectra, Q1 was operated as a mass filter. For cross section measurements, Q1 was operated as an RF-only ion guide, and Q3 was operated as a mass filter. Uncertainties in cross sections are the standard deviations of three measurements.

2.2.3 Ion Masses

Masses of dimers and heme-deficient dimers from unoxidized or oxidized hemoglobins, 20 μM in 10% methanol (MeOH)/90% water (v/v), 10 mM ammonium acetate (NH$_4$Ac), were measured with a linear quadrupole ion trap time-of-flight mass spectrometer system (LIT-TOF MS) [83]. To record spectra of apo-monomers with the LIT-TOF MS, proteins were denatured in 50% MeOH with 0.5% acetic acid. ES tuning mix (for LC/MSD Ion Trap, Agilent, Santa Clara, CA, USA) was used for mass calibration.

2.2.4 Solutions and Reagents

Human ^{oxy}Hb ("fresh Hb") was prepared via standard procedures [20, 154]. Fresh human blood was centrifuged (Sorvall RC-5B Plus; Mandel Scientific, Newton, CT, USA) at 3,000 g for 10 min at 10 ℃, and the clear supernatant, plasma and buffy coat, were discarded by suction. The collected red blood cell pellets were then re-suspended in a five-fold (v/v) excess of 0.9% (w/v) sodium chloride solution and washed four times with centrifugation at 5,500 g for 20 min at 4 ℃. After mixing with an equal volume of cold water/toluene 90/10 (v/v) to extract stromal cell impurities, centrifugation of packed red blood cells at 15,000 g for 30 min at 10 ℃ gave an aqueous layer of purified hemolysate,

which was then dialyzed at 4 ℃ with 10 mM NH₄Ac for 42 hours with four buffer

exchanges, using a cellulose membrane (MWCO 3.5 kDa; Spectra/Por, Rancho

Dominguez, CA, USA). The concentration of ^{oxy}Hb (as tetramer) was determined to be

0.4 mM with UV-Vis spectrometry (Cary 5000 UV spectrophotometer; Varian, Inc., Palo

Alto, CA, USA), with the standard pyridine hemochromogen method [155, 156].

Desalted ^{oxy}Hb was oxidized to ^{met}Hb with a 1.5-fold stoichiometric excess of potassium

ferricyanide ($K_3Fe(CN)_6$) for 5 min at 25 ℃ [157]. The ^{met}Hb solution was then frozen

with liquid nitrogen and stored at -80 ℃. Before MS analysis, the solution was quickly

thawed and desalted on a 3×25 cm G-25 Sephadex column (GE Healthcare,

Buckinghamshire, UK).

Freshly prepared human Hb stock solution (50 μL, ca. 0.4 mM) was freeze dried

in a Manifold Freeze-Dryer (Flexi-DryTM MP; FTS systems, Bohemia, NY, USA) at

$5×10^{-2}$ Torr at −80 ℃ for two hours. The lyophilized powders were then dissolved in 50

μL water with 10 mM NH₄Ac to give the concentration prior to freeze drying (ca. 0.4

mM).

Commercial human and bovine ^{met}Hb were purchased from Sigma-Aldrich (St.

Louis, MO, USA). Stock solutions were prepared by dissolving the lyophilized powder in

10 mM NH₄Ac with the same concentration as fresh Hb. Dialysis and storage of

commercial Hb were as with fresh Hb.

Commercial and fresh human Hb were oxidized by adding 30% highly purified

hydrogen peroxide (H_2O_2, TraceSelectUltra, Sigma-Aldrich, St. Louis. MO, USA) to

produce a solution of 20 μM Hb in 200 μM to 300 μM peroxide, and the oxidation was

allowed to proceed for 1 hr. Excess H_2O_2 was removed by buffer exchange with equal volumes of 10 mM NH$_4$Ac [158] with centrifugation (MSE MicroCentaur; London, UK) at 13,000 rpm for 10 min, with five repeats.

For MS of native or near-native proteins, the fresh and commercial Hb solutions were diluted to 20 µM or 5 µM with 10% MeOH or 10% acetonitrile (ACN) in 10 mM NH$_4$Ac at pH 6.8 (measured with a Accumet model 15 pH meter (Fisher Scientific, Fairlawn, NJ, USA)).

Acetic acid (99.99%), pyridine (99.9%), and $K_3Fe(CN)_6$ (ACS grade) were from Sigma-Aldrich, St. Louis, MO, USA. Methanol, ACN, toluene (all HPLC grade), and NH$_4$Ac (ACS grade) were from Fisher Scientific, Fairlawn, NJ, USA. Nitrogen and argon (manufacturer's stated purity 99.999%), and air (breathing grade) were from Praxair, Mississauga, ON, Canada.

2.3 Results and Discussion

2.3.1 Mass Spectra of Hemoglobin

Figure 2.3 shows ESI mass spectra of freshly prepared human Hb in different solvents recorded with the triple quadrupole system. With a 20 µM Hb solution in 10% MeOH (Figure 2.3a), tetramer ions $(\alpha^h\beta^h)_2$ with charge states from +15 to +17 dominate the spectrum. Only low levels of monomer and dimer ions are observed. With a 5 µM fresh
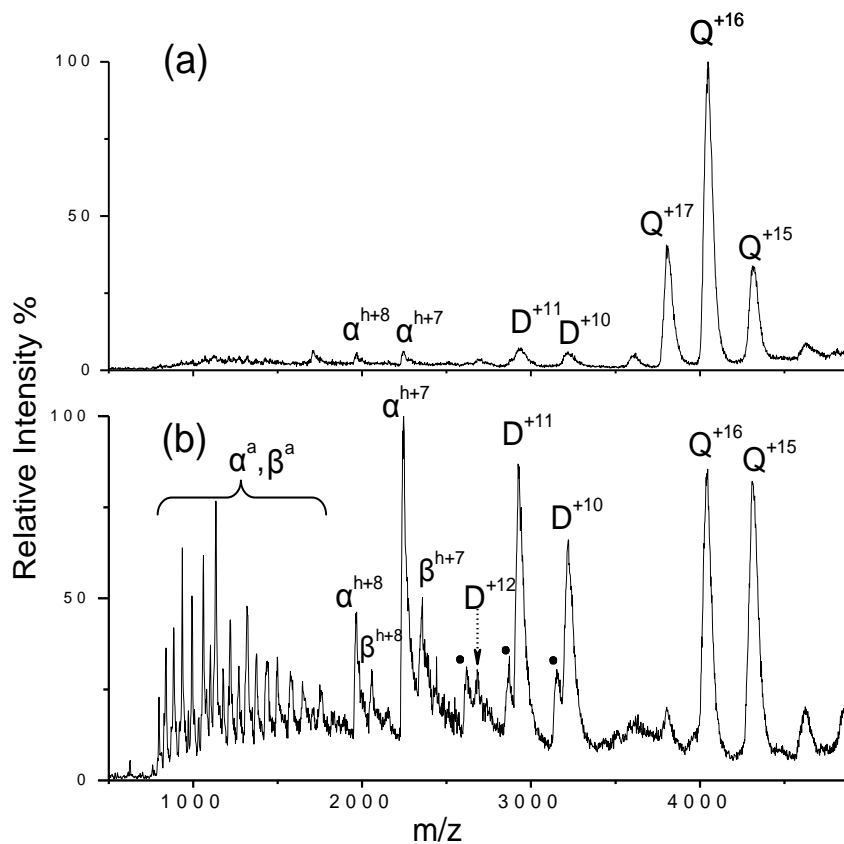
Figure 2.3. ESI mass spectra of fresh human Hb, (a) 20 μM Hb in 10% MeOH, and (b) 5 μM Hb in 10% ACN. Notation: α^a, β^a, apo-monomers; α^h, β^h, holo-monomers; D, dimers, $\alpha^h\beta^h$; Q, tetramers, $(\alpha^h\beta^h)_2$. Peaks labeled with a filled circle correspond to heme-deficient dimers.

Hb solution containing 10% ACN (Figure 2.3b), more intense ions of holo-monomers, α^h, β^h (+7, +8), and dimers, $\alpha^h\beta^h$ (+10 to +12), are seen. The maximum charges of folded holo-alpha, dimer and tetramer ions are estimated to be 10, 14 and 20 respectively [equation (1.1)], in reasonable agreement with the charges observed in the mass spectra.

44

Apo-monomers, α^a, β^a, in high charge states, and some heme-deficient dimers ($\alpha^h\beta^a$ or

$\alpha^a\beta^h$) are also observed. These were previously shown by others to be present with

commercial Hb [7, 20, 93, 151] but not with fresh Hb [20, 61]. Here with fresh Hb,

masses of the heme-deficient dimers, measured with the TOF system, are as expected

from the sequence (see discussion below). Thus the fresh protein is not oxidized and the

formation of heme-deficient dimers is likely due to the addition of ACN which partially

destabilizes the protein. The solution with ACN (5 μM Hb) was used to produce dimer

and monomer ions for cross section measurements. Dilution of the 20 μM solution of Hb

in 10% MeOH, gave only slight increases in intensities of the monomer and dimer ions.

These results indicate that addition of ACN apparently leads to dissociation of tetramers

to dimers and monomers.

Figure 2.4 shows ESI mass spectra of Hb from human and bovine, obtained

commercially, and oxidized commercial human Hb, recorded with the triple quadrupole

system. With the same solution (10% MeOH) and mass spectrometer operating

conditions, commercial human Hb, bovine Hb and oxidized human Hb gave similar mass

spectra, and produced higher levels of monomers (α^h, α^a, β^a) and dimers ($\alpha^h\beta^h$) than fresh

human Hb (Figure 2.3a). Heme-deficient dimers were also observed with all the

commercial proteins, consistent with previous reports [7, 20, 93, 151]. In contrast to fresh

Hb, these dimers, assigned $\alpha^h\beta^a$ structures [7, 20], have masses 32 Da greater than

expected, indicating that the commercial proteins were partially oxidized. These

observations agree partially with those of Boys et al. [20] who also found that that dimer

and monomer ions are more abundant with commercial Hb than with fresh Hb in spectra

with their TOF mass spectrometer. However they found that tetramer ions still dominated
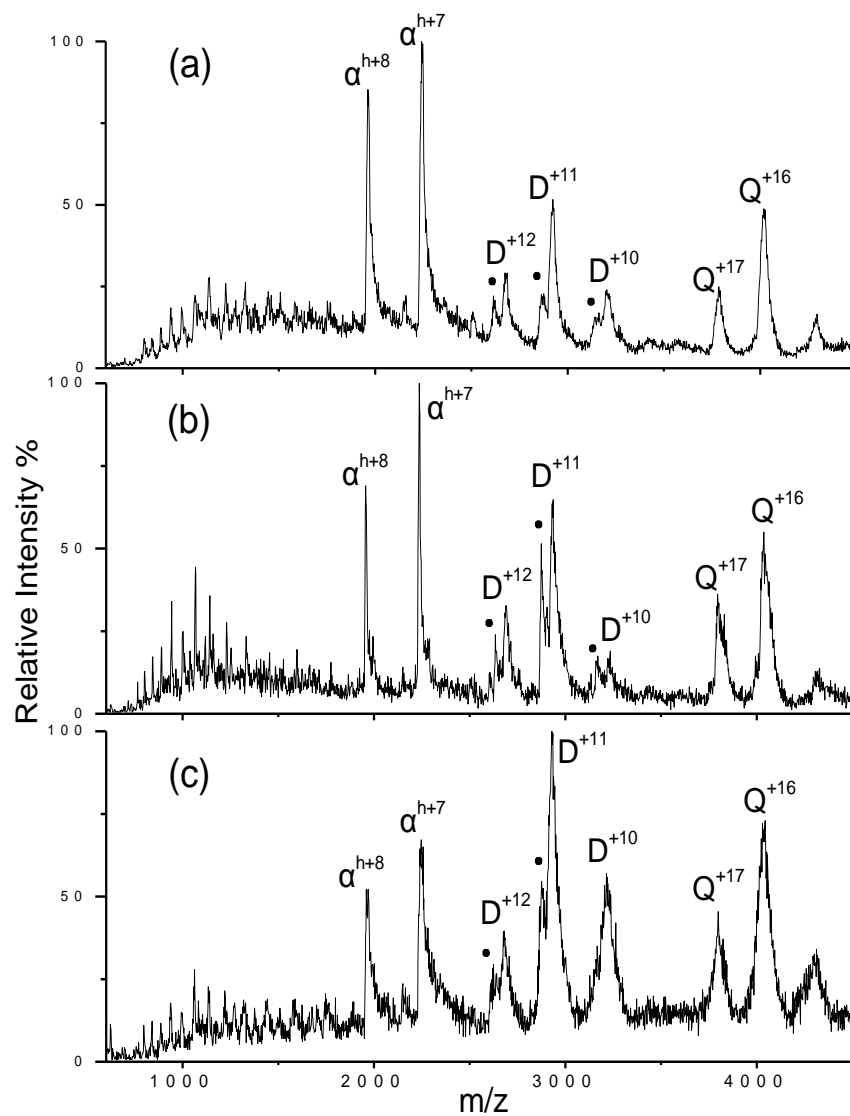
Figure 2.4. ESI mass spectra of (a) commercial human Hb, (b) commercial bovine Hb and (c) oxidized commercial human Hb. Notation as in Figure 2.3.

the spectra with both fresh and commercial bovine Hb, whereas we find much higher levels of monomers and dimers with commercial Hb. In aqueous solution, the tetramer-dimer dissociation constant K_d for ^{met}Hb (H$_2$O) was reported to be 4.0×10^{-6} M at neutral pH (0.1 M KCl, 10 mM bis-Tris) [159]. With this K_d, and 20 µM Hb, ca. 20% of the tetramers should dissociate to dimers, so some dimers might be expected in the mass spectrum. The K_d value for dissociation of αβ dimers to α and β monomers (^{CO}Hb) is much lower, approximately 10^{-12} M [128, 129], so minimal dissociation of dimers to monomers is expected. The solvent composition can strongly affect K_d. For ^{deoxy}Hb, in 0.1 M phosphate buffer alone a $K_d \approx 10^{-7}$ M was found [126] for dissociation of tetramers, while in a different solution (0.1 M Tris, 0.1 M NaCl, 1 mM Na$_2$EDTA), K_d decreased to ca. 10^{-11} M [127]. Addition of 10% organic solvent, MeOH or ACN (Figure 2.3a and 2.3b) may also change the degree of dissociation in solution. Note that Boys et al. did not use 10% MeOH in their Hb solutions. Mass spectra also depend strongly on MS system operating conditions. With a higher pressure in Q0 or a lower voltage difference between the orifice and skimmer (ΔV_{os}), more tetramers are seen [83]. If the mass spectrometer is optimized for maximum transmission of the tetramers, as was done by Boys et al. [20], monomer and dimer ions might be expected to decrease in relative intensity [83]. Thus it is difficult to determine the levels of dissociation in solution by ESI MS, and spectra with different instruments cannot be compared directly.

Figure 2.5 shows ESI mass spectra of Hb denatured in solution, recorded with the TOF system. Peaks from apo-alpha and apo-beta ions can be seen. In Figure 2.5c peaks from holo-alpha ions from bovine Hb can also be seen. The insets show the β^{a+16} and α^{a+15} peaks in detail. Here the TOF mass analyzer was used to give higher resolution and
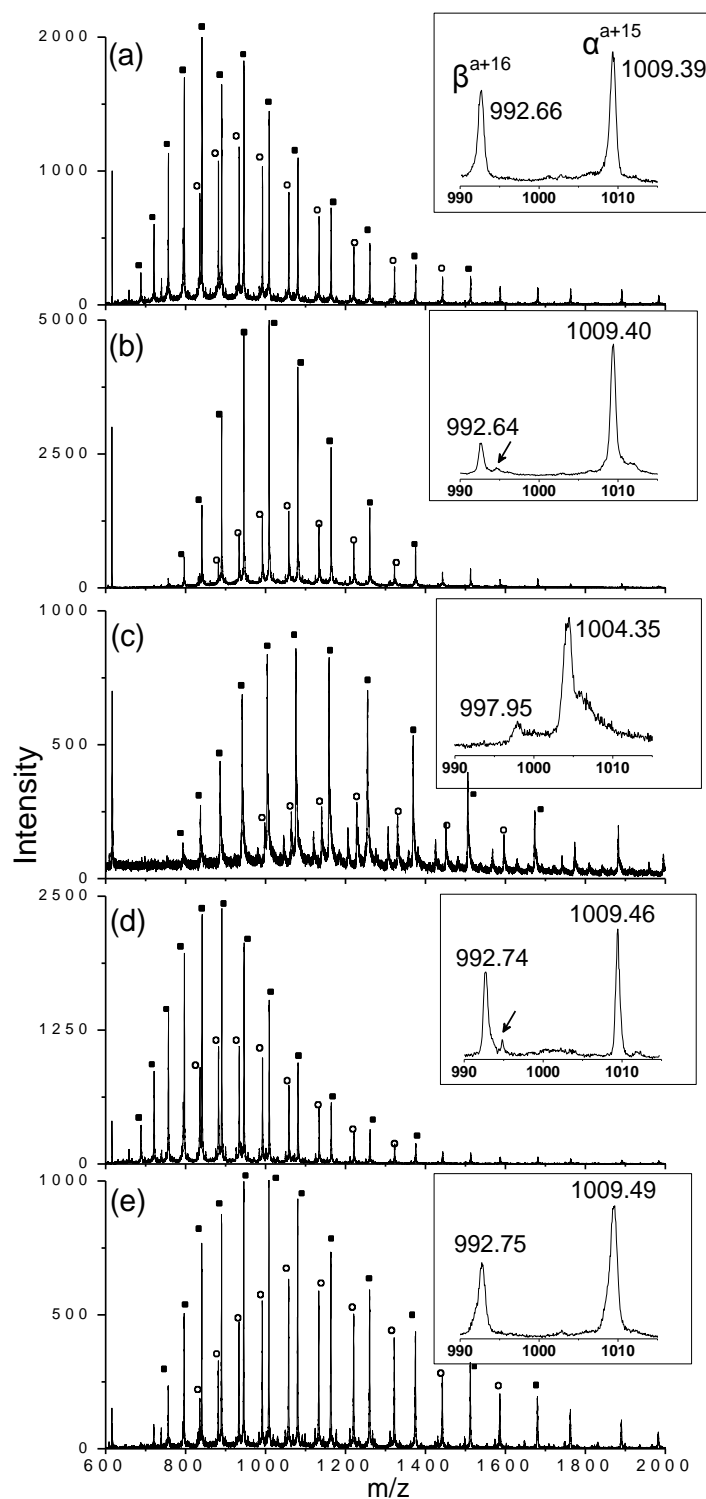
Figure 2.5. Mass spectra of apo-monomer ions, α^a (filled squares), β^a (open circles), from (a) fresh human Hb, (b) commercial human Hb, (c) commercial bovine Hb, (d) oxidized fresh human Hb, and (e) lyophilized fresh human Hb, in denaturing solutions. The insets show peaks of the β^{a+16} and α^{a+15} ions with the measured mass to charge ratios (m/z) labeled. Arrows in (b) and (d) indicate β^{a+16} ions with masses 32 Da higher than expected. Minor peaks adjacent to β^a peaks in (c) are from holo-alpha ions.

48

higher mass accuracy (the FWHM of monomer peaks is ca. 0.7 Th; the expected width from the isotopic distribution is ca. 0.6 Th). Measured masses of the alpha subunits of fresh human Hb and commercial human Hb agree within 0.8 Da (0.005% or better) with masses calculated from the protein sequences (Table 2.1); of commercial bovine Hb within 3 Da (0.02%). Thus the alpha chains of the proteins were not oxidized. Additional peaks on the high mass side of the apo-beta peaks of the commercial proteins (Figure 2.5b) are consistent with partial oxidation of the proteins. Thus partial oxidation of the Hb leads to the observation of oxidized heme-deficient dimers in the spectrum as noted by Boys et al. [20]. High mass tails of the peaks of the apo-alpha ions with commercial Hb may be attributed to some impurity adducts or chemical decomposition occurring during the freeze drying process or storage of the freeze-dried solid [160, 161]. Figure 2.5d shows that oxidation of fresh human Hb with H_2O_2 gives β^a ions with a 32 Da increase in mass. Figure 2.5e show that lyophilization of fresh human Hb does not give β^a ions with a 32 Da increase in mass, and thus does not oxidize the protein.

Table 2.1. Molecular weights of human and bovine Hb species (Da).

Species	α^a	α^h	β^a	β^h	$\alpha^h\beta^h$	$(\alpha^h\beta^h)_2$
Human Hb	15126	15743	15867	16484	32227	64453
Bovine Hb	15053	15669	15954	16571	32240	64480

The sulphur-containing residues, methionine (Met) and cysteine (Cys) are easily oxidized [162]. Human Hb contains two Met and one Cys in the α chain, and one Met and two Cys in the β chain [124]. Initial oxidation of Met generates methionine sulfoxide ($-(CH_2)_2-(S=O)-CH_3$), which, with more intense chemical attack [162], can then form the irreversible product Met sulfone ($-(CH_2)_2-(O=S=O)-CH_3$). Cysteine residues are more susceptible to oxidation than Met residues, and the possible irreversible oxidation products are the sulfenic acid ($-CH_2-SOH$), the sulfinic acid ($-CH_2-SO_2H$), and the sulfonic acid ($-CH_2-SO_3H$) [158, 163]. Hydrogen peroxide is a biologically relevant oxidant [158, 164]. At low concentrations of H_2O_2, hydroxyl radicals are required for oxidation, catalyzed by trace transition metal ions [165]. Here we used a relatively high concentration of H_2O_2, in which the oxidation is a direct effect, independent of intermediate hydroxyl radicals [158, 166]. Extensive exposure to H_2O_2 can substantially increase a protein's hydrophilicity which can lead to irreversible conformational changes [167]. With Hb, β subunits are more susceptible to oxidation [158]. The ratio $[H_2O_2]/[Hb]$ and reaction time were carefully controlled to minimize conformational changes to Hb. In our experiments, ratios of $[H_2O_2]/[Hb]$ in the range 10 to 15 were chosen. Greater than a 15-fold excess of H_2O_2 was found to cause irreversible collapse of the tetrameric structures, so that only monomers appeared in the mass spectra.

Commercial human Hb was chosen for further oxidation for comparison to the cross section results of Wright and Douglas who used commercial Hb. Although the total ion intensity decreased (by about half) after oxidation, the mass spectrum (Figure 2.4c) still showed abundant tetramer ions, indicating that the folded structure in solution was well preserved. Mass spectra of Hb that was oxidized with H_2O_2 and denatured in

solution, recorded with the TOF mass analyzer, showing peaks from the α^a and β^a monomers, are presented in Figure 2.6. An adduct corresponding to an increase in mass of 32 Da is seen with both monomers. The β chain shows a greater degree of oxidation.
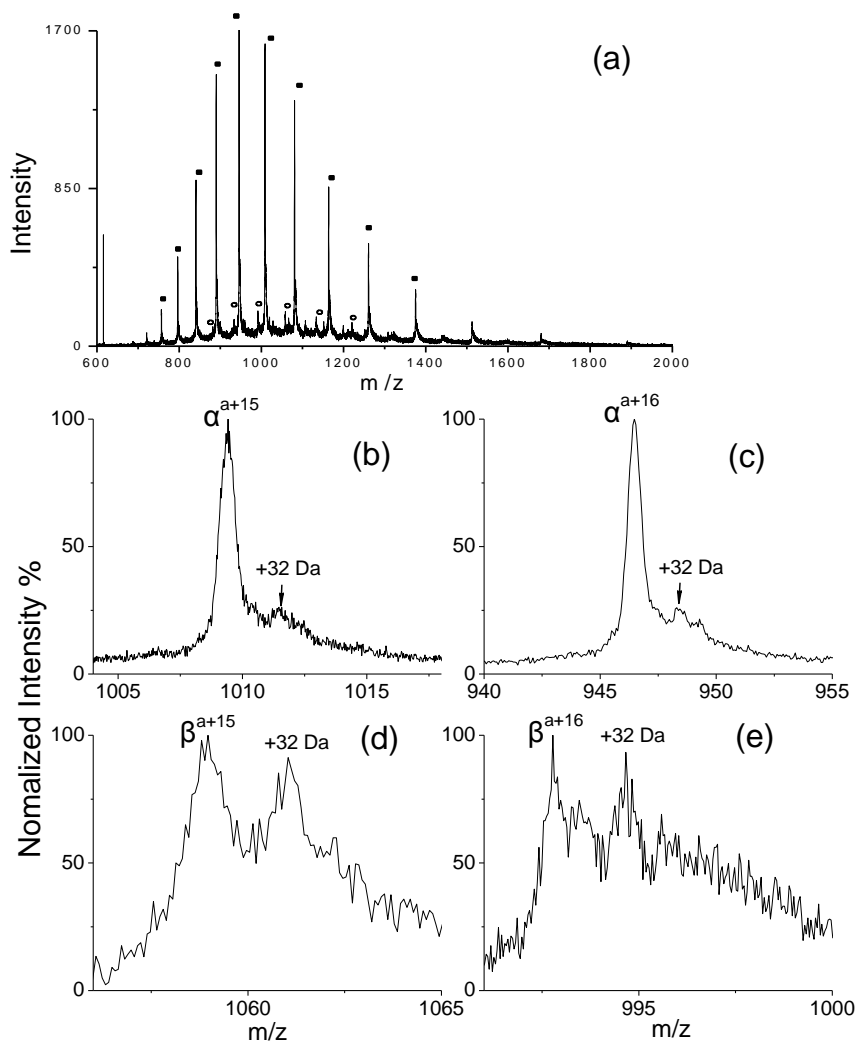
Figure 2.6. (a) Mass spectrum of commercial human Hb further oxidized with H_2O_2 and denatured in solution (α^a, filled squares, β^a, open circles) and detailed views of the (b) α^{a+15} (c) α^{a+16} (d) β^{a+15} (e) β^{a+16} peaks. The main peaks observed correspond to unmodified α- and β- globins. Mass shifts from the oxidative modifications are indicated.

Chemically oxidized commercial human Hb showed a spectrum (Figure 2.4c) similar to human Hb without reaction with H_2O_2 (Figure 2.4a), indicating that this further oxidation does not cause significant changes to the mass spectra of commercial human Hb.

The effects of oxidation and lyophilization on the spectra of fresh human Hb folded in solution were then investigated. Figure 2.7 shows mass spectra of fresh human Hb before and after oxidation, lyophilization, and both lyophilization and oxidation, recorded with the TOF system. Also shown is the spectrum of commercial Hb recorded with the same instrument. The proteins were in 10% MeOH/90% H_2O to avoid destabilizing the hemoglobins which can lead to the formation of heme-deficient dimers (such as with ACN, Figure 2.3b). The insets show the regions of the spectra near the peaks of the +11 dimer ions. Comparison of Figure 2.7a and 2.7b shows that oxidation of human Hb increases the intensities of the dimer $\alpha^h\beta^h$ (+11,+12) and monomer α^h (+7,+8) peaks, and causes the appearance of heme-deficient dimer ions with masses 32 Da higher than expected in the mass spectrum. Comparison of Figure 2.7a and 2.7c shows that lyophilization also increases the intensities of monomers and dimers, but does not in itself lead to formation of a heme-deficient dimer. Comparison of Figure 2.7a and 2.7d shows that lyophilization of the protein, followed by oxidation causes the appearance of an oxidized heme-deficient dimer. This provides direct evidence that oxidation, not lyophilization, leads to the appearance of the heme-deficient dimer ions. Lyophilization, however, seems to produce some subtle changes to the protein that increase the relative intensities of monomer and dimer ions, but are not readily detected by mass spectrometry. Finally, comparison of Figure 2.7e to Figures 2.7a-d shows that the commercial protein has the highest levels of dimers, monomers and heme-deficient dimers.
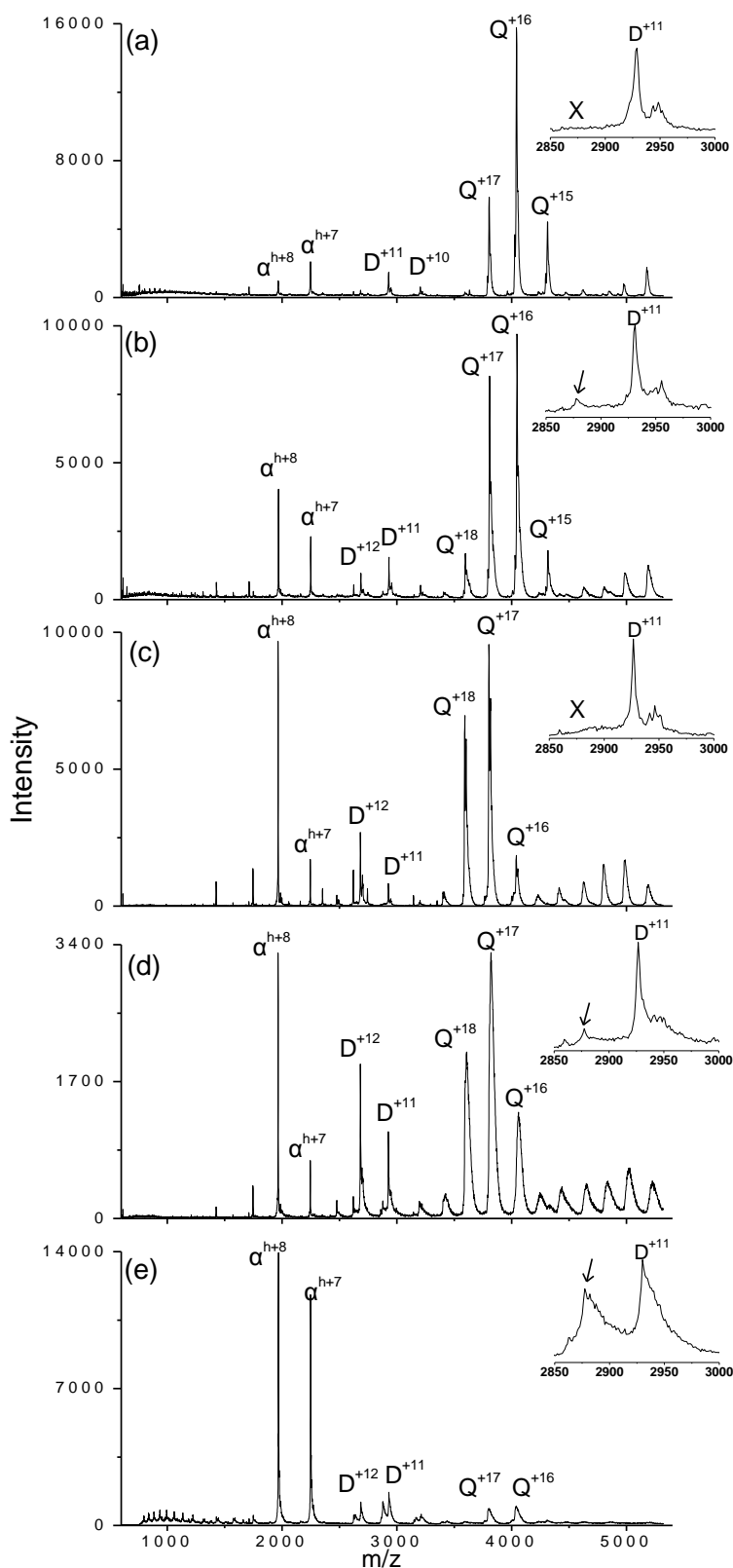
Figure 2.7. Mass spectra of (a) fresh human Hb, (b) oxidized fresh human Hb, (c) lyophilized fresh human Hb, (d) fresh human Hb oxidized after lyophilization, and (e) commercial human Hb. The insets show peaks from the +11 dimer ions in detail. Spectra (b), (d), and (e) show heme-deficient dimer ions (indicated with the arrow) with a 32 Da mass shift, while (a) and (e) do not show these peaks. Solutions were 20 μM Hb in 10% MeOH and 10 mM NH$_4$Ac. Notation is the same as in Figure 2.3.

2.3.2 Collision Cross Sections

Collision cross sections provide information on the overall "size" of ions in the gas phase. Table 2.2 lists cross sections of monomer (α^h, +7, +8), dimer ($\alpha^h\beta^h$, +11, +12) and tetramer (($\alpha^h\beta^h$)$_2$, +16, +17) ions formed from fresh human Hb, commercial human Hb, commercial bovine Hb and human Hb further oxidized with H_2O_2. Also shown are cross sections measured by Douglas and Wright [83] and Faull et al. [7]. In all cases studied here, cross sections of gas-phase dimer ions are intermediate between cross sections of monomer and tetramer ions. More dissociation of tetramers is observed when changing the solvent composition from 10% MeOH to 10% ACN, but collision cross sections are the same with gas-phase tetramer ions formed from these two solutions.

To compare with sizes of the same species of human Hb in solution, the radius of gyration, r_g, measured by small angle X-ray scattering [168, 169], and the Stokes radius, r_s, measured by size exclusion chromatography [170-172], are used [83]. Areas $A_s = \pi r_s^2$ and $A_g = \left(\frac{5}{3}\right)\pi r_g^2$ [169], calculated from r_s and r_g, are shown in Figure 2.8. Average cross sections of monomer ions are similar (within 10%) to A_s. Average cross sections of dimer ions fall between A_g and A_s. Average cross sections of tetramers are similar to A_g (within 5 %), and are only 1.2 times larger than A_s. Thus gas-phase monomer, dimer, and tetramer ions from fresh Hb and commercial Hb have compact structures, similar to the folded native conformations in solution.

Table 2.2. Collision cross sections of Hb ions ($\mathring{A}^2$).

Species	Charges	Douglas and Wright commercial bovine Hb [83]	Faull et al. commercial human Hb[a] [7]	Fresh human Hb	Commercial human Hb	Commercial bovine Hb	Oxidized commercial human Hb
α^h	+7	1339±76	1420	1310±10	1258±14	1415±30	1317±17
	+8	1530±127	1525	1420±34	1339±38	1510±42	1367±10
$\alpha^h\beta^h$	+11	1225±101	2355	2402±100	2232±36	2498±86	2137±113
	+12	1225±191	2484	2420±44	2421±100	2548±54	
$(\alpha^h\beta^h)_2$	+16	2826±292	3460	3672±13	3414±34	4113±143	3476±88
	+17	2763±330	3649	3672±98	3445±123	3854±72	

[a]at pH 9.5 in buffered ammonium acetate.
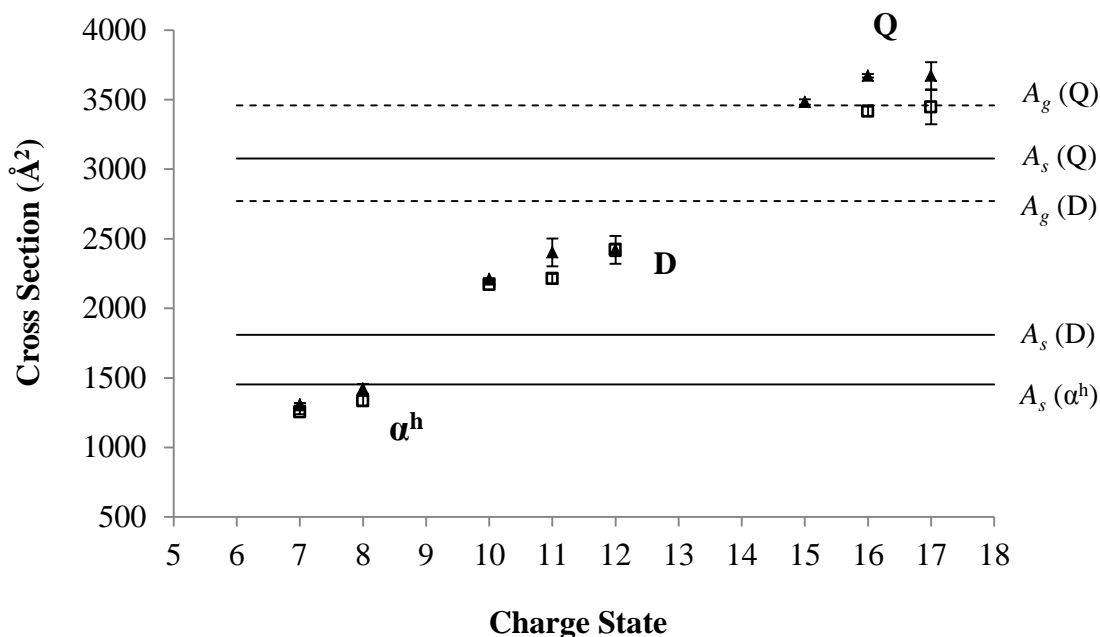
Figure 2.8. Collision cross sections as a function of charge state for fresh human Hb (filled triangles) and commercial human Hb (open squares). Notation is the same as in Figure 2.3. Solid lines show cross sections, A_s, of tetramer, dimer and monomer ions calculated from the Stokes radii. Dashed lines show cross sections, A_g, of dimer and tetramer ions calculated from the radii of gyration.

Collision cross sections of human Hb ions have been reported by Faull et al. [7] and Scarff et al. [61]. With fresh human Hb, our cross sections for monomers, dimers and tetramers generally agree with those of Faull et al. within 8% or better. Both Faull et al. and Scarff et al. found that dimer cross sections are intermediate between monomer and tetramer cross sections. The cross sections estimated by Scarff et al. from travelling wave ion mobility measurements, are somewhat larger than those reported here and by Faull et

al. with linear drift tube ion mobility (35% larger for monomers, 20% for dimers, and 17% for tetramers). The difference may be due to the calibration procedure used by Scarff et al. in which only relative cross sections are estimated. With commercial human Hb, our monomer ion cross sections are within 6% of the cross sections of commercial bovine Hb reported by Wright and Douglas [83] (Table 2.2). The major difference is with the dimer ions; cross sections of dimer ions measured here are consistently greater than cross sections of monomer ions. We also find cross sections of tetramer ions about 25% larger than reported by Wright and Douglas. Variations in sequences of Hb from diverse species [173], may give different cross sections. Tetramer ions from Hb S, with the point mutation E6V[β], have slightly larger (6%) cross sections than those of Hb A [61] (see also chapter 3). For comparison, we also re-measured cross sections of ions from commercial bovine Hb (Table 2.2). Slightly larger cross sections were observed for bovine Hb (ca. 12% for monomers, 8% for dimers, and 16% for tetramer ions) than Hb A. These small differences may be attributed to sequence differences. Bovine and human Hb share 88% sequence homology in the α chain and 83% in the β chain. However the differences in the sequences do not substantially change the cross sections of these protein ions and do not make dimer ions more compact than monomer ions.

The larger cross sections of tetramer ions measured here, in comparison to cross sections reported by Wright and Douglas [83], may be the result of the different degree of solvation or adduct formation of the tetramer ions. When ions pass through the orifice-skimmer region ($\Delta V_{os} = 100$ V), ion activation mainly causes desolvation and removal of adducts from ions. Following this, internal energy added to the ions can cause the ions to unfold. Thus highly desolvated ions, or ions with fewer adducts, tend to have greater

cross sections. In our experiments, when the flow rate of the nitrogen curtain gas was approximate 2 L/min, tetramer ions from fresh and commercial Hb were found to be relatively highly desolvated or have fewer adducts. The peak widths (FWHM) of +16, +17 ions were ~15 Th and mass shifts, if attributed to solvation, corresponded to only ~ 4 water molecules (Q1 scan), much less than seen in the study of Wright and Douglas (FWHM ≈ 50 Th; if attributed to solvation, ca. 17 attached water molecules). Monomer and dimer ions do not show solvation and so this effect only applies to the tetramer ions. The lower degree of solvation here may be a result of the changes to the ion sampling interface.

Because some commercial Hb has been found to be oxidized, the effect of further oxidation on cross sections was investigated. Table 2.2 shows cross sections of human Hb that was chemically oxidized. Only cross sections of ions with the highest intensity (+7, +8 α^h, +11 $\alpha^h\beta^h$, and +16 $(\alpha^h\beta^h)_2$) are shown. Oxidized human Hb and fresh human Hb produce ions with nearly the same cross sections, within the combined uncertainties. Thus the unusual dimer ion cross sections of Wright and Douglas cannot be attributed to oxidation of the protein.

2.4 Summary

With the same solution and mass spectrometer conditions, fresh human Hb, oxidized fresh human Hb, lyophilized fresh human Hb, lyophilized and oxidized fresh human Hb and commercial human Hb all give somewhat different mass spectra. More dimer and monomer ions are seen with oxidized fresh human Hb, lyophilized fresh human Hb,

lyophilized and oxidized fresh human Hb and the commercial Hb used here. All commercial Hb samples showed similar spectra, independent of protein sequence or oxidation. The different spectra with fresh and commercial Hb are partially due to oxidation and freeze drying of the commercial proteins, but may also be due to some other subtle change to the commercial proteins.

Fresh and commercial human Hb give cross sections of dimer ions intermediate between tetramer and holo-alpha ions, and cross sections similar to the same species in solution. Commercial bovine Hb had cross sections 10% to 20% larger than commercial human Hb, possibly a result of the differences in the sequences. Further oxidation of commercial lyophilized Hb does not have a substantial effect on cross sections as long as the protein remains folded. Both human and bovine Hb give dimer ions with cross sections greater than monomer ions. We have not been able to reproduce the unusual result of Wright and Douglas, even with protein samples from the same bottle. Neither the sequence difference between bovine Hb and human Hb nor additional oxidation of Hb gives dimer ions with cross sections less than those of monomer ions. To some extent, the use of commercial Hb is an uncontrolled experiment because the history of the sample is unknown and may vary from sample to sample. As we show here, lyophilization of the proteins produces changes to the mass spectra. Thus there may be some other subtle change to the protein that accounts for the unusual result of Wright and Douglas.

Chapter 3 Gas-Phase Ions of Human Hemoglobin A, F, and S

3.1 Introduction

Electrospray ionization mass spectrometry (ESI MS) has been widely employed to study Hb A and its variants, from peptide sequencing, to the analysis of higher-order assemblies, and interactions with other large molecules [133, 134]. In the analysis of primary structure, Hb variants can be identified with direct mass analysis of globin chains [174], measurements of tryptic peptide masses [175], or tandem mass spectrometry of Hb chains or peptides [176, 177].

Hemoglobin is also of interest as a model protein−protein complex. Studies of the structure of Hb tetramers or subunits with ESI MS provide information on the physical properties of Hb ions in the gas phase. Collision cross sections and hydrogen/deuterium exchange (H/Dx) levels provide insights into the conformations of ions. Recently, studies of Hb cross sections have come from measurements of migration time with ion mobility mass spectrometry (IM MS). Using traveling-wave IM MS, Scarff et al. have shown that gas-phase tetramer ions of Hb S +15 to +18 have greater cross sections than those of Hb A. The ratio of Hb S cross section to Hb A cross section increased with the charge on the ion from ca. 1.02 for +15 ions to 1.07 for +18 ions [61]. An alternative approach to determining cross sections is to measure ion axial kinetic energy losses with a triple quadrupole mass spectrometer [83, 178]. In chapter 2, we showed that oxidation of methionine and cysteine residues on the β chain, and lyophilization of Hb, change the appearance of Hb mass spectra but do not influence the cross sections of gas-phase Hb ions [178]. Hydrogen/deuterium exchange combined with MS is another strategy in structure analysis. With Hb A, H/Dx has been done in solution prior to injection of Hb into an ESI source [93] or directly in the gas-phase with trapped ions exposed to D_2O

61

vapor [83].

In MS/MS, ions of large noncovalently bound complexes such as Hb dissociate into smaller constituents. The gas-phase binding strength and stability of ions from different Hb variants can be examined and compared. With Hb, the binding strength is related to the noncovalent interactions at the $\alpha_1\beta_2$ ($\alpha_1\gamma_2$) or $\alpha_2\beta_1$ ($\alpha_2\gamma_1$) interfaces between the dimer pairs and the $\alpha_1\beta_1$ ($\alpha_1\gamma_1$) or $\alpha_2\beta_2$ ($\alpha_2\gamma_2$) interfaces between the two individual α- and β (γ)-subunits [125]. In MS, the noncovalent binding at interfaces of human Hb has be broken in a controlled way, either during the ion-sampling process without precursor ion mass selection [62] or in a collision cell after mass selection of a precursor ion [107]. With non-selective fragmentation, Apostol showed that the stability of intact tetramer ions can be affected by single mutations in the beta-globins [62], indicating that a small change in sequence may greatly influence the stability of the entire protein complex in the gas phase.

In work described in this chapter, we have measured collision cross sections, H/Dx levels and MS/MS spectra of gas-phase ions of Hb S and Hb F, and have compared these to the same properties of Hb A. The molecular weights of species of Hb A, S and F are listed in Table 3.1. Physiologically inactive ^{met}Hb was used since it is more stable than ^{oxy}Hb [179]. The proteins were freshly prepared from blood rather than purchased commercially, to allow more reproducible results, as discussed in chapter 2 [178]. We show that although Hb A, S and F give similar mass spectra, the gas-phase ions of the different hemoglobins can have different properties. Tetramer ions of Hb S have greater cross sections and greater H/Dx levels than tetramer ions of Hb A and Hb F. In MS/MS, dimer ions of Hb F dissociate to two monomers with a nearly equal division of the

charges of the precursor ions, while Hb A and Hb S dissociate with asymmetrical charge distributions. Gas-phase tetramers of Hb F are more stable than tetramers of the other two proteins. The order of the binding strengths of the gas-phase dimer ions is: Hb S > Hb A > Hb F. The results with Hb S show that a single mutation in a protein can significantly change the properties of a gas-phase protein complex.

Table 3.1. Molecular weights of human Hb species (Da).

Species[a]	α^a	α^h	β^a or γ^a	β^h or γ^h	$\alpha^h\beta^h$ or $\alpha^h\gamma^h$	$(\alpha^h\beta^h)_2$ or $(\alpha^h\gamma^h)_2$
Hb A	15126	15743	15867	16484	32227	64453
Hb F[b]	15126	15743	15995	16612	32354	64709
Hb S	15126	15743	15837	16454	32196	64392

[a] α^a, apo-alpha, heme-free state; α^h, holo-alpha, heme-bound state

[b] Calculated with γ^G

3.2 Experimental Methods

3.2.1 LIT-TOF System and Gas-Phase H/Dx

Hydrogen/deuterium exchange experiments were performed with a home-made linear quadrupole ion trap reflectron time-of-flight mass spectrometer system (LIT-TOF), as described previously [46, 47, 83, 100, 153] and shown in Figure 3.1. Protonated ions generated by pneumatically assisted ESI (5 kV), pass through an aperture (5 mm diameter)

in a curtain plate (1000 V), a dry nitrogen curtain gas (~ 2 L/min), an orifice (0.25 mm diameter, 220 V), a skimmer (0.75 mm aperture diameter, 20 V) and enter a chamber with two consecutive radio frequency only quadrupoles, a short ion guide, Q0 (5 cm, DC offset = 15 V), and a linear ion trap, Q1 (20 cm, DC offset = 10 V). Ions are trapped in Q1 for gas-phase reaction, e.g. H/Dx. After trapping, ions pass through a stack of four equally spaced focusing lenses (L1- L4) and enter the source region of a reflectron-TOF for mass analysis. In the TOF chamber, ions are extracted into the flight tube with a series of acceleration pulses and detected by a dual microchannel plate (MCP) [83]. The vacuum of this apparatus is maintained by a three-stage differential pumping system, including a rotary pump for the interface region and two turbo molecular pumps for the LIT (~3-10 mTorr) and TOF (~1 $\times 10^{-6}$ Torr) chambers respectively. A solution of cesium iodide (CsI) was used for mass calibration.

For control experiments, the LIT chamber pressure, measured with a precision capacitance manometer (model 120AA; MKS Instruments, Boulder, CO, USA), was kept at 10 mTorr of N_2 by partially closing a gate valve between the chamber and the turbo pump. For exchange experiments, the chamber contained 5 mTorr N_2 and 5 mTorr D_2O vapor, set with a needle valve (SS-SS4-Al; Swagelok, Solon, OH, USA), to keep the total pressure 10 mTorr. For H/Dx, ions are trapped in Q1, and confined axially by timed DC stopping potentials on the entrance lens (Q0/Q1, 4.0 mm aperture covered with a 90% transmitting 50 mesh grid) and exit lens (L1, 0.7 mm aperture). Typical trapping conditions: 50 ms injection (Q0/Q1= −5 V, L1= 60 V), 0-10,000 ms trap (Q0/Q1= 40 V, L1= 60 V), 20 ms detection (Q0/Q1 = 40 V, L1= −15 V), and 50 ms drain (Q0/Q1= −5 V, L1= −15 V).
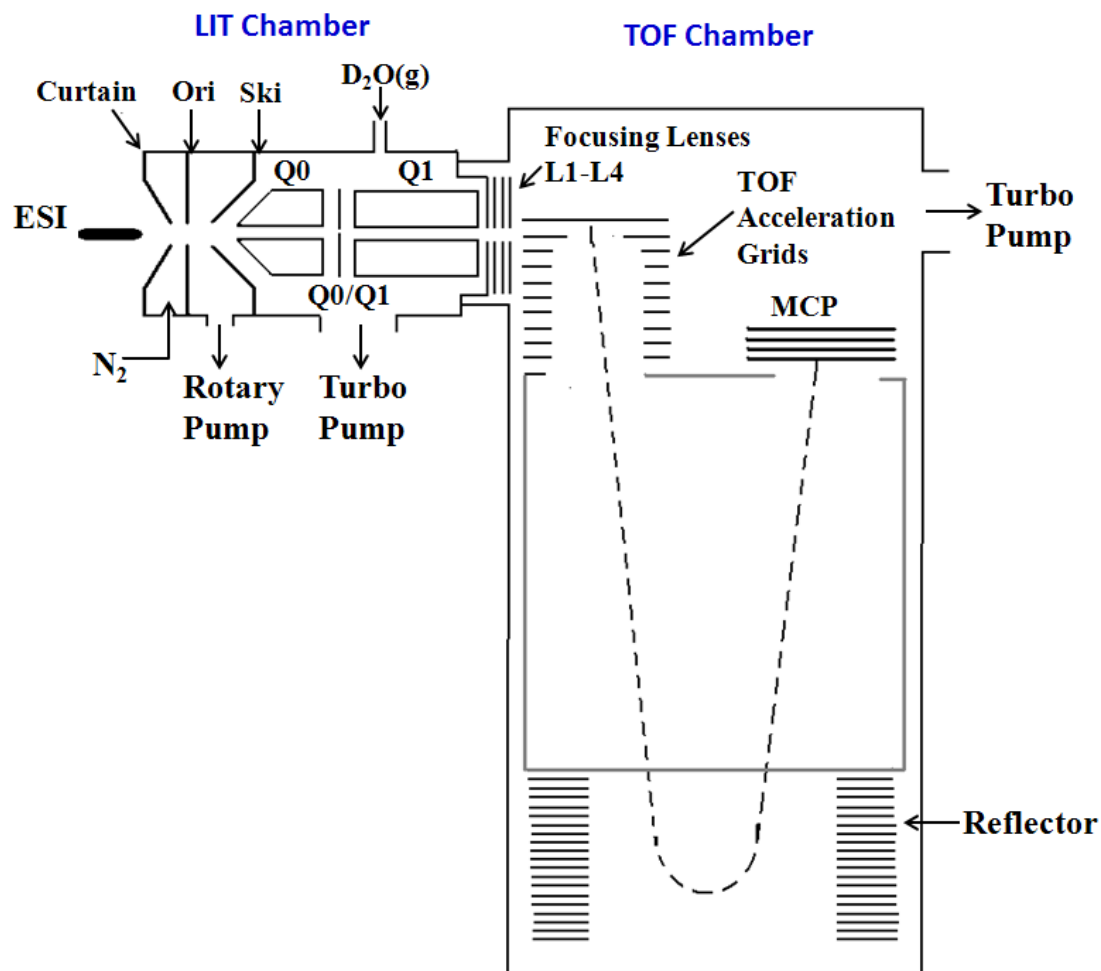
Figure 3.1. Schematic of the LIT-TOF MS system. Notation: Ori, orifice; ski, skimmer; MCP, microchannel plate.

3.2.2 Triple Quadrupole Mass Spectrometer System

For cross section measurements and MS/MS experiments, a home-built ESI triple quadrupole mass spectrometer described previously [78, 80, 178], but modified to increase sensitivity was used [178]. Positive protein ions, formed by pneumatically

assisted ESI (4 kV), pass through a 2.4 mm diameter aperture in a curtain plate (1150 V),

a dry nitrogen curtain gas (~ 2 L/min), and an ion sampling orifice (230 V) into a region

with ca. 0.7 Torr background gas. Ions then pass through a skimmer (130 V), and enter a

quadrupole ion guide Q0 (~ 9 mTorr, DC offset = 120 V), where ions are cooled to

translational energies and energy spreads of about 1-2 eV per charge [152]. After passing

through a short radio frequency quadrupole (DC offset = 108 V), ions enter a quadrupole,

Q1, a collision cell with a quadrupole ion guide, Q2, and a quadrupole, Q3, and are then

detected with pulse counting. For cross section measurements, the Q2 rod offset was

fixed at 105 V and the Q3 rod offset was increased systematically to give ion stopping

curves. For MS/MS experiments, both the Q2 and Q3 rod offsets were varied. In all

experiments the collision gas was argon (Ar).

3.2.3 Collision Cross Sections

Cross sections were measured with axial kinetic energy loss experiments, as described

previously [78, 80, 153] (see chapter 1 and 2). In Q2, ions lose kinetic energy through

multiple collisions with low-density Ar. The energy losses are related to the collision

cross sections with an aerodynamic drag model [81] through equation (1.4)

$$\frac{E}{E^0} = \exp\left(-\frac{C_{Dd}nm_2l\sigma}{m_1}\right)$$

(1.4)

where E is the ion kinetic energy at the exit of Q2, E^0 is the ion kinetic energy at the

entrance to Q2, C_{Dd} is a drag coefficient for diffuse scattering [78], n is the collision gas

number density, m_1 is the mass of the protein ion, m_2 is the mass of the collision gas (Ar),

l is the length of the collision cell (20.6 cm) and σ is the collision cross section. The

pressure of Ar in Q2 was varied between 0.0 and 1.2 mTorr and stopping curves were

obtained at different pressures. Cross sections were then calculated by plotting $-\ln\dfrac{E}{E^0}$

versus $\dfrac{C_{Dd}nm_2l}{m_1}$.

3.2.4 MS/MS of Gas-Phase Ions

In MS/MS experiments, a precursor ion is mass selected in Q1, and then injected into Q2

where multiple collisions with Ar cause dissociation. Fragment ions are then mass

analyzed in Q3. The Q0-Q2 rod offset difference ($\Delta V_{\text{Q0-Q2}}$) and ion charge determine the

initial kinetic energy of an ion, E^0, at the cell entrance. The total internal energy added to

ions in the collision cell, ΔE_{int}, can be calculated with a collision model that considers the

different numbers of collisions of ions with different cross sections, and the losses of

kinetic energies of ions as they pass through the cell [79, 105] by equation (1.11) (see

chapter 1),

$$\Delta E_{\text{int}} \;=\; \Phi\,\frac{m_2}{M}\,E^0\,\frac{m_1}{m_2}\,\frac{1}{C_{Dd}}\left[1-\exp\left(-\frac{C_{Dd}nm_2\sigma l}{m_1}\right)\right] \tag{1.11}$$

where Φ is the average fraction of center-of-mass kinetic energy transferred to internal

energy in a collision (taken to be 1.0) [79], and $M = m_1 + m_2$. During experiments $\Delta V_{\text{Q0-Q2}}$

was systematically increased and the initial energy, E^0, was calculated from the $\Delta V_{\text{Q0-Q2}}$

that gave 50% precursor ion loss. The corresponding $\Delta V_{\text{Q0-Q2}}$ is called the "dissociation

voltage". The pressure of Ar in Q2 was 1.5 mTorr for dissociation of monomers, 2.0 mTorr for dimers and 3.0 mTorr for tetramers. In all experiments the pressures in Q2 were measured with a precision capacitance manometer (model 120AA; MKS Instruments, Boulder, CO, USA).

3.2.4 Protein Purification

Approximately 3 ml of fresh human sickle blood (Hb S, 80%) and 3 ml of cord blood (Hb F, 80%) were provided by BC Children's Hospital, and immediately extracted following standard procedures [154], as described in detail in chapter 2 [178]. After dialysis of ~1 ml of purified hemolysate, the concentration of ^{oxy}Hb (as tetramer) was determined to be 1.0 mM of Hb S and 1.8 mM of Hb F, with a UV-Vis spectrometer (Nanodrop 1000; Thermal Scientific, Wilmington, DE, USA) and the standard pyridine hemochromogen method [155, 156]. The ^{oxy}Hb was then oxidized to ^{met}Hb with a 1.5-fold stoichiometric excess of potassium ferricyanide ($K_3Fe(CN)_6$) for 5 min at 20 °C [157]. To minimize salt content for electrospray ionization the Hb was further desalted on a 3×25 cm G-25 Sephadex column (GE Healthcare, Buckinghamshire, UK) to remove excess $K_3Fe(CN)_6$. The ^{met}Hb solution was then frozen with liquid nitrogen and stored at -80 °C. Before MS analysis, the solution was quickly thawed. Fresh Hb A was prepared as described in chapter 2 [178] and oxidized to ^{met}Hb prior to MS analysis.

3.2.5 Solutions and Reagents

For MS of native or near-native proteins, the Hb solutions were diluted to 20 μM or 10 μM with 10% methanol (MeOH) or 10% acetonitrile (ACN) in 10 mM ammonium acetate (NH_4Ac) at pH 6.8 (measured with a Accumet model 15 pH meter (Fisher Scientific, Fairlawn, NJ)). For MS of denatured Hb to measure monomer masses, proteins were prepared in 50/50 (v/v) MeOH/ H_2O with 0.5% acetic acid. Samples were infused into the ESI sources with a syringe pump (Harvard Apparatus, St. Laurent, QC, Canada) at 1 μL/min.

Acetic acid (99.99%), pyridine (99.9%), CsI (99%) and $K_3Fe(CN)_6$ (ACS grade) were from Sigma-Aldrich, St. Louis, MO, USA. Methanol (HPLC grade), ACN (HPLC grade), and NH_4Ac (ACS grade) were from Fisher Scientific, Fairlawn, NJ, USA. Nitrogen and argon (manufacturer's stated purity 99.999%), and air (breathing grade) were from Praxair, Mississauga, ON, Canada.

3.3 Results and Discussion

3.3.1 Mass Spectra of Hemoglobins

With the same operating and solution conditions (10% MeOH, 10 mM NH_4Ac), 20 μM Hb F and Hb S gave similar mass spectra with the triple quadrupole system, as shown in Figure 3.2a and 3.2b. Protein tetramers with charge +16 dominate the mass spectra with
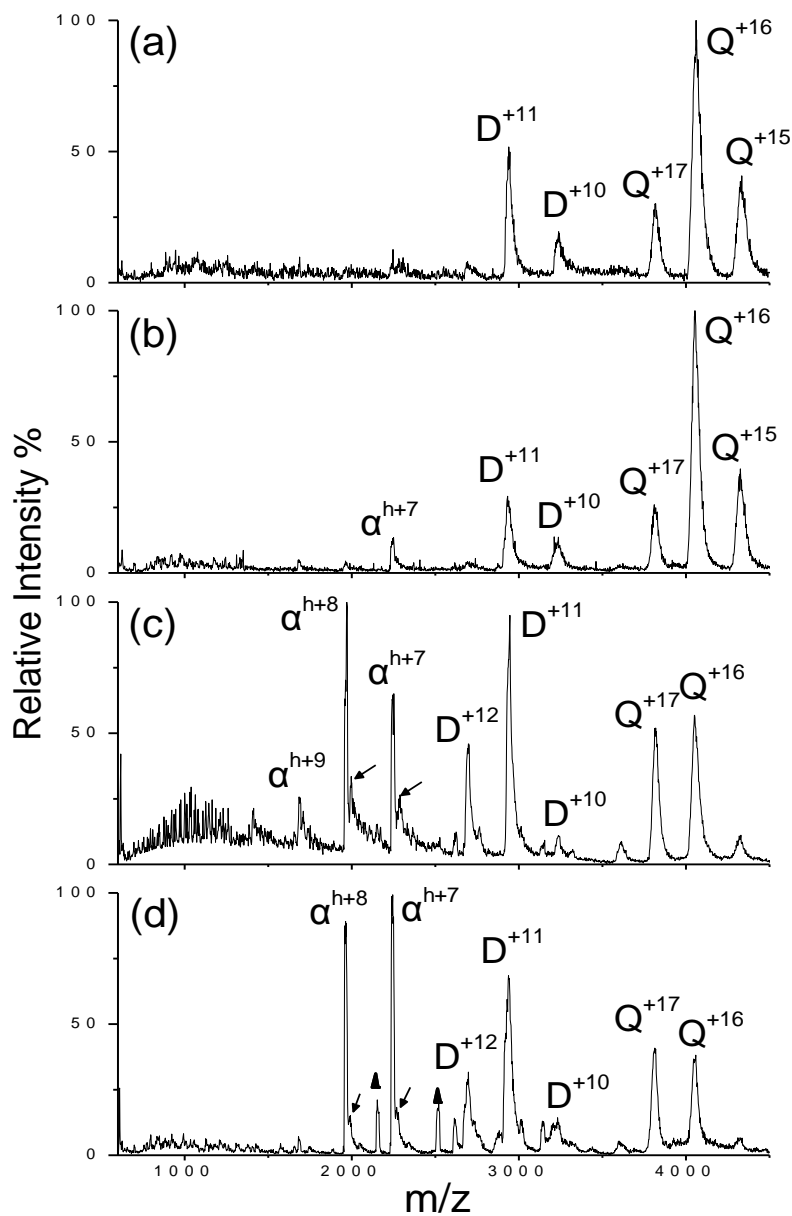
Figure 3.2. ESI mass spectra of (a), Hb F, 20 μM with 10% MeOH; (b), Hb S, 20 μM with 10% MeOH; (c), Hb F, 10 μM with 10% ACN; and (d), Hb S, 10 μM with 10% ACN. Notation: D, dimers; Q, tetramers. Holo-alpha ions, α^h, are labeled; apo-alpha ions, α^a, are marked with filled triangles. Black arrows indicate low-intensity γ^a or β^a ions.

lower intensities of +15, +17 tetramer ions and +10, +11 dimer ions. With 10% MeOH

solutions nearly no monomer ions are seen with Hb F, and only low-abundance α^{h+7} ions

are observed with Hb S. The β and γ chains are not seen due to the low abundance of

monomers and the lower sensitivity of these chains in ESI (see below). As well, oxidation

of methionine and cysteine residues in the β chains of Hb A, which is sometimes found

with commercial proteins, leads to the formation of heme-deficient dimer ions in mass

spectra [20, 178]. We do not observe heme-deficient dimers, which is consistent with

previous studies of fresh Hb S [61] and Hb F [180]. Furthermore, measurements of the

masses of the apo-monomer ions from denaturing solutions with our TOF system do not

show alpha or beta monomers with mass shifts of +16 or +32. Thus we conclude that our

fresh proteins do not contain oxidative modifications. Lowering the Hb concentration to

10 μM and changing the solvent to 10% ACN, which slightly destabilizes the protein,

increases the levels of monomer ions (apo- and holo-) and dimer ions (Figure 3.2c and

3.2d), as in our previous study described in chapter 2 [178], making measurement of the

properties of monomer and dimer ions possible. In this case the variant β chains of Hb S

and the γ chains of Hb F can be seen but with much lower intensity than the α chains,

similar to Hb A [20, 83, 90].

In aqueous solution, usually liganded hemoglobins, ^{CO}Hb or ^{oxy}Hb, have been

used to measure the dissociation equilibrium constant of the tetramer, K_d [125]. For the

tetramer-dimer equilibrium at neutral pH, K_d of ^{CO}Hb S is reported to be 0.196 μM [181],

or 0.4 μM [182]. With these K_d, ca. 5% and 7% of the tetramers initially at 20 μM

dissociate to dimers respectively. The K_d for dissociation of ^{CO}Hb F is reported to be 0.66

μM (100 mM tris-HCl, 0.1 M NaCl, 5 mM EDTA at pH 7.4) [132] and 0.01 μM (150

mM tris-Ac buffer at pH 7.5) [131], which cause ca. 9% and 1% tetramer dissociation respectively. The 66× difference in K_d of Hb F between these two studies was not explained.

The estimated K_d for dissociation of dimers to monomers in solution of ^{CO}Hb F is much smaller (1.63×10^{-13} M) [128]. As expected from the small dissociation constant, we find low levels of monomer ions in mass spectra. However we generally find higher levels of dimer ions in mass spectra than calculated from the solution K_d values. Solution conditions, including buffers and organic solvents, as discussed above, have an effect on the degree of dissociation in solution. As well, mass spectra strongly depend on MS system operating conditions [20, 83, 178], making it difficult to compare ion abundances in mass spectra directly with calculated levels of species in solution.

3.3.2 Collision Cross Sections

Table 3.2 lists cross sections of holo-monomer (α^h, +7,+8), dimer (+11, +12) and tetramer (+16, +17) ions formed from fresh human Hb F and Hb S, and compares these with our previous results with Hb A (see chapter 2) [178]. Generally cross sections of dimer ions are intermediate between cross sections of monomer and tetramer ions (Figure 3.3) and as found in solution (see below). Monomers of Hb F and Hb S have similar cross sections, roughly 10% larger than Hb A. For dimers, the order of the cross sections is Hb S > Hb F > Hb A. Dimers of Hb S have cross sections 11% larger than dimers of Hb A, and 6% larger than dimers of Hb F. Cross sections of Hb S tetramer ions are ca. 13% greater than cross sections of Hb F and Hb A tetramer ions, which have the same cross sections within

Table 3.2. Collision cross section (Å^2) of variant Hb ions[a].

Species	Charge	Hb F	Hb S	Hb A
α^h	+7	1478±34	1510±38	1310±10
	+8	1531±18	1546±65	1420±34
Dimer	+11	2504±46	2664±87	2402±100
	+12	2580±70	2686±100	2420±44
Tetramer	+16	3512±24	4044±92	3672±13
	+17	3774±21	4220±83	3672±98

[a]Uncertainties are the standard deviations of three measurements.

Figure 3.3. Collision cross sections as a function of charge state for Hb A (triangles), Hb F (open circles), and Hb S (diamonds). Notation as in Figure 3.2.

the combined uncertainties. The single localized mutation βGlu6Val in Hb S evidently changes the conformation of monomer, dimer and tetramer ions in the gas phase. Previously, Scarff et al., using IM MS, showed collision cross sections of gas-phase Hb S tetramer ions (+15 to +18) are ca. 4% larger (averaged over charge states) than Hb A tetramer ions [61]. The cross sections of Hb S and Hb A measured by Scarff et al. are ca. 7% and 17% greater than ours, respectively. Collision cross sections of the monomer and dimer ions of Hb S and Hb F have not been reported previously.

One issue involved in studies of gas-phase conformations of proteins is how they compare with the native conformations in solution. The Stokes radius (r_s), measured by size exclusion chromatography, and radius of gyration (r_g), measured by small angle x-ray or multi-angle light scattering, can be used to estimate "sizes" of proteins in solution. The Stokes radius of a protein correlates with the molecular weight [170]. The Hb A dimer has r_s (24 Å) [171], intermediate between that of the tetramer (31.3 Å) [172] and holo-monomer (21.5 Å) [170]. Because Hb A, F and S tetramers have nearly the same molecular weight (within 0.5%) (Table 3.1), they might be expected to show similar r_s values. With light scattering, the r_g values of ^{CO}Hb in 50 mM sodium phosphate buffer were determined to be 29 Å for Hb A and Hb S, and 30 Å for Hb F [22]. Calculated "cross sections", $A_g = \left(\frac{5}{3}\right)\pi r_g^2$ [169], are 4403 Å^2 and 4712 Å^2, respectively. Thus in these solution measurements Hb S does not show larger "cross sections" than the other two proteins. However Scarff et al. [61] have estimated cross sections of Hb S and Hb A from the crystal structures and found that the Hb S tetramers have cross sections ca. 10% greater than Hb A tetramers, similar to the differences in cross sections seen here.

3.3.3 Gas-Phase H/D Exchange

Table 3.3 lists the numbers of hydrogens exchanged, the number of exchangeable hydrogens calculated from the sequences, and the percent of the exchangeable hydrogens exchanged, of monomer (α^h, +7, +8), dimer (+11, +12) and tetramer (+16, +17) ions from fresh Hb A, S and F. The β and γ ions show H/Dx levels similar to the α ions. In theory, increasing charge can give an increasing degree of structural perturbation [78, 80, 96, 97, 99, 150] and thus a different H/Dx level. For the ions studied, increasing the charge by one does not cause significant changes in the H/Dx levels, indicating that the conformations do not greatly change for ions differing by only one charge. This is consistent with our cross section results. The holo-monomer and dimer ions of variant hemoglobins show similar H/Dx levels within the combined uncertainties, although they have different cross sections. As noted, ions with different cross sections may not show different gas-phase H/D exchange levels [96, 97, 99]. With tetramer ions, Hb S shows a ca. 16% higher H/Dx level than Hb A and Hb F. Thus, in the gas-phase, Hb S tetramer ions have both larger cross sections and greater H/Dx levels.

The cross section measurements and the H/Dx measurements occur on different time scales. After ion formation, cross sections are measured in less than the ca. 2 ms required for ions to pass through the triple quadrupole system, while the H/D exchange requires up to 10^4 ms in the trap before ion detection. Monomers α^h from Hb F and Hb S show larger cross sections than monomers α^h from Hb A, but all α^h monomers show the same exchange levels within the combined uncertainties. It is conceivable that the monomers retain some memory of their conformation when formed, but lose this memory on the time scale of seconds [116, 117]. Cross sections show that Hb S tetramers are

Table 3.3. Numbers of hydrogens exchanged (H/Dx), numbers of exchangeable hydrogens (H/Dx^{max}) and percent of the hydrogens exchanged (%H/Dx) for variant Hb ions at ΔV_{os} = 200 V after 10 s exchange with 5.0 mTorr of D_2O.

Species	Charge	Hb F			Hb S			Hb A		
		H/Dx	H/Dx^{max}	%H/Dx	H/Dx	H/Dx^{max}	%H/Dx	H/Dx	H/Dx^{max}	%H/Dx
α^h	+7	75±2	233	32.2±0.8	83±5	233	35.6±2.1	79±5	233	33.9±2.1
	+8	79±5	234	33.8±2.1	86±3	234	36.7±1.3	80±5	234	34.2±2.1
Dimer	+11	149±2	484	30.8±0.4	147±4	472	31.1±0.8	146±13	472	30.9±2.7
	+12	149±6	485	30.7±1.2	148±5	473	31.3±1.0	146±10	473	30.9±2.1
Tetramer	+16	331±19	962	34.4±2.0	376±6	938	40.1±0.6	321±21	938	34.2±2.2
	+17	339±9	963	35.2±0.9	388±2	939	41.3±0.2	330±29	939	35.1±3.1

larger than Hb A and Hb F tetramers at times of a few milliseconds. The H/Dx

experiments show they retain different and perhaps more unfolded conformations than

Hb A and Hb F, for up to 10 s.

When comparing H/Dx levels among monomer, dimer and tetramer ions, relative

exchange levels, %H/Dx, are more informative. The order of the relative exchange levels

might be expected to be monomer > dimer > tetramer, because when monomers bind to

form dimers or tetramers some of the exchangeable amino acid residues are buried in the

interface. This has been observed in solution H/Dx with commercial bovine ^{met}Hb with an

exchange time of 53 ms [93] and with fresh human ^{met}Hb with an exchange time of 1 s or

less (see chapter 4). However in the gas phase, this trend is not seen (Figure 3.4). Dimer

ions show 31% hydrogens exchanged on average, slightly less than that of α^h and

tetramer ions. With Hb A and Hb F, the relative exchange levels of tetramer ions (ca.

34.7%) are similar to α^h ions (ca. 33.5%). With Hb S, tetramer ions show slightly higher

relative exchange levels than α^h ions (40.7% and 36.2% respectively). The difference is

not as large as gas-phase H/Dx results reported previously with commercial bovine ^{met}Hb

where 60% of hydrogens on tetramers and 40% on monomers were exchanged [83].

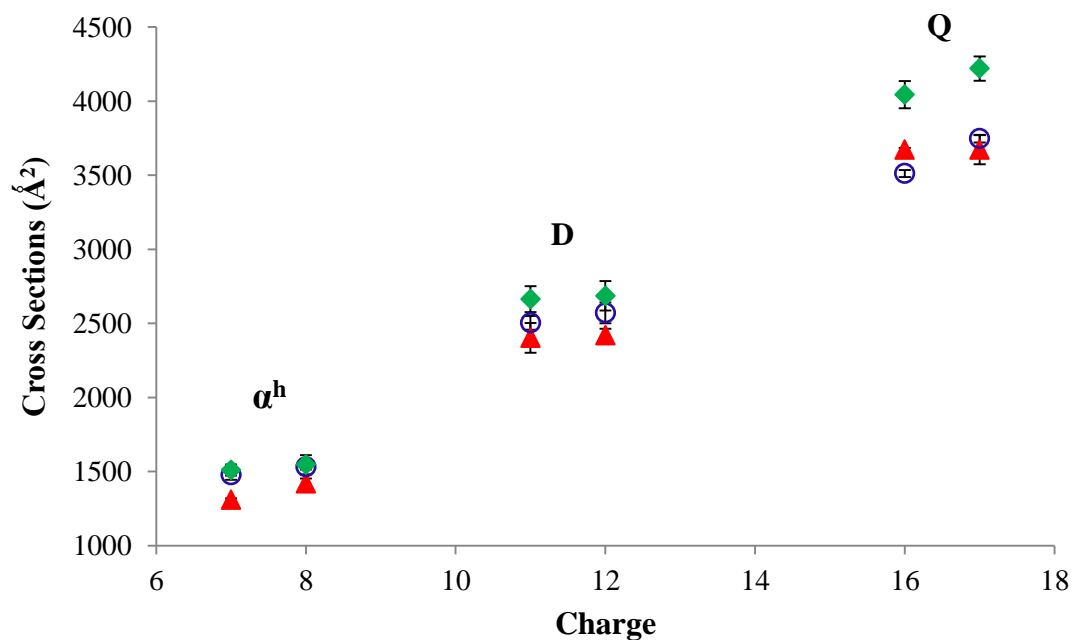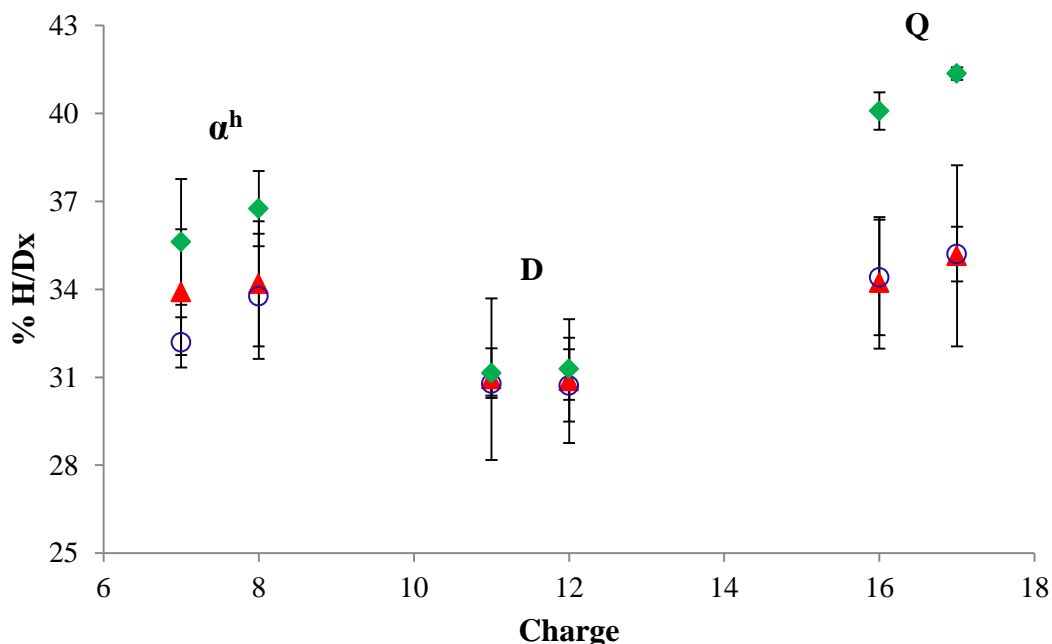**Figure 3.4.** Percent of hydrogens exchanged (% H/Dx) after 10 s trapping as a function of charge state for Hb A (triangles), Hb F (open circles), and Hb S (diamonds). Notation as in Figure 3.2.

3.3.4 MS/MS and Binding Strengths

Tandem mass spectrometry of monomer (α^h, +7, +8), dimer (+11, +12) and tetramer (+16, +17) ions from Hb A, F and S was used to determine relative binding strengths in the gas-phase ions. Holo-alpha ions dissociate to apo-alpha ions with the release of a charged heme (Figure 3.5), for example, $\alpha^{h+7} \rightarrow \alpha^{a+6} + h^+$. Less than 5% neutral heme loss was observed. This is expected because heme is overall singly charged in ^{met}Hb and neutral in ^{oxy}Hb. The results are consistent with previous MS/MS studies of myoglobin which has a globular structure similar to the Hb alpha monomer [84, 183].
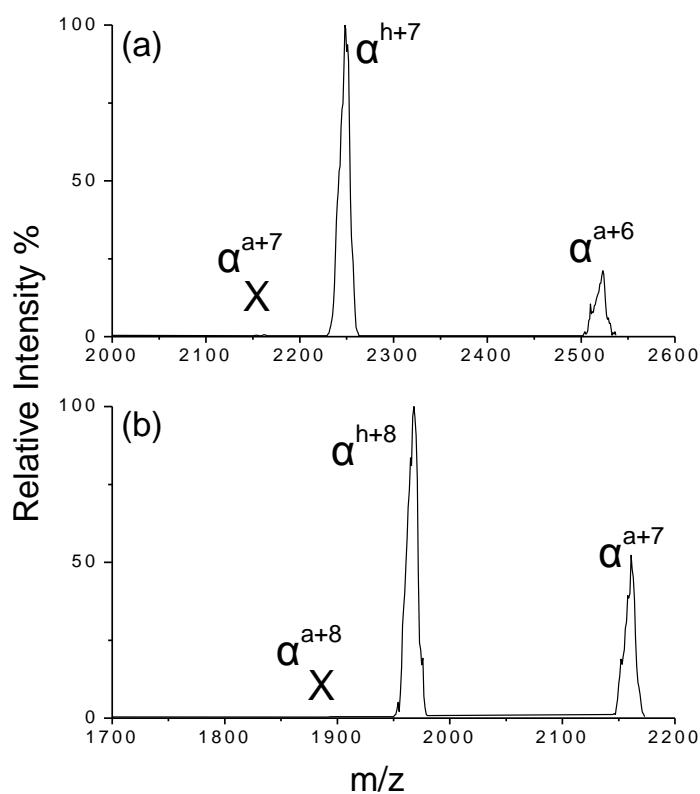
Figure 3.5. MS/MS spectra of (a) +7 and (b) +8 holo-alpha ions from Hb A, with a pressure in Q2 of 1.5 mTorr of Ar, and $\Delta V_{Q0\text{-}Q2}$ of 70 V and 60 V respectively. No +7 apo-alpha ions in (a) or +8 apo-alpha ions in (b) were observed (indicated with the "X").

Dimer ions dissociate into two monomers, as in solution. One clear difference between the hemoglobins is shown in the MS/MS spectra of Figure 3.6. Under conditions where nearly half of the +11 charged Hb A and Hb S dimer ions dissociate, +7 alpha ions and +4 beta ions, both holo- and apo-, are preferentially formed. With Hb F, two holo-monomers with charges +5 and +6 are the main product ions. This effect also is also seen with the +12 dimers; Hb F +12 ions mainly dissociate to two +6 holo-monomer ions,
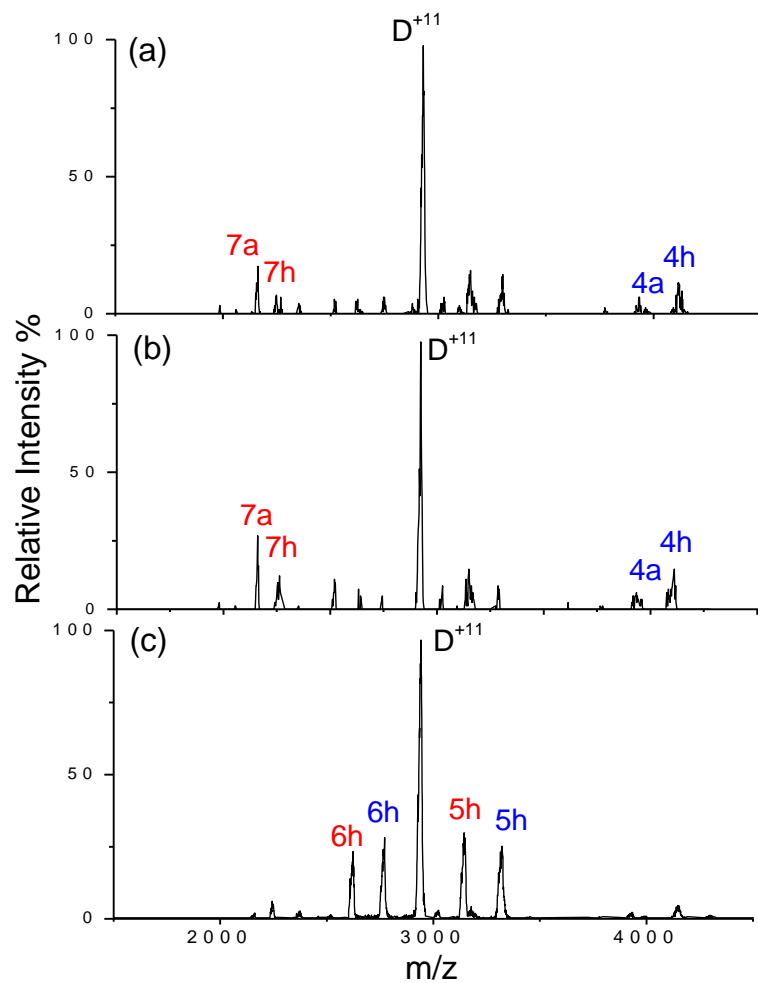
Figure 3.6. MS/MS spectra of +11 dimer ions from (a) Hb A, (b) Hb S, and (c) Hb F with a pressure in Q2 of 2 mTorr of Ar, and $\Delta V_{Q0\text{-}Q2}$ of 70 V for Hb A and S, of 65 V for Hb F, and with ca. 50% dissociation of precursors. Fragments, α ions (red) and β (or γ) ions (blue) are shown; a-apo, h-holo.

whereas Hb A and Hb S +12 ions preferentially form +8 alpha and +4 beta ions. Apo-monomers can be formed by further dissociation of holo-monomers. More highly charged holo-monomers, require less energy for dissociation because of Coulomb repulsion in the ions [84]. Thus the +7 holo-monomers show a greater degree of dissociation to apo-monomers than the +4 holo-monomers (Figure 3.6a and 3.6b). The asymmetric dimer dissociation of Hb A and Hb S is similar to the asymmetric charge partitioning of dimers from commercial Hb A seen in a previous study [107]. Asymmetric charge division has also been observed with other dimeric protein assemblies [184]. That Hb F dimers form monomers with nearly equal charges is somewhat unusual. Charge partitioning is influenced by a number of factors, including the number of charges, the gas-phase conformation of the precursor ion, and the conformational flexibility of the monomer in the protein complex [185, 186]. Assymmetric dissociation occurs when one subunit unfolds during trasition state so that it can accomodate more charges, while for symmetric charge partitioning a complex dissociates before unfolding of its subunit [186]. Of 39 different residues between the β- and γ-subunits, three occur at the $\alpha_1\gamma_1$ or $\alpha_1\beta_1$ dimer interface: β112Cys, 116His and 125Pro are replaced by γ112Thr, 116Ile and 125Glu [124]. These sequence alternations may be the reason for the different dissociation patterns. The internal energy added to the ion is another factor [187]. With relatively low internal energy (ca. 50% dimer dissociation), holo-monomers dominate the MS/MS spectra and Hb F shows symmetric charge division (Figure 3.6c); when ΔE_{int} is increased so that there is about 80% dissociation, all dimers, including Hb F, show fragments with asymmetric charge partitioning and mostly apo-monomers since holo-monomers can have additional collisions and gain enough internal energy to lose heme.

Tetramer ions dissociate to highly charged monomers (apo- or holo-) and trimers with 0 to 4 hemes, consistent with previous studies with commercial human Hb A [107], and in contrast to the known dissociation in solution where two dimers are formed [20, 126, 127]. Trimers with four hemes have also been reported by Versluis and Heck [107], indicating that an apo-alpha ion may be directly expelled from the intact holo-tetramer. Versluis and Heck showed that +17 tetramer ions of Hb A predominantly dissociate to single alpha ions (+10 to +6) and an $\alpha\beta_2$ trimer. However we find that tetramers of Hb A, +16 and +17, dissociate to $\alpha_2\beta$ trimer ions as well as $\alpha\beta_2$ trimer ions (+8, +9). The +7 trimers are outside the mass range of our triple quadrupole system (up to 6500 m/z) and so cannot be seen. However the complementary α and β (+8, +9) ions are seen in the MS/MS spectrum of Hb A (Figure 3.7a). Here only the monomer regions of the MS/MS spectra are shown for clear comparison of the different hemoglobins. Hossain and Konermann also observed apo-alpha and apo-beta ions as MS/MS products in their study on bovine ^{met}Hb [93]. Hemoglobin S shows dissociation pathways similar to Hb A (Figure 3.7b) in that both alpha and beta monomer ions are produced. In contrast, MS/MS of Hb F shows more intense alpha ions than gamma ions (Figure 3.7c), suggesting the preferred pathway is $\alpha_2\gamma_2 \rightarrow \alpha + \alpha\gamma_2$.
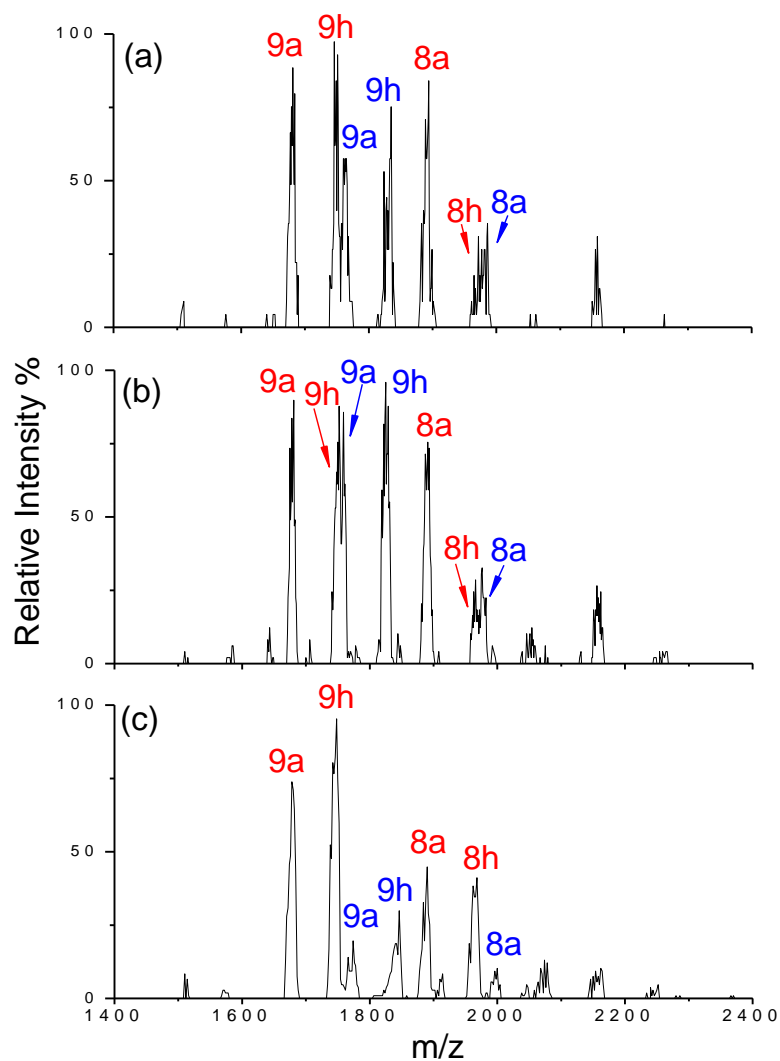
Figure 3.7. Monomer regions of MS/MS spectra of +16 tetramer ions from (a) Hb A, (b) Hb S, and (c) Hb F, with a pressure in Q2 of 3.0 mTorr of Ar. The MS/MS spectra are obtained with nearly 50% dissociation of tetramer precursor ions, at $\Delta V_{Q0-Q2} = 40$ V with Hb A, $\Delta V_{Q0-Q2} = 45$ V with Hb S, and $\Delta V_{Q0-Q2} = 30$ V with Hb F. Notation as in Figure 3.6.

Table 3.4 lists the dissociation voltages ($\Delta V_{Q0\text{-}Q2}$, shown as ΔV for short) and calculated ΔE_{int} values for α^h, dimer and tetramer ions from Hb A, S and F. The ΔE_{int} results are compared with an orifice-skimmer voltage ΔV_{os} of 100 V, to match the conditions used for cross section measurements. Higher ΔE_{int} values indicate that ions must acquire greater additional internal energy in Q2 to dissociate, and thus are more stable in the gas phase. Comparison of ΔE_{int} values for complexes that differ substantially

Table 3.4. Dissociation voltages (ΔV) and ΔE_{int} values (eV) of ions from variant Hb with 50% precursor ion dissociation.

Species	Charge	ΔV_{os} (V)	Hb F		Hb S		Hb A	
			ΔV	ΔE_{int} [a]	ΔV	ΔE_{int}	ΔV	ΔE_{int}
α^h	+7	100	79 ± 1	140 ± 2	76 ± 2	137 ± 4	77 ± 4	126 ± 7
	+8		64 ± 1	132 ± 1	63 ± 2	130 ± 5	62 ± 3	122 ± 6
Dimer	+11		64 ± 1	186 ± 3	72 ± 2	221 ± 8	70 ± 2	201 ± 8
	+12		45 ± 1	146 ± 4	52 ± 3	172 ± 10	52 ± 2	162 ± 6
Tetramer	+16	100	87 ± 3	382 ± 13	72 ± 4	341 ± 18	78 ± 2	351 ± 9
		150	78 ± 1	340 ± 5	63 ± 4	295 ± 19	68 ± 1	305 ± 5
	+17	100	73 ± 3	352 ± 14	62 ± 2	315 ± 11	66 ± 2	314 ± 7
		150	62 ± 1	298 ± 5	51 ± 1	259 ± 6	56 ± 1	265 ± 6

[a]Uncertainties of ΔE_{int} are obtained by propagation of the errors of ΔV and cross sections.

in binding energy requires correction for the different reaction times in Q2 [58, 79, 84].

Under the conditions that give 50% fragment yield, the dissociation occurs over a length

of ca. 5 cm near the cell exit [79]. The times available for reaction can be calculated

based on equation (1.4), using the kinetic energy near the cell exit with $l = 18.1$ cm,

expressed as follows,

$$t = \frac{l'}{\left(\dfrac{2E^0}{m_1} \exp\left(-\dfrac{C_{Dd} n m_2 l \sigma}{m_1} \right) \right)^{1/2}}$$

(3.1)

where l' is distance over which dissociation occurs (5 cm). The corresponding reaction

times for monomer, dimer and tetramer ions of the different hemoglobins with various

charges are calculated to be 28 ± 1 μs, 37 ± 3 μs and 42 ± 4 μs on average, respectively.

This small variation in reaction times between the different hemoglobins will not

influence ΔE_{int} significantly [58, 84] and no correction for different reaction times is

necessary. Heme loss from holo-alpha ions of Hb S and Hb F requires similar ΔE_{int}. The

dissociation voltages are nearly the same for Hb S and Hb A, but Hb A has a slightly

lower (ca. 10%) ΔE_{int} (Figure 3.8), because of the smaller α^h cross section of Hb A. The

smaller cross section means the ions have fewer collisions and thus slightly less kinetic

energy is transferred into internal energy. The order of the ΔE_{int} values of the dimer ions

is, Hb S > Hb A > Hb F. Dimers of Hb S require 6% greater ΔE_{int} than Hb A, and 11%

greater ΔE_{int} than Hb F. With tetramers, Hb F requires approximately 11% higher ΔE_{int}

than Hb A or Hb S. For the same species, ions with only one more charge clearly show

lower ΔE_{int} (Table 3.4), indicating increased Coulomb repulsion forces destabilize the

ions in MS/MS. In these experiments, ΔV_{os} was set to 100 V. When ions pass through the

orifice-skimmer region, ion activation first causes desolvation and then increases internal energies of the ions [83]. A nearly 10 V decrease in dissociation voltage was found with tetramer ions when ΔV_{os} was increased from 100 V to 150 V (Table 3.4) because at ΔV_{os} of 150 V the tetramer ions have greater internal energies before they enter the collision cell. However the trend in ΔE_{int} values among the different Hb variants remains the same. This effect was not seen with dimer and monomer ions; ΔV_{os} of 100 V and 150 V give similar ΔE_{int} values.
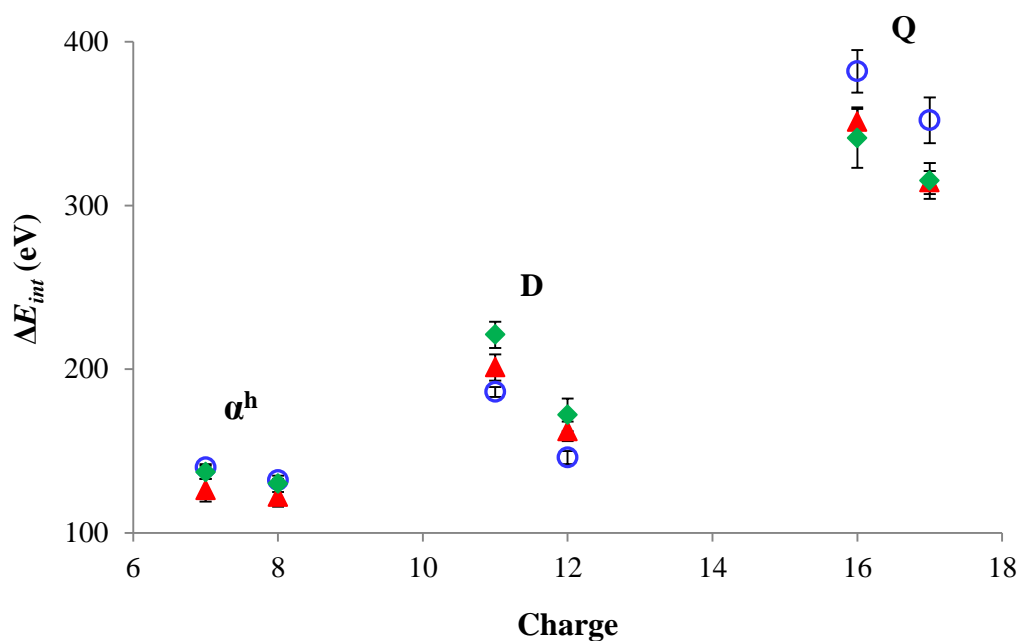
Figure 3.8. Values of ΔE_{int} as a function of charge state for Hb A (triangles), Hb F (open circles), and Hb S (diamonds). Notation as in Figure 3.2. The pressure in Q2 was 1.5 mTorr for α^h, 2.0 mTorr for dimers, and 3.0 mTorr for tetramers.

Correlations between solution and gas-phase stability can be investigated by comparing free energy changes ΔG^0_{sol} and ΔE_{int} for similar dissociation pathways. In solution, dimers of Hb F are more stable than dimers of Hb A because three amino acid replacements increase hydrophobicity on the $\alpha_1\gamma_1$ interface [188], leading to a stronger interface interaction. The dissociation of $\alpha\gamma$ dimers into α and γ is three times slower than the dissociation of $\alpha\beta$ dimers into α and β [128]. The free energy changes (ΔG^0_{sol}) of dimer dissociation of ^{CO}Hb A and ^{CO}Hb F are 16.7 and 17.3 kcal/mol respectively, calculated from reported K_d values (4.7×10^{-13} M and 1.63×10^{-13} M [128]). Thus, in the gas-phase, where Hb F dimers are slightly less stable than Hb A dimers, the dimer binding appears to differ from the binding in solution. This suggests that a more complex mechanism may be involved in gas-phase dissociation than just the immediate contacts at the subunit interface. The lower ΔE_{int} with Hb F may be due to its symmetric charge partitioning. Less internal energy is required to form monomers with equal charges than with asymmetrical charge partitioning [187], giving a lower ΔE_{int} for Hb F dimers to dissociate than Hb S and Hb A.

Tetramers of Hb F are more strongly bound in solution than tetramers of Hb A and Hb S. In 150 mM tris-Ac buffer at pH 7.5, K_d for the tetramer-dimer dissociation of ^{CO}Hb A is 0.68 μM , of ^{CO}Hb F 0.01 μM [131], and of ^{CO}Hb S 0.42 μM [182], and the resultant ΔG^0_{sol} are 8.34 kcal/mol, 10.8 kcal/mol, and 8.61 kcal/mol, respectively. In the gas phase, though Hb F also shows greater stability than Hb A and Hb S, ΔE_{int} cannot be compared with ΔG^0_{sol} values because gas-phase tetramers dissociate to monomers and trimers, not two dimers.

3.4 Summary

With the same solution and mass spectrometer conditions, fresh Hb F and Hb S give similar mass spectra. The organic solvent used in the solution affects the relative abundances of monomer, dimer and tetramer ions in mass spectra. For all proteins studied, Hb A, Hb S and Hb F, dimers give cross sections intermediate between monomer and tetramer ions. Gas-phase dimer ions exchange a slightly smaller fraction of their exchangeable hydrogens than monomer or tetramer ions. Hemoglobin S shows larger collision cross sections of monomer, dimer and tetramer ions and greater H/Dx levels of tetramer ions than Hb A and Hb F. Comparison of ΔE_{int} and $\Delta G^0{}_{sol}$ values for dissociation of dimers suggests that the binding in gas-phase dimers may differ from that in solution. In solution, $\alpha^h\gamma^h$ is more strongly bound, however, in the gas phase, requires less energy to dissociate in MS/MS. In addition, $\alpha^h\gamma^h$ dimers show MS/MS dissociation pathways distinct from $\alpha^h\beta^h$ dimers, with symmetrical versus asymmetrical charge division of monomers. Tetramer ions dissociate to monomers and trimers, unlike solution Hb, which dissociates to dimers. Hemoglobin F tetramer ions require greater internal energy to dissociate than Hb A and Hb S. Thus we do not find consistent relationships between solution stability and gas-phase dissociation energies. The different sequence of the γ chain of Hb F compared to the β chain of Hb A might be expected to change the physical properties of the gas-phase ions, as is observed. The results with Hb S show that substitution of a single residue in the β chain can also change the physical properties in this gas-phase protein−protein complex.

Chapter 4 Solution Hydrogen/Deuterium Exchange of Human Hemoglobin A, F and S

4.1 Introduction

Recently, electrospray ionization mass spectrometry (ESI MS) has been combined with a continuous-flow mixing technique for on-line "pulsed labeling" H/Dx of proteins with millisecond time resolution [24, 93]. The exchange is initiated by rapidly mixing protein and D_2O-containing solutions, and then proceeds in a "labeling" capillary that is connected to an ESI source. This "time-resolved" ESI MS is suitable for monitoring fast conformational changes, and allows the simultaneous detection of coexisting protein conformations [70] which cannot be detected by conventional spectroscopic or NMR methods. This device is easy to operate and readily modified. For example, a double mixing setup has been developed to employ H/Dx for detecting protein conformational changes upon sudden initiation of refolding [71]. Continuous mixing devices have also been used in other investigations, such as studies of the unfolding [151] and refolding kinetics of hemoglobins [149] determined from changes of ion intensities and charge state distributions in mass spectra.

In this chapter, "time-resolved" ESI is used to investigate the solution H/Dx behavior of a model noncovalent protein−protein complex, hemoglobin (Hb). Previous solution H/Dx studies of Hb A have provided insights into its native global structures [21, 91, 141-144]. Localized conformations have also been studied, either with proteolytic peptides [91, 142, 145, 146] or MS-based fragmentation [93]. Abaturov et al. studied the effects of external (pH, temperature) [141] or internal (heme removal, isolated monomers) [21, 145, 146] changes on the H/Dx kinetics of various forms of human Hb A. In their studies, IR spectroscopy was used to detect the labeling after gel filtration through a column equilibrated with D_2O. To probe local functional fluctuations, Englander et al.

utilized HPLC-MS to study the dynamics of ^{deoxy}Hb A or liganded Hb A with an isotope exchange-in/out method in which proteins were first incubated in deuterium or tritium followed by gel filtration with H_2O buffer [91]. In most previous work, the isotope labeling was done on relatively long time scales (>1 min). An exception is the ESI MS/MS study of bovine ^{met}Hb A monomers, dimers and tetramers with pulsed (53 ms) H/Dx at mildly basic pH by Hossain and Konermann [93].

With H/Dx of large noncovalent protein−protein complexes, the reversible inter-exchange between protein and its subunits must be considered. For native hemoglobin, the equilibrium can be expressed as, tetramer ↔ dimer ↔ monomer. If the exchange time is long compared to the interconversion time, different species may show the same relative exchange levels (%H/Dx) (the number of hydrogens exchanged divided by the number of exchangeable hydrogens, expressed as a percent). For example, tetramers may show the exchange of twice as many hydrogens as dimers (the same relative exchange level as dimers) if the protected sites, buried in interface contacts in the tetramers are exposed and complete H/Dx when dissociating into dimers before recombining into tetramers. The resulting H/Dx levels are a mix of the levels of dimers and tetramers rather than those of the individual species. Thus, to study the exchange levels of monomers, dimers and tetramers separately, the exchange time should be short compared to the time for tetramer-dimer interconversion (seconds [147, 148]), or dimer-monomer interconversion (minutes [128]), but sufficiently long for unprotected amides to complete exchange at a neutral pH (0.3 s to 1 s).

Here, with a home-made ESI source that substantially reduces the labeling time, millisecond H/Dx is employed to search for conformational differences of three human

met-hemoglobins (Fe^{3+} in the heme), Hb A, fetal Hb (Hb F) and sickle Hb (Hb S) at neutral pH. We are not aware of any previous solution H/Dx studies of these two variant hemoglobins.

In chapter 3, we reported a study of the gas-phase conformations of ions of Hb A, F and S. Hemoglobin S ions showed 13% larger collision cross sections and exchanged 16% more hydrogens than ions of Hb A and Hb F [189], indicating a different, and possibly more unfolded, conformation in gas-phase Hb S ions. Here, with solution H/Dx exchange times from 195 ms to 3 s, no significantly different exchange levels are found in holo-monomers, dimers and tetramers of these three hemoglobins. With Hb A, where comparison with literature values is possible, our results agree with a previous study [93]. The H/Dx kinetics is also discussed. The relative exchange levels with exchange times less than about 1 s are, tetramers < dimers < monomers, and these change to tetramer ≈ dimer < monomer with 2 s of exchange. Holo-alpha monomers consistently give greater relative exchange levels than dimers and tetramers within 3 s of H/Dx, consistent with the relaxation of the dimer-monomer equilibrium occurring on a longer time scale than that of the tetramer-dimer equilibrium. At times greater than about 1 s, the relative exchange levels of tetramers and dimers are equal, as expected from the interconversion kinetics of tetramers and dimers.

4.2 Experimental Methods

4.2.1 Mixing System

Solution H/Dx was performed with a continuous-flow on-line mixing system [24, 70, 93] (Figure 4.1a). Syringe 1 (volume 250 μL) contained aqueous hemoglobin (40 μM) solutions with 10 mM NH_4Ac and 20% MeOH (pH = 6.8, measured with a Accumet model 15 pH meter (Fisher Scientific, Fairlawn, NJ, USA)). Syringe 2 (volume 1 ml) contained solutions with H_2O/CH_3OH (4/1, v/v) for control experiments with no exchange, or D_2O/CD_3OD (4/1, v/v) for H/Dx experiments. These two syringes are advanced simultaneously by one syringe pump (Harvard Apparatus, St. Laurent, QC, Canada) at flow rates of 4 and 16 μL/min, respectively. The solutions, flowing in two fused silica capillaries (48.6±0.6 μm i.d., Polymicro Technologies, Phoenix, AZ, USA) are combined at a mixing tee (P-727; IDEX Health & Science, Oak Harbor, WA, USA), which then empties into another capillary of the same i.d. that is connected to the ESI source with a total flow rate of 20 μL/min. The exchange of Hb with a final protein concentration of 8 μM takes place in this "labeling" capillary with 80% D_2O/CD_3OD at a pD of 7.2 at room temperature (pD = pH meter reading + 0.4 [190]). With other conditions fixed, the H/Dx time is controlled by the length of the capillary between the mixing point and the ESI source. For short H/Dx times, capillary lengths of 3.5 cm to 56 cm are used, corresponding to protein exchange times from 0.195±0.005 s to 3.1±0.08 s.

(a)

(b)
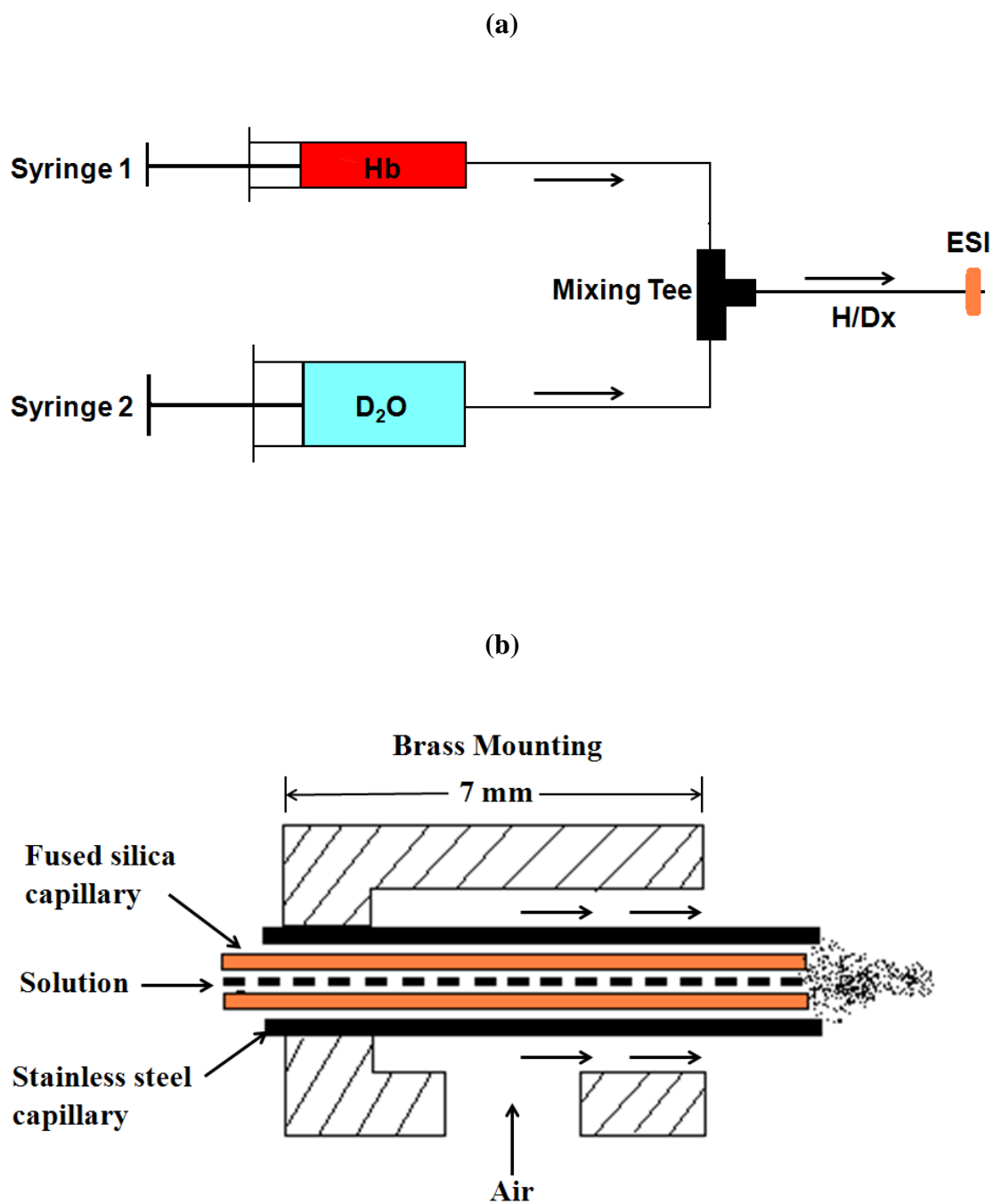
Figure 4.1. Experimental setup for time-resolved ESI with online H/Dx. (a) Flow-mix

system. (b) Home-made ESI source.

A home-made pneumatically assisted ESI source similar to that of Konermann et al. [70] was used (Figure 4.1b). A brass block includes a bore in which a stainless steel tube (i.d. 250 μm and o.d. 380 μm) is mounted. The block also provides on one side an enlarged bore (3 mm diameter), in which a tube is fitted. Air flows through the tube and passes between the block and stainless-steel capillary, to assist nebulization. The capillary with solution is placed in the stainless-steel tube. The whole block is connected to a high voltage supply of up to 5.5 kV. To substantially reduce the time for solutions to flow through the source, the sprayer has an overall length of 7 mm, much shorter than that conventionally used in some commercial instruments (~ 5 cm). For longer exchange times (> 3 s) a commercial sprayer as described in chapter 2 is used (Sciex API 3, Concord, ON, Canada).

4.2.2 ESI LIT-TOF MS System

Protein masses are measured with a linear quadrupole ion trap reflectron time-of-flight mass spectrometer system (LIT-TOF MS) as described in chapter 3 [46, 100, 189]. Ions from the home-made ESI source (5.5 kV) pass through an aperture (5 mm diameter) in a curtain plate (1000 V), a dry nitrogen curtain gas (~ 3 L/min), an orifice (0.25 mm diameter, 170 V to 270 V), a skimmer (0.75 mm orifice diameter, 20 V) and enter a chamber with two consecutive RF-only quadrupole ion guides, Q0 (DC offset 15 V) and Q1 (DC offset 10 V), with a Q0/Q1 interquadrupole lens voltage of 12 V. The chamber pressure was kept at 10 mTorr of N_2 by partially closing a gate valve between the chamber and a turbomolecular pump. After passing through a stack of four focusing

lenses, ions are mass analyzed with a reflectron-TOF and detected by a dual microchannel plate. The increase in protein mass after H/Dx is calculated from the m/z shift between control (no H/Dx) and reaction experiments, and corrected by considering the ion charge and incomplete desolvation. For dimer and monomer ions, the mass increase is calculated from

$$\Delta M = [(m/z)_1 - (m/z)_0] \times i - [0.8 \times (M_D - M_H) \times i] \quad . \quad (4.1)$$

Equation 4.1 subtracts the number of charging protons that exchange. The factor 0.8 corrects for the fact that the solution contains 80% D_2O/CD_3OD. Here, $(m/z)_1$ and $(m/z)_0$ correspond to experimental mass to charge ratios of labeled and unlabeled proteins respectively, M_D and M_H are the masses of deuterium and hydrogen, and i is the ion charge. For tetramers, equation (4.1) should be further corrected due to incomplete desolvation. Assuming the solvation is from water and does not include MeOH, and the extents of solvation with H_2O and D_2O are the same, the mass shift can be calculated from

$$\Delta M = [(m/z)_1 - (m/z)_0] \times i - [0.8 \times (M_D - M_H) \times i] - [0.8 \times (M_D - M_H) \times 2n] \quad (4.2)$$

Here, n is the number of attached water molecules. Cluster ions, $Cs_{(n+1)}I_n^+$ [46], are used for mass calibration.

4.2.3 Materials

The procedures for extraction, purification and oxidation of hemoglobin samples from fresh normal adult human blood (Hb A), sickle cell blood (Hb S) and fetal human

blood (Hb F) were described in detail in chapter 2 and 3 [178, 189]. Prior to MS analysis, the ^{met}Hb stock solution aliquot that was stored at -80 ℃ was quickly thawed and diluted for analysis as discussed above.

Cesium iodide (manufacturer's stated purity 99%) was from Sigma-Aldrich, St. Louis, MO, USA. Methanol (HPLC grade), and NH_4Ac (ACS grade) were from Fisher Scientific, Fairlawn, NJ, USA. Deuterium oxide (99.9%) and methanol-d4 (99.8%) were from Cambridge Isotope Laboratories, Inc., Andover, MA, USA. Nitrogen and argon (manufacturer's stated purity 99.999%), and air (breathing grade) were from Praxair, Mississauga, ON, Canada.

4.3 Results and Discussion

4.3.1 Mass Spectra and Home-Made ESI

Figures 4.2a, 4.2b and 4.2c show mass spectra of Hb S obtained with the home-made sprayer and the commercial sprayer without H/Dx, and the home-made sprayer with H/Dx, respectively. With the home-made sprayer (Figure 4.2a and 4.2c), tetramer ions (+17, +18) dominate the spectra, with lower-intensity dimer ions (+11, +12) and holo-alpha monomer ions (+7, +8). With the same solution and operating conditions and with both sprayers, similar ESI-MS spectra are obtained with Hb A, Hb F and Hb S,
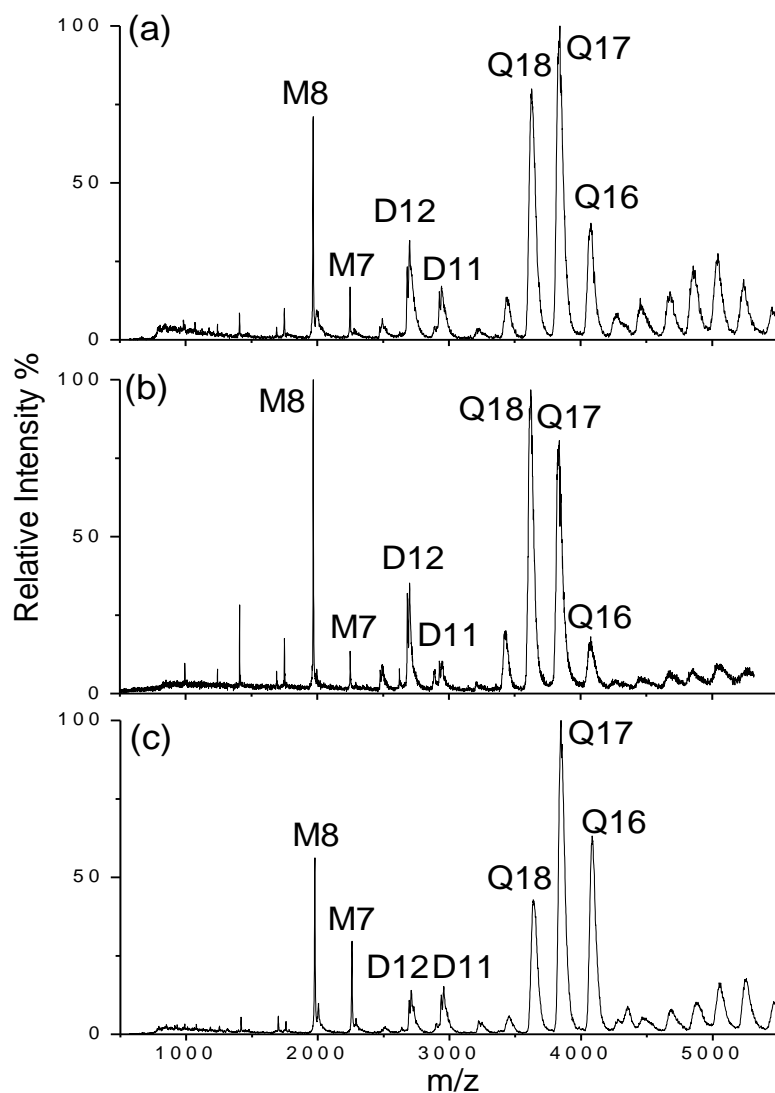
Figure 4.2. ESI LIT-TOF mass spectra of Hb S (8 μM, 20% MeOH), with (a) the home-made sprayer at a flow rate of 20 μL/min, no H/Dx; (b) the commercial sprayer at a flow rate of 1 μL/min, no H/Dx; and (c) the home-made sprayer at a flow rate of 20 μL/min, with 389 ms H/Dx. Notation: Q, tetramers; D, dimers; M, holo-alpha monomers. Charges are labeled.

consistent with previous results presented in chapter 2 and 3 [178, 189]. Although this home-made ESI source has a different configuration, with optimized conditions, it gives mass spectra similar to those with the commercial sprayer (Figure 4.2b). Intensity ratios of tetramer, dimer and monomer ions are similar in these two spectra. However, the home-made sprayer gives somewhat greater levels of higher-order multimers such as hexamers and octamers (at m/z > 4500). These have been shown to be artifacts of ESI [93].

When incubated in D_2O-containing solutions (Figure 4.2c), tetramer ions of Hb S appear to show somewhat less dissociation than with H_2O solutions. Compared to the spectrum with H_2O (Figure 4.2a), the intensity ratio of tetramer to holo-alpha ions with Hb S in Figure 4.2c increases about 20%, and the ratio of tetramer to dimer ions doubles. Also, ions with lower charges increase in relative intensity. For example, tetramers from H_2O have lower intensities of +16 ions than +18 ions, but from D_2O give greater-intensity +16 ions than +18 ions. Dimers from H_2O give levels of +11 ions half of +12 ions, but from D_2O show levels of +11 ions equal to +12 ions. This was also seen with Hb A and Hb F, with both the commercial and home-made sprayers. This may reflect the higher stability of the globular protein in D_2O compared to H_2O [191]. The hydrophobic interaction is strengthened in D_2O, resulting in more stable Hb tetramers.

Increasing the organic solvent content improves ionization efficiency with the home-made sprayer. Solutions of 10% MeOH (previously used in work described in chapter 2 and 3 [178, 189]) and 20% MeOH both give spectra with tetramers, dimers and monomers. However the addition of 20% MeOH apparently increases the intensities of ions in ESI spectra. It also gives higher levels of monomers and dimers in spectra

compared to spectra from a solution with 10% MeOH under the same conditions, making measurements of exchange levels of monomers and dimers easier. The addition of 20% MeOH to the solution does not change the H/Dx levels as compared to 10% MeOH, and it is not detrimental to the folded conformation of Hb proteins, consistent with a previous study on methanol-induced conformations of myoglobin [19].

4.3.2 Optimizing Conditions for H/Dx

To obtain structural information on Hb subunits (dimers and monomers) in solution, in-source dissociation of tetramers in the gas phase should be minimized. Dissociation can occur in the orifice-skimmer region or skimmer-Q0 region of the mass spectrometer used here (see also chapter 5) [192]. With the skimmer-Q0 voltage difference of only 5 V used here, increasing the orifice-skimmer voltage difference (ΔV_{os}) can apparently increase dissociation of tetramer ions to monomer ions, to produce +7 to +11 charged holo-monomers and apo-monomers while leaving the relative intensities of dimer ions almost unchanged. This is consistent with the dissociation of gas-phase tetramer ions in MS/MS experiments described in chapter 3, where monomer and trimer ions are formed [189]. To minimize this dissociation, values of ΔV_{o}s were decreased to 150 V. Further decreases did not increase the tetramer to holo-monomer ion intensity ratio. After the initial ion intensity changes of Hb ions in the deuterating solution at the beginning of H/Dx compared to Hb ions from H_2O, no further changes in intensity ratios over the 3 s of H/Dx are seen. Thus at least most of the monomers and dimers in the

spectra derive from the species in solution, rather from dissociation in the ion sampling process.

In mass measurements of tetramers, incomplete desolvation is seen. This complicates relating mass shifts to H/Dx levels. Accurate corrections are difficult, due to possible differences in the extents of attachment of H_2O and D_2O, and possible attachment of CH_3OH or CD_3OD. Higher degrees of solvation of the protein may introduce greater errors in calculating the number of hydrogens exchanged. To reduce the labeling time, a relatively high flow rate (20 μL/min) is used. This increases the solvation of the ions. Solvation of tetramers was reduced as much as possible as follows. The increased MeOH in solution helped increase solvent evaporation. The ESI source was moved further away from the sampling orifice. The flow rates of the nebulizer gas and the curtain gas were carefully increased to enhance desolvation while maintaining acceptable ion intensity. For measurements of tetramer H/Dx, ΔV_{os} was increased to 200 V, to further desolvate ions in the gas phase. With these optimized conditions, the number of water molecules attached to tetramers was reduced to about 15. The peak widths of tetramers at 80% maximum is around 20 m/z (Figure 4.3c, below), similar to those of the fragment monomer ions studied by Hossain and Konermann, who chose MS/MS to study H/Dx of Hb tetramers to avoid solvation problems [93]. Solvation of monomer and dimer ions was not seen and did not affect the calculated H/D exchange levels (Figure 4.3a and 4.3b, below).

4.3.3 H/Dx Levels

Figure 4.3 shows detailed mass spectra of monomer, dimer and tetramer ions of Hb F with different exchange times. For each species, single peaks that move to higher masses are observed as the exchange time is increased from 195 ms to 3 s, suggesting an EX2 mechanism, as is usually seen with the native conformations of proteins [1]. The calculated numbers of exchangeable hydrogens on holo-alpha globin, holo-beta globin, and holo-gamma globin are 229, 235 and 247, respectively.
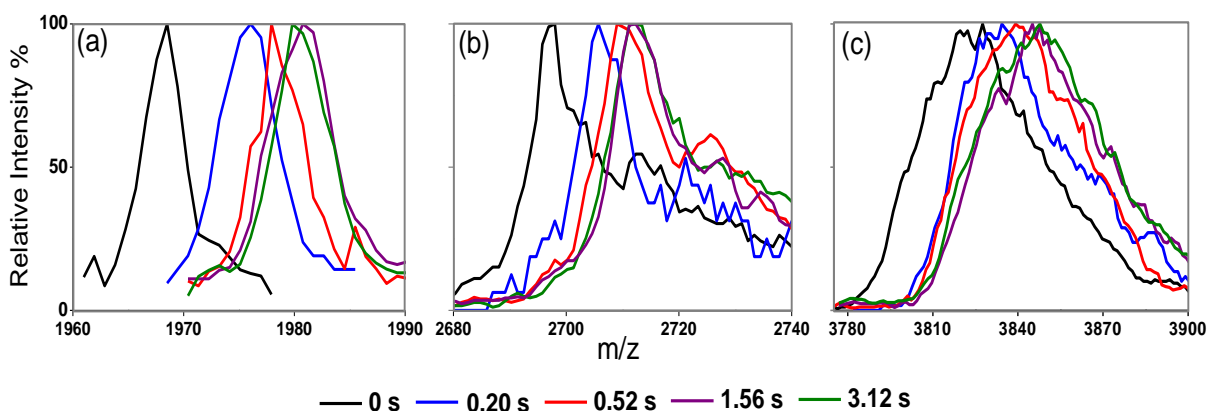
Figure 4.3. Mass spectra of Hb F, (a) holo-alpha (+8), (b) dimer (+12), and (c) tetramer (+17), with different exchange times. Results with no exchange (0 s) are obtained from control experiments.

With Hb A, with 0.5 s labeling, the number of hydrogens exchanged averaged over charge states are 254 ± 17 (%H/Dx of $27.5 \pm 1.8\%$) for tetramers (+16 to +18), 152 ± 6 ($33.0 \pm 1.4\%$) for dimers (+11, +12), and 95 ± 7 ($42.0 \pm 3.3\%$) for holo-monomers (+7, +8).

In ^{deoxy}Hb, about 31 and 33 amino acid residues are involved in the $\alpha_1\beta_2$ interfaces between dimer pairs and in the $\alpha_1\beta_1$ interfaces between α- and β- subunits [124], corresponding to 56 and 50 exchangeable hydrogens respectively. Our results show that about 50 and 40 hydrogens are protected against H/Dx when binding from dimers to tetramers and from monomers to dimers, slightly less than the numbers of exchangeable hydrogens at the interfaces. In the study of Hossain and Konermann, with commercially obtained bovine ^{met}Hb A and 53 ms deuterium labeling at pD = 8.5, the estimated averaged %H/Dx was 31.4% for tetramers (+15 to +18), 35.3% for dimers (+11, +12), and 39.4% for monomers (+7, +8) [93], in reasonable agreement with our results.

Figure 4.4a, 4.4b and 4.4c show %H/Dx vs. exchange time for Hb A, Hb S and Hb F holo-monomer (+8), dimer (+12) and tetramer (+17) ions respectively. For the same species, similar H/Dx levels are seen with ions with different charges (Figure 4.5, below). Similar exchange levels are observed with dimers and monomers of different hemoglobins (Figure 4.4a and 4.4b). Thus no pronounced conformational differences in solution are found by H/Dx. For tetramers (Figure 4.4c), with exchange times less than 0.5 s, Hb F exchanges slightly fewer (~10%) hydrogens than Hb A and Hb S, while between 0.5 s to 2 s, similar H/Dx levels are seen within the combined uncertainties. At 3 s, Hb F tetramers exchange 33% of their exchangeable hydrogens, less than Hb A and S with 37% hydrogens exchanged. Though the difference is not pronounced, it is possible that Hb F adopts a somewhat more folded or less flexible conformation than Hb A or Hb S. In solution Hb F is more strongly bound than Hb A and Hb S [131, 182]. The proteins' "sizes" can be estimated from the radii of gyration, r_g, measured by light scattering in solution. For ^{CO}Hb in 50 mM sodium phosphate buffer, Hb F has an r_g of 30±1 Å, while
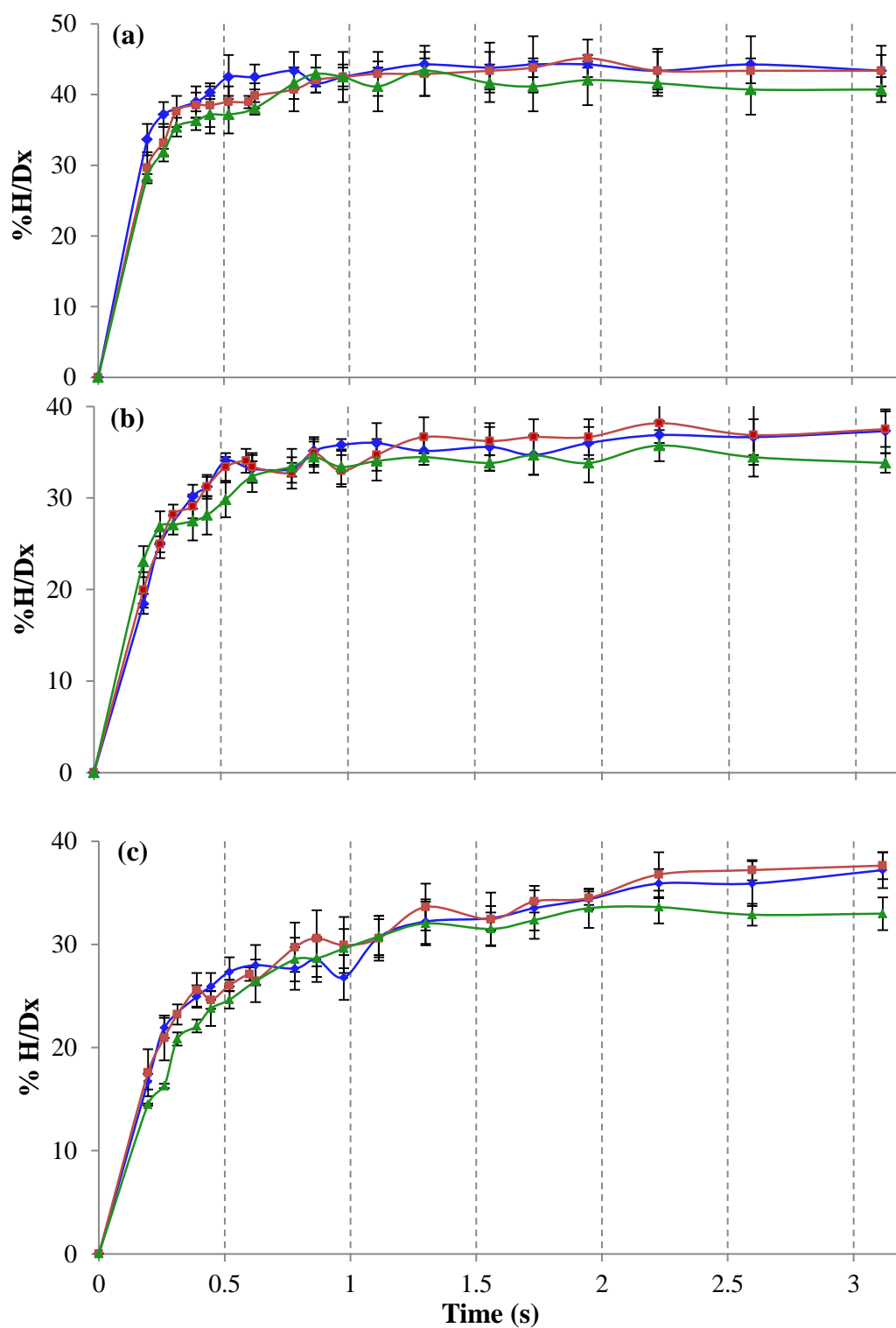
Figure 4.4. Relative exchange levels of Hb A (blue), Hb F (green) and Hb S (red), measured with (a) +8 holo-alpha, (b) +12 dimer, and (c) +17 tetramer ions. Uncertainties are standard deviations of three repeat measurements.

Hb A and Hb S, have r_g values of 29±1 Å and 29±2 Å respectively [22], so little difference in the solution conformations is seen by light scattering. Another study found small differences in the maximum H/Dx levels of [met]Hb A (81.8%) and Hb S (84.8%) when comparing sorption results of H_2O and D_2O vapor on protein crystals [193]. However, that experiment was carried out on solid-phase Hb, so that the "vapor" exchange cannot be directly compared to our solution H/Dx.

The solution H/Dx was also measured with exchange times from 2 min to 1 hr with the commercial sprayer. The results with 2 min H/Dx are similar to those at 3 s with the home-made sprayer. After about 5 min incubation in D_2O, H/Dx levels of all species increase. At 10 min, tetramers, dimers and monomers show similar %H/Dx, exchanging ~500 (54%), ~250 (54%), and ~120 (53%) hydrogens, respectively. These numbers are similar to those of Hb A with a denatured or more unfolded conformation [142] where at pH 2.7, 0 °C, Hb A exchanged ~250 hydrogens per dimer (~500 hydrogens per tetramer), determined by hydrogen-tritium exchange measurements as well as modeling calculations. Abaturov et al. [141] measured H/Dx levels of [oxy]Hb A and [CNmet]Hb A and found that after 100 minutes exchange (20 °C, pD≈7.4) both proteins exchanged ca. 55% of their hydrogens, in agreement with our observations for [met]Hb A. They also found [145] that after 100 minutes α monomers, chemically isolated from tetramers, exchanged about 70% of their hydrogens, in qualitative agreement with our observations at short times which show higher %H/Dx levels for the monomers than tetramers. Englander and co-workers also studied exchange out of deoxy or liganded human Hb A that had been incubated in tritium for 15 or 22 hours [91, 143, 144]. The shortest exchange-out time was ca. 3 min [143, 144], where about 80 tritiums per monomer remained unexchanged.

Here we show that in 3 min, Hb can exchange about 85 hydrogens per monomer, so it is possible the fully tritiated Hb used by Englander et al. exchanged 85+80 =165 hydrogens per monomer or about 660 hydrogens per tetramer, somewhat greater than the 500 seen in 10 minutes here. The greater number may be due to the longer exchange time (at least 15 hours) and higher incubation temperature (37 °C).

4.3.4 Kinetic Studies

Hemoglobin A, F and S give similar H/Dx kinetics, as shown in Figure 4.5 with Hb F as an example. With monomers and dimers, exchange is complete within 1 s (Figure 4.5). With 3 s reaction, dimers show consistently lower %H/Dx than monomers, indicating the interconversion between dimer and monomers does not occur extensively on this time scale, in agreement with previous kinetic studies [128]. The exchange kinetics of tetramers is more complex, as shown in Figure 4.5. From 0.4 s to 0.6 s, about 26% of the hydrogens are exchanged. Then H/Dx levels gradually continue to increase. At 1 s, nearly 30% of the hydrogens are exchanged, still lower than the relative exchange levels of dimers or monomers. From 1 s to 1.5 s, the %H/Dx of tetramers increases to more than 30%, close to that of the dimers. After 1.5 s, tetramers and dimers show similar %H/Dx. It is concluded that the interconversion of tetramers and dimers is significant after ca. 1 s. In detail, the times for tetramers and dimers to show equal relative exchange levels are approximately 1.5 s for Hb A, 1.7 s for Hb S, and 1.1 s for Hb F. Thus exchange times of 1 s or less are necessary to determine the separate

exchange levels of tetramers and dimers. This is consistent with kinetic studies that show that the tetramer and dimer re-equilibrate on the order of seconds [147, 148].
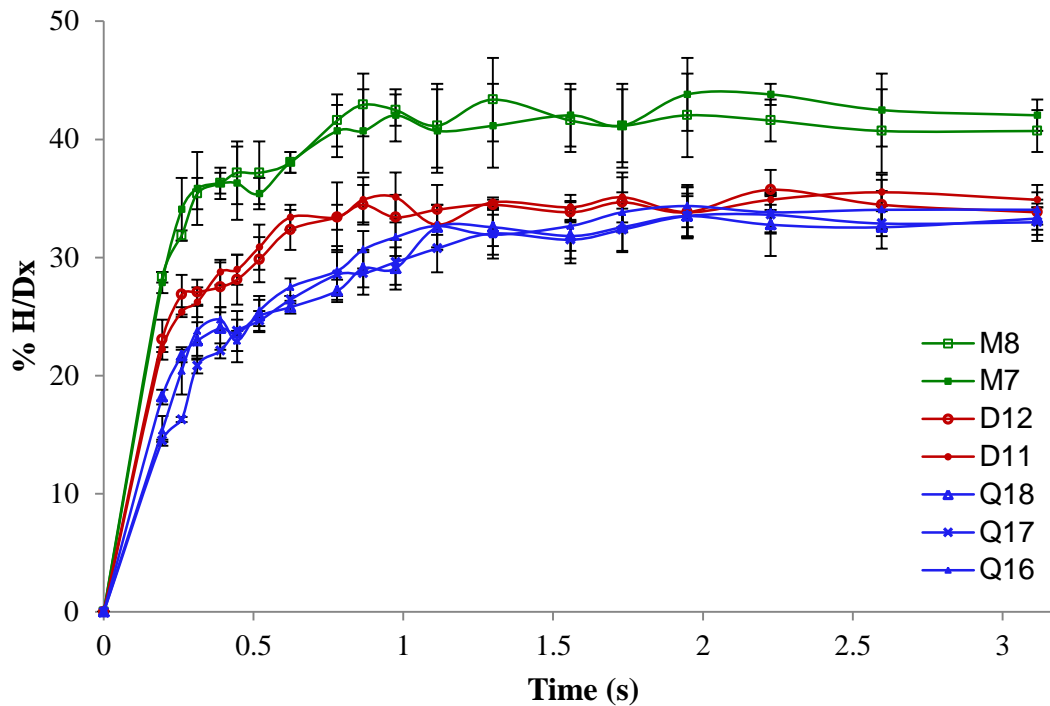
Figure 4.5. Relative exchange levels measured with +7, +8 holo-alpha (green), +11, +12 dimer (red) and +16 to +18 tetramer (blue) ions with Hb F as a function of labeling time. Uncertainties are standard deviations of three repeat measurements. Notation is shown in the figure.

Fitting curves of the H/Dx levels ($N(t)$, where t (s) is reaction time) into a first-order rate equation, $N(t) = A \times (1 - e^{-kt})$, gives the rate constants, k (s^{-1}). Table 4.1 lists the k values averaged over different charge states of Hb A, F and S, for reaction times of 0.5 s, 1 s and 3 s, respectively. Similar rates are obtained for these three proteins. Holo-alpha monomers exchange slightly faster than dimers and tetramers, possibly because of the higher intramolecular mobility in Hb monomers [21]. With times up to 1 s, dimers and tetramers show similar exchange rates within the combined uncertainties. With millisecond H/Dx, the exchange predominantly takes place on the unprotected exposed areas of the protein, with similar exchange rates, while the protected regions are sufficiently stable against H/Dx. For monomers and dimers, fitting rates to data collected with different reaction times (e.g. 0.5 s, 1 s, and 3 s) gives similar rate constants. For tetramers, the rate constants obtained with 3 s exchange are apparently smaller than those within 1 s, and smaller than the rate constants of the dimers. After 1 s reaction, the rate constants of tetramers become closer to the half time of tetramer-dimer dissociation and the calculated tetramer-dimer equilibrium relaxation time. Using an association rate constant ($k_a = 1.5 \times 10^5$ M^{-1} s^{-1}) and a dissociation equilibrium constant ($K_d = 2 \times 10^{-6}$ M) [126], the calculated tetramer-dimer dissociation rate constant is 0.3 s^{-1}, corresponding to a half time of 2.3 s. The calculated relaxation rate constant for 8 μM Hb is 0.48 s^{-1}, which corresponds to a relaxation time of 2.1 s. Thus after 1 s, the protein kinetic studies cannot reveal the conformation-dependant H/Dx rates of tetramers because the interconversion between tetramers and dimers makes interpreting the exchange process ambiguous.

Table 4.1. H/Dx rate constants (s^{-1}) of Hb A, F and S[a].

Species Time	Monomer			Dimer			Tetramer		
	Hb A	Hb F	Hb S	Hb A	Hb F	Hb S	Hb A	Hb F	Hb S
0.5 s	8.0±1.1	7.5±1.2	6.4±0.9	4.3±0.9	6.1±0.7	3.7±0.9	4.9±0.8	5.0±1.0	4.3±0.6
1.0 s	7.5±0.6	5.9±0.7	6.3±0.4	5.0±0.4	5.1±0.5	4.8±0.5	5.5±0.4	4.0±0.5	4.9±0.6
3.0 s	6.9±0.5	5.5±0.3	5.5±0.3	4.7±0.2	4.8±0.3	4.3±0.3	2.9±0.5	3.0±0.3	2.9±0.4

a. Averaged over data from +7 and +8 ions of holo-alpha monomers, +11 and +12 ions of dimers, and +16 to +18 ions of tetramers.

4.4 Summary

The solution H/Dx behavior of intact Hb A, Hb F and Hb S, measured with time-resolved ESI, is reported. The home-made sprayer gives mass spectra comparable to those obtained with a conventional commercial sprayer. The instrument operating conditions required re-optimization to minimize dissociation in the ion sampling interface and to minimize solvation of tetramers. In monomers or dimers, hemoglobin A, S and F show similar exchange rates and exchange levels. In tetramers, Hb A and Hb S show similar exchange levels which are slightly greater than Hb F with labeling times of less than 0.5 s and between 2 s to 3 s. Thus no substantial conformational differences in these Hb variants are found by H/Dx. With exchange times of less than 1 s, the order of the relative exchange levels is, tetramer < dimer < monomer. This result further demonstrates that the dimers and monomers studied here are mostly from solution rather than from gas-phase dissociation. With H/Dx times longer than 1 s, where the interconversion between tetramer and dimer is involved, the relative exchange levels of tetramers increase, and become similar to the relative exchange levels of dimers, as expected from previous kinetic studies of tetramer-dimer dissociation and recombination. Thus when using solution H/Dx to study the conformations of a protein−protein noncovalent complex even in equilibrium studies, it is necessary to limit the exchange to times less than that required for dissociation and recombination of the complex. In cases where the rates of dissociation and recombination are not known, measurements of H/Dx levels at different exchange times can reveal approximately the interconversion kinetics.

Chapter 5 Solution and Gas-Phase Hydrogen Deuterium

Exchange of Protein–Small-Molecule Complexes:

Cex and Its Inhibitors

5.1 Introduction

Studies by ESI MS of the noncovalent binding of proteins to small molecules continue to be of interest, with the potential for a better understanding of noncovalent binding properties, both in solution and in gas-phase ions. If conditions can be found where gas-phase binding is related to solution binding, mass spectrometry may be more widely applied to systematically determine the relative binding strengths of a variety of molecules with a target protein, with the advantages over other methods of speed, sensitivity and specificity.

In some cases, changes to conformations of an entire protein or domains of a protein when binding a ligand, are involved in the biological function of a protein. In work described in this chapter, we have used collision cross section measurements and solution and gas-phase H/Dx coupled with MS, to probe the conformations of a protein and the protein binding small-molecule inhibitors. Tandem mass spectrometry (MS/MS) has also been used to study the relative gas-phase binding strengths of ligand-bound protein ions [58, 84, 189].

Here, binding of the catalytic domain of the enzyme exo-1,4-β-D-glycanase (cellulasexylanase or "Cex") with three aza-sugar inhibitors, serves as a model to study conformations in solution and in the gas phase of protein−small-molecule noncovalent complexes. Three small-molecule inhibitors that noncovalently bind at the active site of the catalytic domain of Cex (Cex-cd) with high affinity have been used. These are deoxynojirimycin (X_2DNJ), isofagomine lactam (X_2IL), and isofagomine (X_2IF) (see chapter 1) [139]. Comparison of the interactive maps via X-ray crystallographic studies

with these inhibitors has been described in detail [16]. The dissociation or inhibition

constants, indicating binding strengths in solution, K_i, have been determined through

kinetic analysis [9], and are listed in Table 5.1. In solution, the Cex−X$_2$DNJ complex has

the lowest binding strength, Cex−X$_2$IL is intermediate and Cex−X$_2$IF has the highest

binding strength.

Previously in this lab, the binding in ions of the gas-phase complexes of wild type

Cex and three variants of Cex with the noncovalent inhibitors, X$_2$IF, X$_2$IL and X$_2$DNJ

was studied with collision cross section measurements and MS/MS experiments [58].

Mass spectra showed ions of Cex, Cex binding both a single inhibitor and two inhibitors.

Because Cex has only a single binding site, the minor peak corresponding to Cex with

two inhibitors was attributed to non-specific binding. Triple quadrupole tandem MS

showed that the relative binding strengths of +9, +10 and +11 ions of all forms of Cex

binding each of the three inhibitors in the gas phase parallel the free energy changes,

ΔG^0_{sol}, for binding in solution, calculated from the inhibition constants K_i (Table 5.1).

Complexes have lower cross sections than free protein ions, and the cross sections of the

complexes decrease as the gas-phase binding strengths increase. It was concluded that all

the hydrogen bonds between the inhibitors and the enzyme that are involved in solution

binding are preserved in the gas-phase complexes, and therefore that the gas-phase

enzyme retains its specific solution binding characteristics.

In this study, we have extended our earlier work by using solution and gas-phase

H/Dx of Cex with the three noncovalent inhibitors, X$_2$IF, X$_2$IL and X$_2$DNJ, to gain

further insights into the properties of the solution and gas-phase complexes. Here a

different version of the catalytic domain of Cex with a 6-histidine tag (H_6-Cex-cd) is used. Compared with the Cex-cd used previously (MW 34,850.1 Da), H_6-Cex-cd (MW 35,824.9 Da) has 3 additional amino acid residues and differs in 50 residues. Despite the sequence difference, the -1 and -2 binding sub-sites are identical in these two proteins, as shown in Scheme 5.1. Because this enzyme has a different sequence and gives slightly different charge states in mass spectra (+11 and +12 here, +10 and +11 in [58]), we have repeated the cross section and tandem mass spectrometry measurements with ions of +11 and +12 charge states. With the +11 ions, the results of both experiments are in good agreement with the previous study [58], indicating that the sequence changes at non-binding sites do not significantly influence the binding strengths or conformations of the gas-phase Cex-inhibitor complexes.

Mass spectra show higher abundances of free protein than the abundances calculated to be present in solution from K_i values. We show that these protein ions are mostly formed by dissociation of ions of the complexes in the ion sampling process. In solution, complexes have lower H/Dx levels than free Cex. The complexes and Cex from a solution with the inhibitors show the same H/Dx levels, showing that the protein is almost entirely bound in solution, as calculated, and providing additional evidence that the protein ions observed in the mass spectra are formed in the ion sampling process. As seen previously [58], cross section measurements here show ions of the complexes have more compact conformations than ions of Cex from a solution of Cex alone. Surprisingly, Cex ions from solutions with an inhibitor have lower cross sections than Cex ions from a solution of Cex alone, and cross sections similar to the complexes, suggesting that these Cex ions "remember" their solution conformations. In gas-phase H/Dx, ions of the

114

complexes generally show *greater* H/Dx levels than ions of Cex with the same charge.

Unlike the cross sections, the H/Dx levels of the complexes do not correlate with the

relative gas-phase binding strengths measured by MS/MS, suggesting the ions may fold

or unfold when trapped for up to 15 s for H/Dx. Cex ions from solutions with Cex alone,

and Cex ions from solutions with an inhibitor, which have different cross sections, show

the *same* H/Dx levels after 15 s, also suggesting ions may fold or unfold when trapped for

H/Dx. Overall, the gas-phase complexes have more compact conformations than free

protein ions on the ca. 1 ms time scale of cross section measurements, and retain different

and possibly more folded conformations than the Cex ions on the seconds time scale of

H/Dx experiments.

Table 5.1. Inhibition constants, calculated Cex and complex concentrations, and ratios of complex to Cex concentration with initial total solution concentrations of Cex and inhibitor of 10 μM and 33 μM respectively.

Inhibitor	K_i (μM)[a]	[Cex] (μM)	[complex] (μM)	[complex]/[Cex]
X_2DNJ	5.8	1.89	8.11	4.29
X_2IL	0.33	0.14	9.86	70.4
X_2IF	0.13	0.056	9.94	177

[a] $K_i = \dfrac{[\text{Cex}] \times [\text{inhibitor}]}{[\text{complex}]}$

(a) Cex-cd

VVKPAQA
RTTPAPGHPA RGARTALRTT
LAAAAATLVV GATVVLPAQA
ATTLKEAADG AGRDFGFALD
PNRLSEAQYK AIADSEFNLV
VAENAMKWDA TEPSQNSFSF
GAGDRVASYA ADTGKELYGH
TLVWHSQLPD WAKNLNGSAF
ESAMVNHVTK VADHFEGKVA
SWDVVNEAFA DGGGRRQDSA
FQQKLGNGYI ETAFRAARAA
DPTAKLCIND YNVEGINAKS
NSLYDLVKDF KARGVPLDCV
GFQSHLIVGQ VPGDFRQNLQ
RFADLGVDVR ITELDIRMRT
PSDATKLATQ AADYKKVVQA
CMQVTRCQGV TVWGITGAS

(b) H6-Cex-cd

ASHH HHHHIEGRAS
ATTLKEAADG AGRDFGFALD
PNRLSEAQYK AIADSEFNLV
VAENAMKWDA TEPSQNSFSF
GAGDRVASYA ADTGKELYGH
TLVWHSQLPD WAKNLNGSAF
ESAMVNHVTK VADHFEGKVA
SWDVVNEAFA DGGGRRQDSA
FQQKLGNGYI ETAFRAARAA
DPTAKLCIND YNVEGINAKS
NSLYDLVKDF KARGVPLDCV
GFQSHLIVGQ VPGDFRQNLQ
RFADLGVDVR ITELDIRMRT
PSDATKLATQ AADYKKVVQA
CMQVTRCQGV TVWGITDKYS
WVPDVFPGEG AALVWDASYA
KKPAYAAVME AFGAS

X: binding sites for the distal xylose from X_2DNJ
X: binding sites for the proximal sugar from X_2DNJ

Scheme 5.1. Sequence of the Cex catalytic domain, (a) Cex-cd used in [58] and (b) H6-Cex-cd used in this work. Residues involved in binding the proximal aza-sugar and distal xylose of X_2DNJ are shown in red. Differences in sequence at the N and C termini are shown in blue.

116

5.2 Experimental Section

5.2.1 Triple Quadrupole MS System and Solution H/Dx

For solution H/Dx experiments, a home-built triple quadrupole mass spectrometer described previously was used [58, 78]. Stock solutions of Cex and inhibitors were mixed to a concentration of 160 μM of Cex and 528 μM of inhibitor. For H/Dx analysis, the solutions were diluted in 10 mM deuterated ammonium acetate and 90/10 (v/v) D_2O/ CD_3OD, to a final concentration of 10 μM in Cex and 33 μM in inhibitor. The same solvent was used for H/Dx of Cex alone. The corrected pD in solution was 7.1 at room temperature (pD = pH meter reading + 0.4) [190]. Samples in D_2O were immediately infused into a pneumatically assisted ESI source with a syringe pump (Harvard Apparatus, St. Laurent, QC, Canada) at 1 μL/min. Positively charged gaseous ions pass through an aperture in a curtain plate, an orifice-skimmer region with a voltage difference ($\Delta V_{ori\text{-}ski}$) of 100 V, then enter a quadrupole ion guide Q0 operated at 9 mTorr (N_2) for collisional cooling [152]. After passing through a short radio frequency quadrupole, ions enter a quadrupole Q1 for mass analysis with quadrupoles Q2 and Q3 used as ion guides. Pulse counting is used for ion detection. Spectra were then recorded repeatedly at different time intervals for one hour. The number of hydrogens exchanged is calculated from the mass difference between the intact protein and the deuterated protein. ES Tuning mix (Agilent, Santa Clara, CA, USA) was used for mass calibration.

5.2.2 Collision Cross Sections and MS/MS

For cross section and MS/MS measurements, experiments were done with the same triple quadrupole mass spectrometer with modifications to the ion sampling and vacuum system to increase sensitivity, as described in chapter 2 [178]. For cross section experiments, Q1 is operated as an ion guide and Q3 as a mass filter. For MS/MS, both Q1 and Q3 are operated as mass filters and Q2 as a collision cell.

When ions pass through low-density gas (argon) in Q2, they lose axial kinetic energy through multiple non-reactive collisions. The energy losses can be related to collision cross sections with an aerodynamic drag model [81] by [78, 153, 178, 189] (equation 1.4),

$$\frac{E}{E^0} = \exp\left(-\frac{C_{Dd}nm_2l\sigma}{m_1} \right)$$

(1.4)

where E is the ion kinetic energy at the cell exit, E^0 is the ion kinetic energy at the cell entrance, C_{Dd} is a drag coefficient, n is the gas number density, m_1 is the protein ion mass, m_2 is the collision gas mass, l is the length of the collision cell and σ is the collision cross section. To determine energy losses, the Q2 pressure was systematically increased from 0.0 to 1.2 mTorr, measured with a precision capacitance manometer (model 120AA; MKS Instruments, Boulder, CO, USA). Stopping curves were measured at each pressure by systematically increasing the Q3 rod offset voltage. Cross sections were then

calculated by plotting $-\ln\dfrac{E}{E^0}$ versus $\dfrac{C_{Dd}nm_2l}{m_1}$.

In MS/MS, precursor complex ions are mass selected in Q1, and have multiple

energetic collisions with Ar in Q2 leading to dissociation. Fragment ions are then mass

analyzed in Q3. To compare relative binding strengths of the complexes, the total internal

energies added to ions in Q2, ΔE_{int}, are determined with a collision model [58, 79, 189]

which corrects for losses of kinetic energy as the precursor ions move through the cell

and for the different numbers of collisions of ions with different collision cross sections.

Values of ΔE_{int} are calculated from (equation 1.11)

$$\Delta E_{int} = \Phi \frac{m_2}{M} E^0 \frac{m_1}{m_2} \frac{1}{C_{Dd}} \left[1 - \exp\left(-\frac{C_{Dd} n m_2 \sigma l}{m_1} \right) \right]$$

(1.11)

where Φ is the average fraction of center-of-mass kinetic energy transferred to internal

energy in a collision (taken to be 1.0), and $M = m_1 + m_2$. The initial kinetic energy of the

complex ions per charge, E^0, is taken as the difference in rod offsets between Q0 and Q2

which causes one half of the precursor ions to dissociate in Q2. For each complex, values

of ΔE_{int} were determined with at least three cell pressures from 0.5 mTorr to 2.74 mTorr.

At each pressure the time available for reaction occurring over a length of ca. 5 cm near

the cell exit was determined as previously described (see equation 3.1) [58, 79].

5.2.3 Trap-TOF MS System and Gas-Phase H/Dx

Gas-phase H/Dx experiments were done with a home-built linear quadrupole ion trap

reflectron time-of-flight mass spectrometer system (LIT-TOF MS), as described in

chapter 3 [46, 100, 153, 194]. Ions, generated by pneumatically assisted ESI, pass

through a curtain plate, a dry nitrogen curtain gas, and an orifice-skimmer region with a voltage difference of 150 V to 180 V. In control experiments, Cex or Cex complex ions continuously pass through a chamber with two consecutive ion guide quadrupoles, Q0 (ΔV_{ski-Q0} = 5 V) and Q1, in the presence of 10 mTorr of N_2, with the pressure controlled by a gate valve between the chamber and a turbo pump. For H/Dx experiments, the chamber was maintained at 4 mTorr of N_2, then filled with 6 mTorr of D_2O vapor controlled with a needle valve (SS-SS4-Al; Swagelok, Solon, OH, USA), to a total pressure of 10 mTorr. Ions are confined axially in Q1 by adding timed DC stopping potentials to the entrance and exit lenses for up to 20 seconds [189]. Following this, the exit lens voltage is lowered and ions drain through a stack of lens for mass analysis with a reflectron TOF. The extent of exchange is determined by the mass increase between the control and exchange experiments. Mass spectra for non-deuterated Cex were recorded repeatedly at the beginning and the end of each trial to ensure no instrumental mass drift occurred. A solution of CsI was used for mass calibration.

5.2.4 Solutions and Reagents

Cex and the inhibitors were provided by Stephen Withers' group, UBC. Cex stock solution (8 µL, 20 mg/ml) was desalted by buffer exchange with 550 µL NH_4Ac (12.5 mM) with a 10 kDa MWCO membrane (Millipore, Carrigtwohill, Co. Cork, Ireland), with centrifugation at 11,000 rpm for 10 min each, with eight cycles (MSE MicroCentaur, London, UK), to give a pure Cex stock solution of 200 µM in 12.5 mM NH_4Ac.

For mass spectra of Cex alone, the Cex stock solution was diluted to 10 μM in 10 mM NH$_4$Ac and H$_2$O/MeOH 90/10 (v/v) at pH 6.6 measured with a Accumet model 15 pH meter (Fisher Scientific, Fairlawn, NJ, USA). For mass spectra of the complexes, the inhibitors were mixed with Cex at room temperature. The final solutions contained 10 μM Cex and 33 μM inhibitor with the same solvent composition as the solution with Cex alone. Deuterated solutions are described above.

Cesium iodide (manufacturer's stated purity 99%) was from Sigma-Aldrich, St. Louis, MO, USA. Methanol (HPLC grade) and NH$_4$Ac (ACS grade) were from Fisher Scientific, Fairlawn, NJ, USA. Deuterium oxide (99.9%) and methanol-d4 (99.8%) were from Cambridge Isotope Laboratories, Inc., Andover, MA, USA. Nitrogen and argon (manufacturer's stated purity 99.999%), and air (breathing grade) were from Praxair, Mississauga, ON, Canada.

5.3 Results and Discussion

5.3.1 Mass Spectra

Figure 5.1a and 5.1b show ESI triple quadrupole MS spectra of Cex and Cex−X$_2$IL complexes over the +10 to +14 charge state region. Cex binds specifically to one inhibitor molecule. With both Cex and the complexes, the +11 and +12 ions dominate the mass spectra, with +10 ions of lower intensity. With the two other complexes,

121
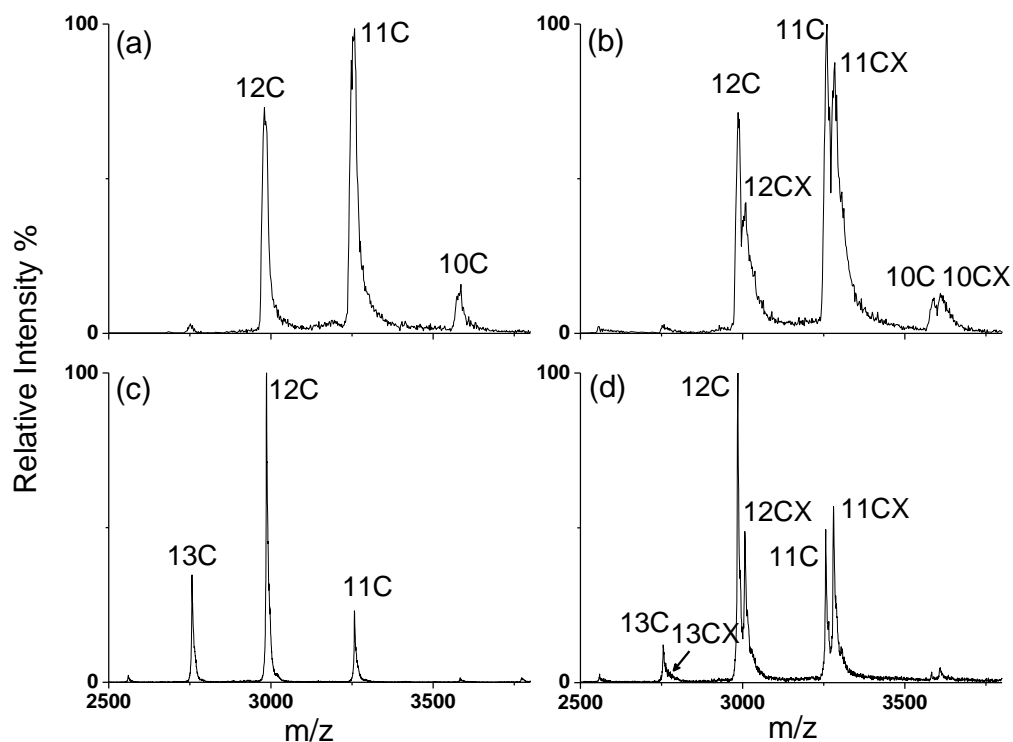
Figure 5.1. ESI MS spectra recorded with the triple quadrupole MS of (a) Cex alone and (b) Cex complexes with X_2IL, and with the LIT-TOF MS of (c) Cex alone and (d) Cex with X_2IL. Charges are labeled. Notation: C, Cex; CX, Cex-inhibitor complex.

Cex−X_2DNJ and Cex−X_2IF, spectra were similar with slightly less intense +12 ions and slightly more intense +10 ions (data not shown). Compared to previous spectra with Cex-cd with the triple quadrupole MS [58], the H_6-Cex-cd protein and its complexes produce significantly more abundant +12 ions, less abundant +10 ions, and no +9 ions. This was seen with both our old and new ion sampling interfaces, indicating the differences in mass spectra do not come from the instrumental changes but may be attributed to the

sequence differences. The six-histidine tags near the N-terminus of H_6-Cex-cd may increase the charging of the protein.

Figure 5.1c and 5.1d show mass spectra of Cex and Cex−X_2IL complexes recorded with the LIT-TOF MS which gives higher resolution and better peak shapes. Ions with +11 to +13 charges appear in the mass spectra. On average the ions appear somewhat more highly charged, compared with spectra with the triple quadrupole MS. This may due to the different ion sampling processes and instrumental operating conditions of these two systems. When Cex binds the inhibitor, the +13 ions decrease in intensity and the +11 ions increase in intensity. Similar spectra are seen with Cex−X_2DNJ and Cex−X_2IF.

The ratios of intensities of complex ions to Cex ions in the mass spectra do not match the ratios of the solution abundances calculated from the values of K_i, listed in Table 5.1. The observed ratios are substantially affected by the instrument operating conditions. In experiments with the triple quadrupole MS, with the orifice-skimmer voltage difference kept at 100V, increasing the voltage difference between the skimmer and Q0 (ΔV_{ski-Q0}) produces more Cex ions because the increased internal energy added to the complexes in Q0 causes greater dissociation of the complexes. For example, if ΔV_{ski-Q0} is set to 30 V, almost equal levels of ions of Cex and complexes are seen. If ΔV_{ski-Q0} is decreased to 10 V, with Cex−X_2DNJ, the ratio of the intensities of ions of the complex to Cex ions increases to about 4 to1, similar to the calculated abundance ratio in solution. At $\Delta V_{ski-Q0} = 10$ V, with Cex−X_2IL and Cex−X_2IF solutions, the intensity ratios of Cex ions to complex ions are less than 0.1 and 0.05, respectively. In experiments with the LIT-

TOF MS, where the skimmer-Q0 voltage difference is only 5.0 V, the orifice-skimmer voltage difference affects the ratio of complex to Cex ions. Higher voltage differences lead to more dissociation of the complexes. The relatively lower abundances of complexes in mass spectra compared to calculated solution abundances then derive at least in part from dissociation of complexes in the ion sampling interfaces.

5.3.2 Collision Cross Sections

Table 5.2 shows collision cross sections of Cex and Cex−inhibitor complex ions with +11 and +12 charges. Uncertainties are standard deviations of three separate measurements. For Cex ions, cross sections were determined in two ways: first, with Cex ions from a solution containing only Cex, and second with Cex ions from solutions of Cex and the inhibitors. With all three inhibitors, Cex−inhibitor complexes (CX) have cross sections lower than Cex ions from a solution of Cex alone, as seen in [58], indicating a more compact structure is adopted by the gas-phase complex ions. Among the different complexes, Cex−X_2DNJ and Cex−X_2IL have similar cross sections, 11% larger than cross sections of Cex−X_2IF. This is reasonable because Cex−X_2IF also has the strongest binding in the gas phase (see below). For the +11 ions of Cex and Cex−inhibitor complexes, where comparisons are possible, the cross sections here agree with those of Tesic et al. [58] within about 2.0%. Thus the global conformations of the protein and complexes are unchanged by the differences in the sequences remote from the binding site. The decrease of cross sections with increasing binding strength in the ions is purely a gas-phase effect. Structures of apo-Cex-cd and its complexes were reported to be

124

"essentially identical" based on NMR [15] and X-ray crystallographic analysis [16, 18, 195]. For the complex ions, and Cex ions formed from the solutions containing an inhibitor, the +12 ions have somewhat larger cross sections than the +11 ions. Adding one charge is sufficient to change the conformations. However within the uncertainties, this effect is not seen with the more unfolded ions of Cex formed from a solution of Cex alone.

Table 5.2. Collision cross sections ($\mathring{A}^2$) of ions of Cex and its complexes.

Charge	Cex	Cex–X$_2$DNJ		Cex–X$_2$IL		Cex–X$_2$IF	
		C[a]	CX[b]	C	CX	C	CX
+11	1816±57	1566±67	1545±53	1602±59	1552±14	1621±52	1387±48
+12	1833±62	1666±69	1617±39	1671±47	1594±53	1709±39	1454±49

[a]C: Cex from a mixture of Cex and inhibitor

[b]CX: Cex-inhibitor complex

Cex ions (C) from solutions of the complexes are also more compact than Cex ions from a solution of Cex alone. With X$_2$DNJ and X$_2$IL, Cex and complex ions gave similar cross sections (within 5%). With X$_2$IF, Cex shows a 17% larger cross section than the complex but still 7% less than Cex from a solution of Cex alone. As discussed above, these Cex ions are mostly formed when complexes are injected into and dissociate in Q0. Interestingly, these Cex ions apparently retain some memory of their origin on the ca. 1

ms time scale of the collision cross section measurements. Solution H/Dx provides additional evidence that these Cex ions are not present in solution, but are formed in the ion sampling process (see below). Knapman et al. [76] measured cross sections of fragment ions formed by loss of monomers in MS/MS experiments with several protein−protein complexes. In some cases, GroEL (a 14-mer), hemoglobin (a tetramer), and a hexamer of a virus capsid protein, MS2, the fragment ions collapsed and had substantially smaller cross sections than expected from a simple removal of a monomer from the multimer. However with major histocompatibility complex class 1(MHC1) and a decamer of the virus capsid protein, fragment ions had cross sections close to what was expected from the species within the complex, and the fragment ions "remembered" their conformations within the complex. Although the dissociation of this protein−small-molecule complex studied here cannot be compared directly to the dissociation of a protein−protein complex, it is interesting that in both cases the proteins appear to retain their conformations within the complex after dissociation.

5.3.3 MS/MS of Noncovalent Complexes

In MS/MS, an enzyme−inhibitor complex ion dissociates to one Cex ion plus a neutral or charged inhibitor, as shown in Figure 5.2. Precursor ions of higher charge (+12) give higher yields of charged inhibitor loss than ions with lower charges (+10 and +11). This was not observed in the previous study with ions of +9 to +11 charges [58]. This charge-dependent MS/MS is most evident with Cex−X_2DNJ. With +10 ions, neutral inhibitor loss dominates (Figure 5.2a). With +11 ions, the ratio of neutral to charged inhibitor loss

126
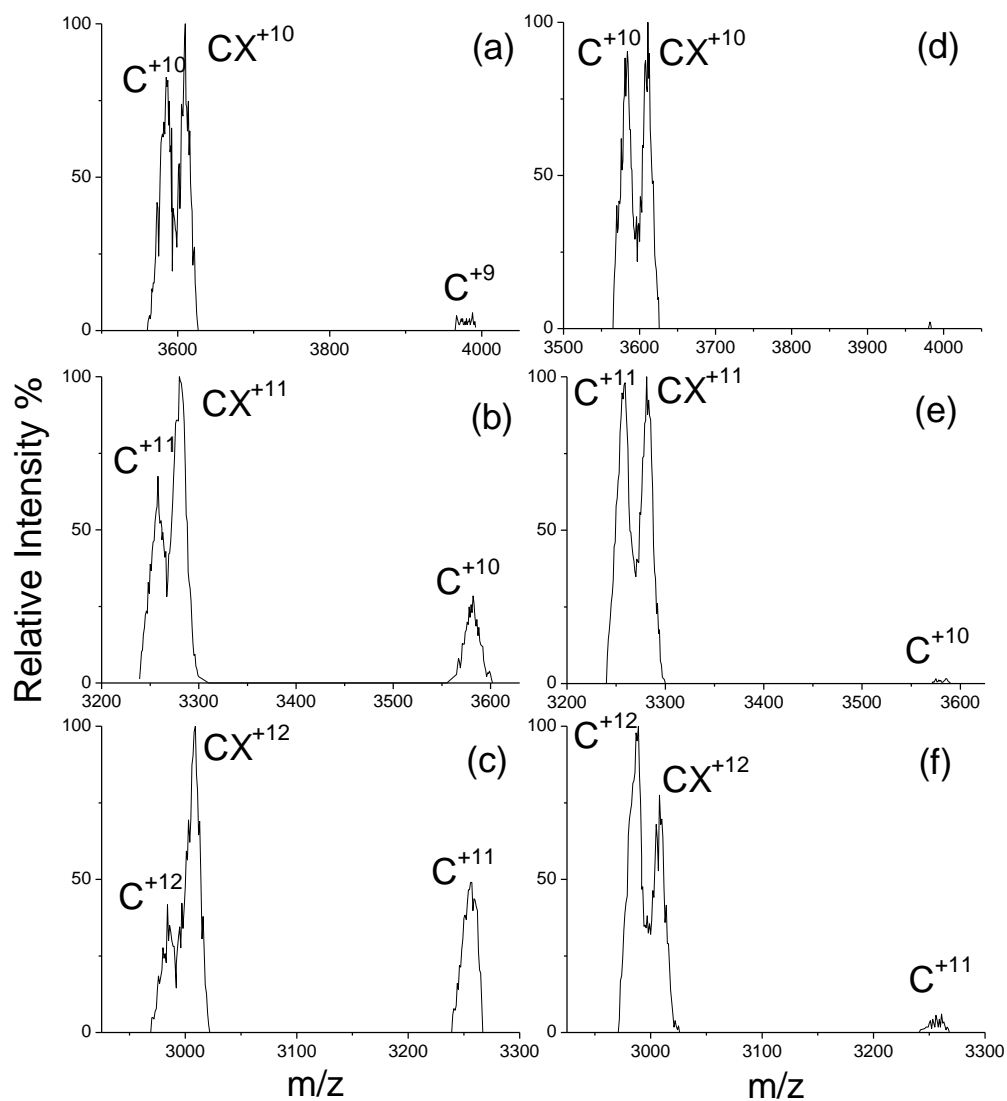
Figure 5.2. MS/MS spectra of +10, +11 and +12 ions of Cex-X$_2$DNJ (a, b, c), and of Cex-X$_2$IL (d, e, f), under conditions with nearly 50% fragment yield.

is approximately 3 to 1 (Figure 5.2b), while +12 ions dissociate by losing neutral and charged inhibitor almost equally (Figure 5.2c). With X_2IL, approximately 4% charged inhibitor loss was found with the +12 charged complexes (Figure 5.2f), while the +11 and +10 ions showed mainly neutral loss (Figure 5.2d and 5.2e). Cex−X_2IF showed predominantly neutral inhibitor loss, consistent with previous results [58].

To compare gas-phase binding strengths quantitatively, the internal energy added to ions in the collision cell, ΔE_{int}, was determined at different cell pressures, which have different times available for reaction. For each complex, ΔE_{int} was plotted vs. the time available for reaction, with the results shown in Figure 5.3. Only small differences in values of ΔE_{int} between the +11 and +12 ions were observed for Cex−X_2IL and Cex−X_2IF. With +12 Cex−X_2DNJ ions, less internal energy, ΔE_{int}, is required for dissociation than with +11 Cex−X_2DNJ ions, possibly because with the charged inhibitor loss, Coulomb repulsion lowers the additional internal energy required [84]. The order of the binding strengths in the gas-phase ions is: $X_2IF > X_2IL > X_2DNJ$, the same order as the values of ΔG^0_{sol} for dissociation in solution, as was found in [58]. For direct comparison with the previous results [58], the values of ΔE_{int} required to induce dissociation in 25 μs were read from the graph, and are shown in Table 5.3. With the +11 ions, where comparisons are possible, the ΔE_{int} values agree with those of Tesic et al. [58] within 7% or better, and within the combined uncertainties, indicating the gas-phase noncovalent binding energy of this version of Cex is not significantly influenced by the sequence alteration.
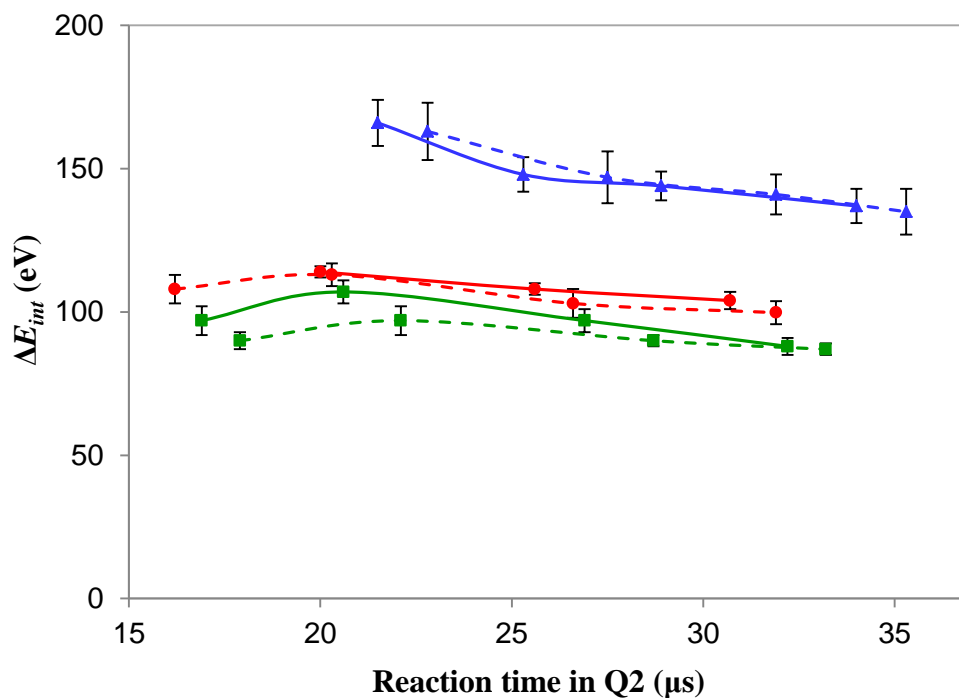
Figure 5.3. Values of ΔE_{int} vs. the time available for reaction for the +11(solid lines) and +12 (dashed lines) ions of Cex$-$X$_2$DNJ (green), Cex$-$X$_2$IL (red) and Cex$-$X$_2$IF (blue).

Table 5.3. Internal energies (eV) required to cause 50% dissociation of the complexes in 25 µs.

ion	+11	+12
Cex$-$X$_2$DNJ	100.5$\pm$5	94.7$\pm$5
Cex$-$X$_2$IL	108.5$\pm$3	105.5$\pm$5
Cex$-$X$_2$IF	149$\pm$8	155$\pm$10

5.3.4 Solution H/Dx

Measurements of solution H/D exchange were performed with solutions containing Cex only, then solutions of Cex with an inhibitor. The exchange levels were monitored at different time intervals over one hour, with an example shown in Figure 5.4 for +11 Cex−X_2IF ions. The first data were collected 3 min after the exchange started and at this time the exchange was already nearly complete. At pD 7.1, 99% of unprotected backbone amide and side chain hydrogens are expected to exchange with D_2O within 1 s [88, 92]. During the exchange, single peaks that moved to higher mass were seen, indicating an EX2 mechanism [1], as expected [15]. The numbers of hydrogens exchanged after 60 min by Cex and the complexes, measured with the +11 ions are listed in Table 5.4. The same exchange levels were measured on the +10 and +12 ions (data not shown). As shown in Table 5.4, Cex ions from a solution of Cex alone consistently show higher exchange levels than Cex−inhibitor complexes and Cex ions from a solution containing the inhibitors. No differences in H/Dx levels were seen with Cex binding to different inhibitors. These noncovalent complexes all have basically the same X-ray structures [15, 16, 18, 195]. Apparently the different inhibitors stabilize the protein against fluctuations that lead to H/D exchange to the same extent.

The H/Dx levels of Cex ions from solutions containing the inhibitors were also measured. Cex from solutions containing the inhibitors show the same exchange levels as the complexes (Figure 5.4 and Table 5.4). As discussed above, these Cex ions are likely formed from dissociation of ions in the skimmer-Q0 region of the triple quadrupole MS. Because the deuterium uptake is complete in solution, and, from the values of K_i it is
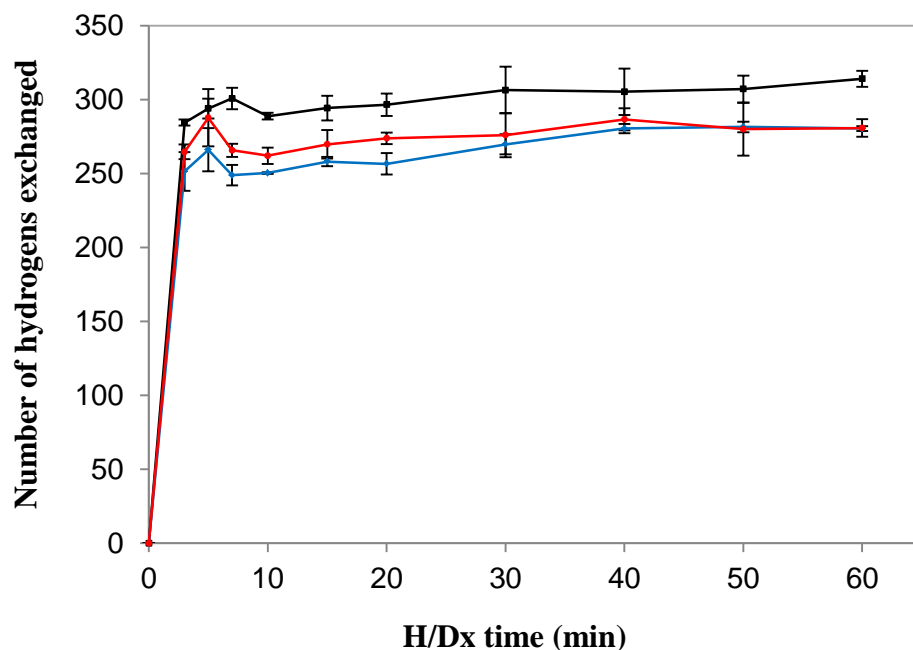
Figure 5.4. Numbers of hydrogens exchanged in solution as a function of reaction time measured with +11 Cex ions from a solution of Cex alone (black), from a solution of Cex with X_2IF (blue), and with +11 ions of the Cex-X_2IF complex (red).

calculated that Cex is almost entirely bound to inhibitors in solution (Table 5.1), these Cex ions come from Cex which is bound to inhibitors in solution, and show the same exchange levels as the complexes.

As shown in Table 5.4, after one hour H/D exchange, Cex from a solution of Cex alone exchanges 314 ± 5 hydrogens, 38 ± 11 (14%) more than Cex$-X_2DNJ$ and 33 ± 11 (12%) more than Cex$-X_2IL$ and Cex$-X_2IF$. Two factors account for the lower H/Dx levels with complexes. First, the interactive maps [16] show that about 10 hydrogens are

Table 5.4. Numbers of hydrogens exchanged after one hour of solution H/Dx.

Cex alone		314 ± 5
Cex–X$_2$DNJ	C[a]	281 ± 14
	CX[b]	276 ± 10
Cex–X$_2$IL	C	280 ± 6
	CX	281 ± 10
Cex–X$_2$IF	C	280 ± 2
	CX	281 ± 6

a. C: Cex from a solution of Cex–inhibitor mixture

b. CX: Cex–inhibitor complex

involved in intermolecular hydrogen bonding between the inhibitor and enzyme. Second, NMR studies by Poon et al. [15, 196], show the enzyme has less flexible conformations after binding the inhibitors, thus reducing fluctuations around the binding site. In their studies, binding of the inhibitor 2,4-dinitrophenyl 2-deoxy-2-fluro-β-cellobioside to Cex-cd was described. This inhibitor has the same noncovalent binding through hydrogen bonds to the enzyme as the inhibitors used here, except that it forms a covalent bond to Glu233 with loss of dinitrophenol. Binding to the inhibitor clearly stabilized fluctuations of Cex-cd, leading to reduced hydrogen exchange in both the short term ($<$ 65 hours) and the long term (500 days) of at least 12 amide protons and their side chains that are clustered around the active site. From their results, it can be calculated that at least 22

hydrogens are protected when the inhibitor is bound. This is fewer than we find because in the NMR experiment not all residues were resolved, and thus only a lower limit to the number of protected hydrogens was given. Because the protein in the complex has the same global conformation as the free protein in solution [15, 16, 18, 195], it is the loss of fluctuations that open up the protein for H/Dx that reduces the number of hydrogens exchanged.

5.3.5 Gas-Phase H/Dx

Gas-phase H/Dx experiments were performed with the +11, +12 and +13 ions of Cex and Cex−inhibitor complexes with the LIT-TOF MS. During the exchange no bimodal isotopic distributions were seen, suggesting that a single conformation is present for each of the ions, or that the ions fluctuate between different conformations on a time scale much shorter than the exchange time (EX2 mechanism). As an example, the numbers of hydrogens exchanged vs. trapping time by gas-phase ions of Cex and gas-phase ions of Cex−X_2DNJ complexes are shown in Figure 5.5. In the first two seconds, Cex and the complexes exchange about the same number of hydrogens. Following this, ions of the complexes show somewhat greater rates of exchange than ions of Cex. After ca. 12 s the exchange is mostly complete. Similar exchange behavior is seen with the Cex−X_2IF and Cex−X_2IL ions (data not shown).
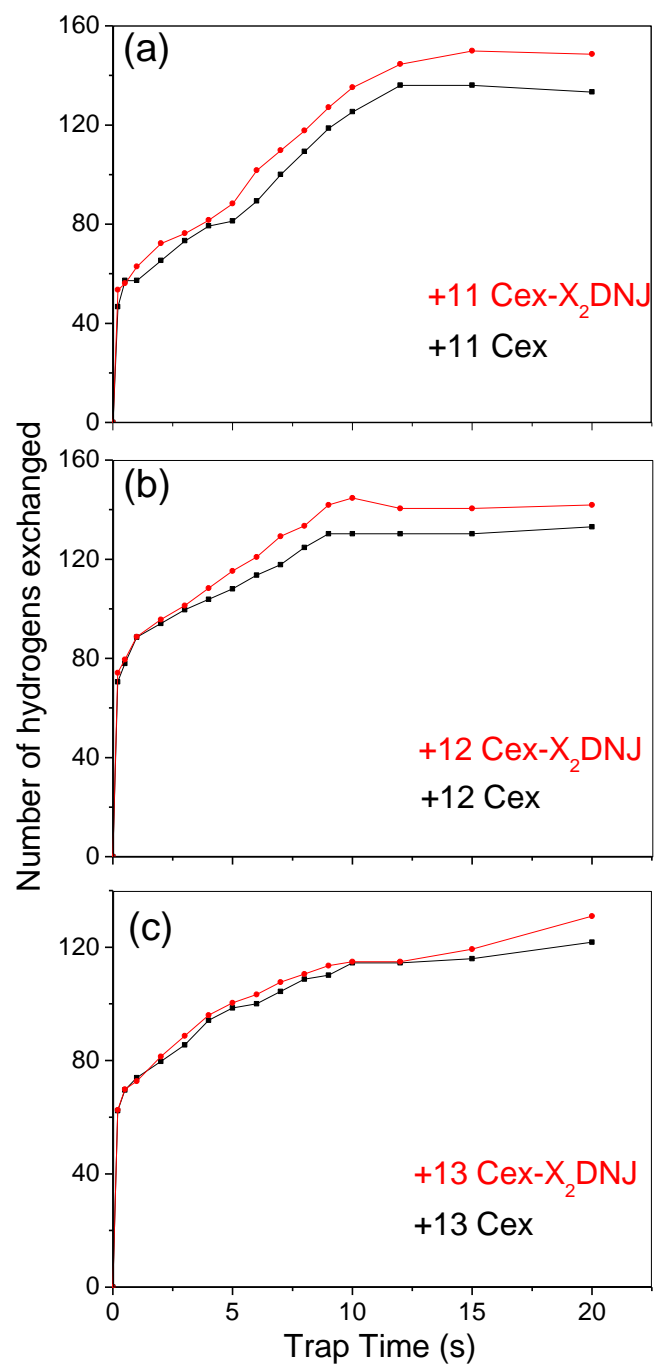
Figure 5.5. Gas-phase H/Dx levels as a function of trap time of Cex (black) and

Cex-X$_2$DNJ (red) ions with (a) +11, (b) +12 and (c) +13 charges.

The numbers of hydrogens exchanged after 15 s of trapping in D_2O vapor are shown in Table 5.5a. For a given charge, the complexes of Cex−X_2DNJ and Cex−X_2IF exchange about the same number of hydrogens. The +11 and +12 ions of Cex−X_2IL exchange fewer hydrogens than the +11 and +12 ions of Cex−X_2DNJ and Cex−X_2IF, but +13 Cex−X_2IL ions exchange almost the same number as +13 ions of Cex−X_2DNJ and Cex−X_2IF. The binding strengths in the gas phase follow the order: Cex−X_2IF > Cex−X_2IL > Cex−X_2DNJ (Table 5.3). Thus the numbers of hydrogens exchanged do not correlate with the binding energies.

Table 5.5. a. Numbers of hydrogens exchanged after 15 s of gas-phase H/Dx. b. Exchange levels of +12 and +13 ions relative to +11 ions.

a			
ion	+11	+12	+13
Cex−X_2DNJ	152±4	141±2	115±6
Cex−X_2IL	140±3	122±2	112±6
Cex−X_2IF	157±2	148±2	108±2
Cex	131±4	124±7	109±5
b			
ion	+11	+12	+13
Cex−X_2DNJ	1.00	0.93±0.03	0.76±0.04
Cex−X_2IL	1.00	0.87±0.02	0.80±0.05
Cex−X_2IF	1.00	0.94±0.02	0.67±0.01
Cex	1.00	0.95±0.06	0.83±0.05

Unexpectedly, the +11 and +12 ions of Cex, exchange *fewer* hydrogens than the +11 and +12 ions of the complexes with all three inhibitors (Table 5.5a). The differences in exchange levels between Cex and the complexes decrease with increasing charge state. The +13 Cex ions and the +13 ions of the complexes exchange about the same number of hydrogens. Adding charges to the complex ions slightly increases the collision cross sections (Table 5.2), but apparently *decreases* the number of hydrogens exchanged (Table 5.5a). Exchange levels of +12 and +13 ions relative to +11 ions are shown in Table 5.5b. The decreases in these relative exchange levels with increasing charge are about the same for ions of the protein alone and the three complexes.

While Cex ions from a solution of protein alone show greater cross sections than Cex ions from a solution containing the inhibitors, Cex ions formed from these two solutions exchange the same number of hydrogens after 15 s of H/Dx in the gas phase. If Cex ions formed from dissociation of complex ions in the orifice-skimmer region of the trap-TOF MS also have more compact conformations than Cex ions from a solution of Cex alone, they appear to adopt similar conformations when trapped in the gas phase for up to 15 s.

Gas-phase H/D exchange occurs via different mechanisms than solution H/Dx, as discussed in chapter 1. Sites that can readily exchange in solution do not necessarily exchange in the gas phase [99]. H_6-Cex-cd has 581 exchangeable hydrogens. In the gas phase, +11 Cex ions exchange 23% of the exchangeable hydrogens, much lower than the 54% in solution. The noncovalent complexes exchange fewer hydrogens than the protein alone in solution, but more in the gas phase. This may be a result of the relay mechanism with D_2O as a reagent in gas-phase H/Dx [87]. For exchange, a hydrogen must be

136

accessible on the surface of the protein, but also must be near a charged site, such as the N-terminal or charged side chains, such as Arg, His and Lys. If binding the inhibitor leads to a more folded structure in the gas phase, as observed in the cross section measurements, some backbone amides on Cex may be closer to the charged sites, making H/Dx possible and leading to an increase in exchange rate as well as exchange level. With Cex alone, the hydrogens in these regions may be unable to complete H/D exchange because charged sites are farther from the exchangeable hydrogens. Increasing the charge on a complex ion or on a Cex ion alone causes the exchange level to decrease, indicating that the addition of a single charge to the ions can change the conformations. This decrease in exchange level can also be explained with the relay mechanism. Ions with more charges generally have greater cross sections, corresponding to more unfolded conformations, which increase the distances between charged and exchange sites and results in a decrease in exchange levels [87].

Collision cross section and gas-phase H/Dx experiments provide insights into the gas-phase protein conformations. The cross section results illustrate that complex ions are more compact than free Cex ions on the ca. 1 ms time scale of the cross section measurements. The H/Dx results show that complex ions retain different and perhaps more folded conformations after 15 s of trapping at a pressure of 10 mTorr.

5.4 Summary

In this study we have probed the conformational changes of an enzyme noncovalently binding with small-molecule inhibitors. The gas-phase conformations and relative binding strengths of complexes are generally unchanged with sequence alterations far from binding sites. The relative gas-phase binding strengths measured by MS/MS follow the order, $X_2IF > X_2IL > X_2DNJ$, the same order as in solution.

Mass spectra of solutions containing the complexes show higher levels of free protein ions than expected. These Cex ions are mostly produced by dissociation of complex ions in the ion sampling process. In solution, Cex is almost entirely bound to inhibitors, and therefore exchanges the same number of hydrogens as the complexes. In the gas phase, these Cex ions show cross sections similar to the complexes, but give H/Dx levels similar to Cex ions from a solution of Cex alone, suggesting these ions "remember" their original solution conformations on the ca. 1 ms time scale of the cross section experiments, but may fold or unfold on the seconds time scale of the H/Dx experiments.

The addition of a single charge is sufficient to change the gas-phase conformations of ions of the noncovalent complexes. As charge is added, cross sections of all the ions slightly increase, while H/Dx levels decrease. The cross sections of ions of the complexes decrease as the binding strengths increase. However the H/Dx levels of the gas-phase complexes do not correlate with the binding strengths, also suggesting the ions may fold or unfold when trapped in the gas phase for several seconds.

In solution, complexes have lower H/Dx levels than Cex alone, consistent with previous NMR results [15] that show binding the inhibitors protects some hydrogens and reduces global fluctuations of the protein. In the gas phase, complex ions give smaller collision cross sections and, interestingly, *greater* H/Dx levels than ions of Cex. The interpretation of the gas-phase H/Dx results requires considering two competing effects. To exchange, an exchangeable proton must be on the surface of the protein, favoring greater exchange levels for more unfolded proteins. However an exchangeable hydrogen must also be near a charged site, favoring greater exchange levels of more folded ions of the same charge. Thus H/Dx gives little insight into the degree of folding. However different H/Dx levels can indicate different conformations of a given ion. Cross sections show complexes have more compact conformations on the time scale of ca. 1 ms. The H/Dx levels show at least the +11 and +12 complex ions retain different conformations from the Cex ions on the time scale of seconds.

The greater exchange levels of the noncovalent complexes are not inconsistent with complexes retaining more compact conformations of the time scale of seconds, but do not provide definitive evidence. In future, pulsed time-resolved gas-phase H/Dx [197] might be used to study conformational changes of these or other trapped ions.

Chapter 6 Conclusions

6.1 Hemoglobin

With 10% MeOH solutions, mass spectra of freshly prepared Hb show ions predominantly of tetrameric species with dimer and monomer subunits in lower abundance. Higher relative levels of monomer and dimer ions were seen when slightly destabilizing the proteins by changing the solvent to 10% ACN or 20% MeOH while lowering the protein concentration. Collision cross sections of holo-monomer, dimer and tetramer ions of Hb A are in good agreement with sizes of the same species measured in solution, indicating compact structures are preserved in the gas-phase ions. Changing the solvent from 10% MeOH to 10% ACN or 20% MeOH induce greater dissociation but did not influence the collision cross section results, indicating complex destabilization is not always indicated by a change in collision cross section.

As compared to fresh Hb, commercially obtained Hb gives higher levels of monomer and dimer ions, which derives at least in part from the oxidation observed on β globins as well as lyophilization of the proteins. The oxidative modification on β chains also leads to the formation of oxidized heme-deficient dimers. The use of commercial protein samples requires caution. Subtle changes to the proteins may produce unusual results.

Although freshly prepared human Hb A, Hb F and Hb S give similar mass spectra, both the single mutation in the β chain of Hb S and the sequence alterations of the γ chain of Hb F have an effect on the gas-phase properties of Hb complexes. Tetramer ions of Hb S have greater collision cross sections and greater gas-phase H/Dx levels than tetramer ions of Hb A and Hb F, indicating gas-phase Hb S tetramers have less compact structures

in the millisecond cross section measurements, and retain different and perhaps more unfolded conformations when trapped for several seconds. In MS/MS, dimers and tetramers of Hb F differ from the other two hemoglobins in binding strengths and dissociation patterns. Gas-phase tetramers of Hb F are more stable than tetramers of Hb A and Hb S. The order of the binding strengths of the gas-phase dimer ions is: Hb S > Hb A > Hb F. Dimer ions of Hb F dissociate to two monomers with a nearly equal division of the charges, while Hb A and Hb S dissociate with asymmetrical charge distributions. Comparison of ΔE_{int} and ΔG^0_{sol} values of dimers suggests that the gas-phase binding in dimers differs from that in solution. In solution, Hb F dimers are more strongly bound, but, in the gas phase, require less energy to dissociate. The stabilities of tetramers in solution and in the gas phase cannot be directly compared, due to the different dissociation pathways. Thus no consistent relationships between gas-phase stability and solution binding strengths are found.

In studies of solution H/Dx of Hb A, F and S, the home-made flow mix and ESI setup that substantially reduces the labeling time are used, making millisecond-H/Dx possible. Operational conditions should be controlled to minimize gas-phase dissociation while maintaining a high extent of desolvation. In contrast to the measurements of gas-phase conformations, no substantial differences in the conformations of these three hemoglobins are seen with solution H/Dx. The H/Dx kinetics of the tetrameric Hb and its subunits are of particular interest. The results are consistent with the known times for inter-conversions of tetramers to dimers (ca. 1 s) and dimers to monomers (minutes). With exchange times of less than 1 s, the H/Dx levels can represent conformations of individual species in solution, and the order of relative exchange levels is, tetramer <

dimer < monomer. With exchange times of 1 s to 3 s where the tetramer-dimer interconversion is involved, tetramers and dimers show the same relative exchange levels, which are less that of monomers. With exchange times of 10 minutes, tetramers, dimers and monomers of all three proteins show the same relative exchange levels. Our results suggest that when employing solution H/Dx in the conformational studies of a protein−protein noncovalent complex in equilibrium with its subunits, it is necessary to limit the exchange to times less than that required for dissociation and recombination of the complex. In cases where the rates of dissociation and recombination are not known, studies of H/Dx at different exchange times provide a potential method to reveal approximately these rates.

6.2 Cex−Inhibitor Complexes

In studies of Cex−inhibitor complexes, abundant Cex ions with intensities more than expected from solution binding constants are observed in mass spectra. These Cex ions are mostly formed by dissociation of complexes in the ion sampling interface. In solution H/Dx, these Cex ions show the same exchange levels as the complexes, since in solution they are almost entirely bound to inhibitors. In the gas phase, these Cex ions "remember" their original solution conformations on a ca. 1 ms time scale, showing collision cross sections similar to the complex ions. However these Cex ions "lose" their compact conformations on a time scale of seconds, showing gas-phase H/Dx levels similar to Cex ions from a solution of Cex alone.

Conformational changes in the enzyme noncovalently binding small-molecule inhibitors in solution and in the gas phase have been studied. In solution, Cex−inhibitor complexes have lower H/Dx levels than free Cex because binding the inhibitors blocks some sites from H/Dx and reduces fluctuations of the protein. In the gas phase, complex ions give smaller collision cross sections and interestingly *greater* H/Dx levels than Cex ions from a solution of Cex alone. The addition of a single charge is sufficient to change the gas-phase conformations of ions of noncovalent complexes. As charge is added, cross sections of all the complex ions slightly increase, while H/Dx levels decrease. The interpretation of gas-phase H/Dx results considers two effects, accessibility of an exchangeable amide and its proximity to a charged site. Thus gas-phase H/Dx alone cannot illustrate the degree of folding. However different H/Dx levels can indicate different conformations of a given ion. Cross sections show complexes have more compact conformations on the time scale of ca. 1 ms. The H/Dx levels show at least the complex ions with +11 and +12 charges retain different conformations from the Cex ions on the time scale of seconds.

The relative gas-phase binding strengths measured by MS/MS follow the order, $X_2IF > X_2IL > X_2DNJ$, the same order as in solution. As the binding strengths increase, the cross sections of complex ions decrease. However, this correlation does not apply to gas-phase H/Dx results, further suggesting the ions may fold or unfold and lose their solution binding characteristics when trapped in the gas phase for several seconds.

6.3 Further Work

Gas-phase H/Dx with D_2O vapor on a seconds time scale does not provide definitive evidence on protein conformations due to the complex reaction mechanism as well as the possible gas-phase structural changes during this exchange period. In future work, pulsed-time (at least millisecond) resolved gas-phase H/Dx might be used to study conformations of trapped protein ions without interruption of folding/unfolding transitions, and to monitor conformational changes over the trapping time for a better understanding of gas-phase H/Dx kinetics. A more efficient deuterium reagent with higher protein affinity can be selected, such as deuterated ammonia (ND_3), for enhanced exchange rates and the potential of proposing a different exchange mechanism [101].

Bibliography

1. Kaltashov, I. A., Eyles, S. J., *Mass Spectrom. Rev.* 2002, *21*, 37-71.

2. Kaltashov, I. A., Eyles, S. J., *Mass Spectrometry in Biophysics: Conformation and Dynamics of Biomolecules*, John Wiley and Sons, Inc., Hoboken 2005.

3. Kaddis, C. S., Lomeli, S. H., Yin, S., Berhane, B., Apostol, M. I., Kickhoefer, V. A., Rome, L. H., Loo, J. A., *J. Am. Soc. Mass Spectrom.* 2007, *18*, 1206-1216.

4. Kool, J., Jonker, N., Irth, H., Niessen, W. M. A., *Anal. Bioanal. Chem.* 2011, *401*, 1109-1125.

5. Hanson, C. L., Robinson, C. V., *J. Biol. Chem.* 2004, *279*, 24907-24910.

6. Heck, A. J. R., van den Heuvel, R. H. H., *Mass Spectrom. Rev.* 2004, *23*, 368-389.

7. Faull, P. A., Korkeila, K. E., Kalapothakis, J. M., Gray, A., McCullough, B. J., Barran, P. E., *Int. J. Mass Spectrom.* 2009, *283*, 140-148.

8. Feng, R., Castelhano, A. L., Billedeau, R., Yuan, Z. Y., *J. Am. Soc. Mass Spectrom.* 1995, *6*, 1105-1111.

9. Wicki, J., Williams, S. J., Withers, S. G., *J. Am. Chem. Soc.* 2007, *129*, 4530-4531.

10. Sun, J., Kitova, E. N., Sun, N., Klassen, J. S., *Anal. Chem.* 2007, *79*, 8301-8311.

11. Wang, W. J., Kitova, E. N., Sun, J. X., Klassen, J. S., *J. Am. Soc. Mass Spectrom.* 2005, *16*, 1583-1594.

12. Stumpf, M. P. H., Thorne, T., de Silva, E., Stewart, R., An, H. J., Lappe, M., Wiuf, C., *Proc. Natl. Acad. Sci. U. S. A.* 2008, *105*, 6959-6964.

13. Sharon, M., *J. Am. Soc. Mass Spectrom.* 2010, *21*, 487-500.

14. Loo, J. A., *Mass Spectrom. Rev.* 1997, *16*, 1-23.

15. Poon, D. K. Y., Ludwiczek, M. L., Schubert, M., Kwan, E. M., Withers, S. G., McIntosh, L. P., *Biochemistry* 2007, *46*, 1759-1770.

16. Notenboom, V., Williams, S. J., Hoos, R., Withers, S. G., Rose, D. R., *Biochemistry* 2000, *39*, 11553-11563.

17. Takano, T., *J. Mol. Biol.* 1977, *110*, 537-568.

18. Williams, S. J., Notenboom, V., Wicki, J., Rose, D. R., Withers, S. G., *J. Am. Chem. Soc.* 2000, *122*, 4229-4230.

19. Babu, K. R., Douglas, D. J., *Biochemistry* 2000, *39*, 14702-14710.

20. Boys, B. L., Kuprowski, M. C., Konermann, L., *Biochemistry* 2007, *46*, 10675-10684.

21. Abaturov, L. V., Yakobashvily, N. N., Jinoria, K. S., Molchanova, T. P., Varshavsky, Y. M., *FEBS Lett.* 1976, *70*, 127-130.

22. Tam, M. F., Chen, J., Tam, T. C. S., Tsai, C. H., Shen, T. J., Simplaceanu, V., Feinstein, T. N., Barrick, D., Ho, C., *Biochemistry* 2005, *44*, 12188-12195.

23. Mathur, S., Badertscher, M., Scott, M., Zenobi, R., *Phys. Chem. Chem. Phys.* 2007, *9*, 6187-6198.

24. Simmons, D. A., Dunn, S. D., Konermann, L., *Biochemistry* 2003, *42*, 9248-9248.

25. Ladbury, J. E., *Biochem. Soc. Trans.* 2010, *38*, 888-893.

26. Thomas, J. M., *Angew. Chem. Int. Ed.* 2006, *45*, 6797-6800.

27. McLafferty, F. W., *Annu. Rev. Anal. Chem.* 2011, *4*, 1-22.

28. Jonsson, A. P., *Cell. Mol. Life Sci.* 2001, *58*, 868-884.

29. Hager, J. W., *Anal. Bioanal. Chem.* 2004, *378*, 845-850.

30. Gaskell, S. J., *J. Mass Spectrom.* 1997, *32*, 677-688.

31. Dole, M., Mack, L. L., Hines, R. L., *J. Chem. Phys.* 1968, *49*, 2240-2249.

32. de la Mora, J. F., *Anal. Chim. Acta* 2000, *406*, 93-104.

33. Iribarne, J. V., Thomson, B. A., *J. Chem. Phys.* 1976, *64*, 2287-2294.

34. Denison, D. R., *J. Vac. Sci. Technol.* 1971, *8*, 266-269.

35. Douglas, D. J., *Mass Spectrom. Rev.* 2009, *28*, 937-960.

36. Douglas, D. J., Frank, A. J., Mao, D. M., *Mass Spectrom. Rev.* 2005, *24*, 1-29.

37. Dawson, P. H., *Quadrupole Mass Spectrometry and Its Applications*, AIP Press: Woodbury, New York 1995, pp. 13-21.

38. Winger, B. E., Lightwahl, K. J., Loo, R. R. O., Udseth, H. R., Smith, R. D., *J. Am. Soc. Mass Spectrom.* 1993, *4*, 536-545.

39. Fenn, J. B., Mann, M., Meng, C. K., Wong, S. F., Whitehouse, C. M., *Science* 1989, *246*, 64-71.

40. Yamashita, M., Fenn, J. B., *J. Phys. Chem.* 1984, *88*, 4451-4459.

41. Chernushevich, I. V., Loboda, A. V., Thomson, B. A., *J. Mass Spectrom.* 2001, *36*, 849-865.

42. Jemal, M., Ouyang, Z., *Rapid Commun. Mass Spectrom.* 2003, *17*, 24-38.

43. Xu, X. Y., Veals, J., Korfmacher, W. A., *Rapid Commun. Mass Spectrom.* 2003, *17*, 832-837.

44. Mamyrin, B. A., Karataev, V. I., Shmikk, D. V., Zagulin, V. A., *Sov. Phys. JETP* 1973, *37*, 45-48.

45. Wiley, W. C., McLaren, I. H., *Rev. Sci. Instrum.* 1955, *26*, 1150-1157.

46. Collings, B. A., Campbell, J. M., Mao, D. M., Douglas, D. J., *Rapid Commun. Mass Spectrom.* 2001, *15*, 1777-1795.

47. Campbell, J. M., Collings, B. A., Douglas, D. J., *Rapid Commun. Mass Spectrom.* 1998, *12*, 1463-1474.

48. Guilhaus, M., Selby, D., Mlynski, V., *Mass Spectrom. Rev.* 2000, *19*, 65-107.

49. Wyttenbach, T., Bowers, M. T., *Annu. Rev. Phys. Chem.* 2007, *58*, 511-533.

50. Siuzdak, G., The Expanding Role of Mass Spectrometry in Biotechnology. MCC Press, San Diego. 2003, 71-94.

51. Ganem, B., Li, Y. T., Henion, J. D., *J. Am. Chem. Soc.* 1991, *113*, 6294-6296.

52. Katta, V., Chait, B. T., *J. Am. Chem. Soc.* 1991, *113*, 8534-8535.

53. Pukala, T. L., Ruotolo, B. T., Zhou, M., Politis, A., Stefanescu, R., Leary, J. A., Robinson, C. V., *Structure* 2009, *17*, 1235-1243.

54. Erba, E. B., Ruotolo, B. T., Barsky, D., Robinson, C. V., *Anal. Chem.* 2010, *82*, 9702-9710.

55. Loo, J. A., Berhane, B., Kaddis, C. S., Wooding, K. M., Xie, Y. M., Kaufman, S. L., Chernushevich, I. V., *J. Am. Soc. Mass Spectrom.* 2005, *16*, 998-1008.

56. Kitova, E. N., Bundle, D. R., Klassen, J. S., *J. Am. Chem. Soc.* 2002, *124*, 9340-9341.

57. Kitova, E. N., Wang, W. J., Bundle, D. R., Klassen, J. S., *J. Am. Chem. Soc.* 2002, *124*, 13980-13981.

58. Tesic, M., Wicki, J., Poon, D. K. Y., Withers, S. G., Douglas, D. J., *J. Am. Soc. Mass Spectrom.* 2007, *18*, 64-73.

59. Bich, C., Zenobi, R., *Curr. Opin. Struct. Biol.* 2009, *19*, 632-639.

60. Sinz, A., *ChemMedChem* 2007, *2*, 425-431.

61. Scarff, C. A., Patel, V. J., Thalassinos, K., Scrivens, J. H., *J. Am. Soc. Mass Spectrom.* 2009, *20*, 625-631.

62. Apostol, I., *Anal. Biochem.* 1999, *272*, 8-18.

63. Chernushevich, I. V., Thomson, B. A., *Anal. Chem.* 2004, *76*, 1754-1760.

64. Mann, M., Hendrickson, R. C., Pandey, A., *Annu. Rev. Biochem.* 2001, *70*, 437-473.

65. Sterling, H. J., Kintzer, A. F., Feld, G. K., Cassou, C. A., Krantz, B. A., Williams, E. R., *J. Am. Soc. Mass Spectrom.* 2012, In press.

66. Lomeli, S. H., Peng, I. X., Yin, S., Loo, R. R. O., Loo, J. A., *J. Am. Soc. Mass Spectrom.* 2011, *21*, 127-131.

67. Sterling, H. J., Prell, J. S., Cassou, C. A., Williams, E. R., *J. Am. Soc. Mass Spectrom.* 2011, *22*, 1178-1186.

68. Konermann, L., Douglas, D. J., *Rapid Commun. Mass Spectrom.* 1998, *12*, 435-442.

69. Griffith, W. P., Kaltashov, I. A., *Biochemistry* 2003, *42*, 10024-10033.

70. Konermann, L., Collings, B. A., Douglas, D. J., *Biochemistry* 1997, *36*, 5554-5559.

71. Pan, J. X., Wilson, D. J., Konermann, L., *Biochemistry* 2005, *44*, 8627-8633.

72. Konermann, L., Douglas, D. J., *J. Am. Soc. Mass Spectrom.* 1998, *9*, 1248-1254.

73. Scarff, C. A., Thalassinos, K., Hilton, G. R., Scrivens, J. H., *Rapid Commun. Mass Spectrom.* 2008, *22*, 3297-3304.

74. Harvey, S. R., MacPhee, C. E., Barran, P. E., *Methods* 2011, *54*, 454-461.

75. Uetrecht, C., Rose, R. J., van Duijn, E., Lorenzen, K., Heck, A. J. R., *Chem. Soc. Rev.* 2010, *39*, 1633-1655.

76. Knapman, T. W., Morton, V. L., Stonehouse, N. J., Stockley, P. G., Ashcroft, A. E., *rapid Commun. Mass Spectrom.* 2010, *24*, 3033-3042.

77. Uetrecht, C., Versluis, C., Watts, N. R., Wingfield, P. T., Steven, A. C., Heck, A. J. R., *Angew. Chem. Int. Ed.* 2008, *47*, 6247-6251.

78. Chen, Y. L., Collings, B. A., Douglas, D. J., *J. Am. Soc. Mass Spectrom.* 1997, *8*, 681-687.

79. Mauk, M. R., Mauk, A. G., Chen, Y. L., Douglas, D. J., *J. Am. Soc. Mass Spectrom.* 2002, *13*, 59-71.

80. Covey, T., Douglas, D. J., *J. Am. Soc. Mass Spectrom.* 1993, *4*, 616-623.

81. Douglas, D. J., *J. Am. Soc. Mass Spectrom.* 1994, *5*, 17-18.

82. Wright, P. J., Zhang, J. M., Douglas, D. J., *J. Am. Soc. Mass Spectrom.* 2008, *19*, 1906-1913.

83. Wright, P. J., Douglas, D. J., *J. Am. Soc. Mass Spectrom.* 2009, *20*, 484-495.

84. Mark, K. J., Douglas, D. J., *Rapid Commun. Mass Spectrom.* 2006, *20*, 111-117.

85. Konermann, L., Pan, J. X., Liu, Y. H., *Chem. Soc. Rev.* 2011, *40*, 1224-1234.

86. Konermann, L., Tong, X., Pan, Y., *J. Mass Spectrom.* 2008, *43*, 1021-1036.

87. Wyttenbach, T., Bowers, M. T., *J. Am. Soc. Mass Spectrom.* 1999, *10*, 9-14.

88. Bai, Y. W., Milne, J. S., Mayne, L., Englander, S. W., *Proteins: Struct. Funct. Genet.* 1993, *17*, 75-86.

89. Wales, T. E., Engen, J. R., *Mass Spectrom. Rev.* 2006, *25*, 158-170.

90. Kuprowski, M. C., Boys, B. L., Konermann, L., *J. Am. Soc. Mass Spectrom.* 2007, *18*, 1279-1285.

91. Englander, J. J., Del Mar, C., Li, W., Englander, S. W., Kim, J. S., Stranz, D. D., Hamuro, Y., Woods, V. L., *Proc. Natl. Acad. Sci. U. S. A.* 2003, *100*, 7057-7062.

92. Creighton, T. E., *Proteins: Structure and Molecular Properties*, W. H. Freeman and Company, New York 1993, p. 282.

93. Hossain, B. M., Konermann, L., *Anal. Chem.* 2006, *78*, 1613-1619.

94. Pan, J., Han, J., Borchers, C. H., Konermann, L., *Anal. Chem.* 2010, *82*, 8591-8597.

95. Cox, H. A., Julian, R. R., Lee, S. W., Beauchamp, J. L., *J. Am. Chem. Soc.* 2004, *126*, 6485-6490.

96. Valentine, S. J., Clemmer, D. E., *J. Am. Soc. Mass Spectrom.* 2002, *13*, 506-517.

97. Evans, S. E., Lueck, N., Marzluff, E. M., *Int. J. Mass Spectrom.* 2003, *222*, 175-187.

98. Freitas, M. A., Hendrickson, C. L., Emmett, M. R., Marshall, A. G., *Int. J. Mass Spectrom.* 1999, *187*, 565-575.

99. Valentine, S. J., Clemmer, D. E., *J. Am. Chem. Soc.* 1997, *119*, 3558-3566.

100. Mao, D. M., Ding, C. F., Douglas, D. J., *Rapid Commun. Mass Spectrom.* 2002, *16*, 1941-1945.

101. Campbell, S., Rodgers, M. T., Marzluff, E. M., Beauchamp, J. L., *J. Am. Chem. Soc.* 1995, *117*, 12840-12854.

102. Butcher, D. J., Asano, K. G., Goeringer, D. E., McLuckey, S. A., *J. Phys. Chem.* 1999, *103*, 8664-8671.

103. Liu, L., Bagal, D., Kitova, E. N., Schnier, P. D., Klassen, J. S., *J. Am. Soc. Mass Spectrom.* 2009, *131*, 15980-15981.

104. Sun, J., Kitova, E. N., Klassen, J. S., *Anal. Chem.* 2007, *79*, 416-425.

105. Chen, Y. L., Campbell, J. M., Collings, B. A., Konermann, L., Douglas, D. J., *Rapid Commun. Mass Spectrom.* 1998, *12*, 1003-1010.

106. Gao, J. M., Wu, Q. Y. Q., Carbeck, J., Lei, Q. P., Smith, R. D., Whitesides, G. M., *Biophys. J.* 1999, *76*, 3253-3260.

107. Versluis, C., Heck, A. J. R., *Int. J. Mass Spectrom.* 2001, *210*, 637-649.

108. Wan, K. X., Gross, M. L., Shibue, T., *J. Am. Soc. Mass Spectrom.* 2000, *11*, 450-457.

109. Benesch, J. L., Robinson, C. V., *Curr. Opin. Struct. Biol.* 2006, *16*, 245-251.

110. Breuker, K., Brueschweiler, S., Tollinger, M., *Angew. Chem. Int. Ed. Engl.* 2011, *50*, 873-877.

111. Barylyuk, K., Balabin, R. M., Grunstein, D., Kikkeri, R., Frankevich, V., Seeberger, P. H., Zenobi, R., *J. Am. Soc. Mass Spectrom.* 2011, *22*, 1167-1177.

112. Xie, Y., Zhang, J., Yin, S., Loo, J. A., *J. Am. Soc. Mass Spectrom.* 2006, *128*, 14432-14433.

113. Rhee, Y. M., Sorin, E. J., Jayachandran, G., Lindahl, E., Pande, V. S., *Proc. Natl. Acad. Sci. U. S. A.* 2004, *101*, 6456-6461.

114. Rostom, A. A., Tame, J. R. H., Ladbury, J. E., Robinson, C. V., *J. Mol. Biol.* 2000, *296*, 269-279.

115. Ruotolo, B. T., Giles, K., Campuzano, I., Sandercock, A. M., Bateman, R. H., Robinson, C. V., *Science* 2005, *310*, 1658-1661.

116. Badman, E. R., Myung, S., Clemmer, D. E., *J. Am. Soc. Mass Spectrom.* 2005, *16*, 1493-1497.

117. Breuker, K., McLafferty, F. W., *Proc. Natl. Acad. Sci. U. S. A.* 2008, *105*, 18145-18152.

118. Clark, S. M., Konermann, L., *Anal. Chem* 2004, *76*, 7077-7083.

119. Jecklin, M. C., Touboul, D., Bovet, C., Wortmann, A., Zenobi, R., *J. Am. Soc. Mass Spectrom.* 2008, *19*, 332-343.

120. Hunter, C. L., Mauk, A. G., Douglas, D. J., *Biochemistry* 1997, *36*, 1018-1025.

121. Wang, W. J., Kitova, E. N., Klassen, J. S., *Anal. Chem.* 2003, *75*, 4945-4955.

122. Gross, D. S., Zhao, Y. X., Williams, E. R., *J. Am. Soc. Mass Spectrom.* 1997, *8*, 519-524.

123. Stadler, J. R., Zurich, V. J., *National Advisory Committee for Aeronautics TN 2423, NACA* 1951.

124. Bunn, H. F., Forget, B. G., *Hemoglobin: Molecular, Genetic and Clinical Aspects*, W.B. Saunders Company, Philadelphia 1986, pp. 24-70.

125. Manning, J. M., Dumoulin, A., Li, X. F., Manning, L. R., *J. Biol. Chem.* 1998, *273*, 19359-19362.

126. Edelstein, S. J., Rehmar, M. J., Olson, J. S., Gibson, Q. H., *J. Biol. Chem.* 1970, *245*, 4372-4381.

127. Ip, S. H. C., Ackers, G. K., *J. Biol. Chem.* 1977, *252*, 82-87.

128. Mrabet, N. T., Shaeffer, J. R., McDonald, M. J., Bunn, H. F., *J. Biol. Chem.* 1986, *261*, 1111-1115.

129. Shaeffer, J. R., McDonald, M. J., Turci, S. M., Dinda, D. M., Bunn, H. F., *J. Biol. Chem.* 1984, *259*, 4544-4547.

130. Kilmartin, J. V., *Brit. Med. Bull.* 1976, *32*, 209-212.

131. Dumoulin, A., Manning, L. R., Jenkins, W. T., Winslow, R. M., Manning, J. M., *J. Biol. Chem.* 1997, *272*, 31326-31332.

132. Yamaguchi, T., Adachi, K., *Biochem. Biophys. Res. Commun.* 2002, *290*, 1382-1387.

133. Griffith, W. P., Kaltashov, I. A., *Curr. Org. Chem.* 2006, *10*, 535-553.

134. Zanella-Cleon, I., Joly, P., Becchi, M., Francina, A., *Clin. Biochem.* 2009, *42*, 1807-1817.

135. Murayama, M., *Clin. Chem.* 1967, *13*, 578-588.

136. Sunshine, H. R., Hofrichter, J., Ferrone, F. A., Eaton, W. A., *J. Mol. Biol.* 1982, *158*, 251-273.

137. Caughey, W. S., *Biochemical and Clinical Aspects of Hemoglobin Abnormalities*, Academic Press, New York 1978, p. 401.

138. Platt, O. S., *N. Engl. J. Med.* 2008, *358*, 1362-1369.

139. Williams, S. J., Hoos, R., Withers, S. G., *J. Am. Chem. Soc.* 2000, *122*, 2223-2235.

140. White, A., Withers, S. G., Gilkes, N. R., Rose, D. R., *Biochemistry* 1994, *33*, 12546-12552.

141. Abaturov, L. V., Nosova, N. G., Shlyapnikov, S. V., Faizullin, D. A., *Mol. Biol.* 2006, *40*, 326-340.

142. Englander, J. J., Rogero, J. R., Englander, S. W., *Anal. Biochem.* 1985, *147*, 234-244.

143. Englander, S. W., *Ann. N.Y. Acad., Sci.* 1975, *244*, 10-27.

144. Englander, S. W., Mauel, C., *J. Biol. Chem.* 1972, *247*, 2387-2394.

145. Abaturov, L. V., Molchanova, T. P., Nosova, N. G., Shlyapnikov, S. V., Faizullin, D. A., *Mol. Biol.* 2006, *40*, 413-426.

146. Abaturov, L. V., Nosova, N. G., Shlyapnikov, S. V., *Mol. Biol.* 2006, *40*, 811-820.

147. Gibson, Q. H., Antonini, E., *J. Biol. Chem.* 1967, *242*, 4678-4681.

148. Griffon, N., Baudin, V., Dieryck, W., Dumoulin, A., Pagnier, J., Poyart, C., Marden, M. C., *Protein Sci.* 1998, *7*, 673-680.

149. Boys, B. L., Konermann, L., *J. Am. Soc. Mass Spectrom.* 2007, *18*, 8-16.

150. Hoaglund-Hyzer, C. S., Counterman, A. E., Clemmer, D. E., *Chem. Rev.* 1999, *99*, 3037-3079.

151. Simmons, D. A., Wilson, D. J., Lajoie, G. A., Doherty-Kirby, A., Konermann, L., *Biochemistry* 2004, *43*, 14792-14801.

152. Douglas, D. J., French, J. B., *J. Am. Soc. Mass Spectrom.* 1992, *3*, 398-408.

153. Mao, D. M., Babu, K. R., Chen, Y. L., Douglas, D. J., *Anal. Chem.* 2003, *75*, 1325-1330.

154. Antonini, E., Brunori, M., *Hemoglobin and Myoglobin in Their Reactions with Ligands*, North-Holland Publishing Company, Amsterdam 1971, pp. 2-6.

155. de Duve, C., *Acta Chem. Scand.* 1948, *2*, 264-289.

156. Paul, K. G., Theorell, H., Akeson, A., *Acta Chem. Scand.* 1953, *7*, 1284-1287.

157. Antonini, E., Brunori, M., Wyman, J., *Biochemistry* 1965, *4*, 545-551.

158. Jia, Y., Buehler, P. W., Boykins, R. A., Venable, R. M., Alayash, A. I., *J. Biol. Chem.* 2007, *282*, 4894-4907.

159. White, S. L., *J. Biol. Chem.* 1975, *250*, 1263-1268.

160. Han, Y., Quan, G. B., Liu, X. Z., Ma, E. P., Liu, A., Jin, P., Cao, W., *Cryobiology* 2005, *51*, 152-164.

161. Pikal, M. J., Dellerman, K. M., Roy, M. L., Riggin, R. M., *Pharm. Res.* 1991, *8*, 427-436.

162. Vogt, W., *Free Radic. Bio. Med.* 1995, *18*, 93-105.

163. Chen, H. J. C., Chang, C. M., Lin, W. P., Cheng, D. L., Leong, M. I., *Chembiochem* 2008, *9*, 312-323.

164. Hardin, S. C., Larue, C. T., Oh, M. H., Jain, V., Huber, S. C., *Biochem. J.* 2009, *422*, 305-312.

165. Winterbourn, C. C., *Biochem. J.* 1981, *198*, 125-131.

166. Hambly, D. M., Gross, M. L., *Anal. Chem.* 2009, *81*, 7235-7242.

167. Chao, C. C., Ma, Y. S., Stadtman, E. R., *Proc. Natl. Acad. Sci. U. S. A.* 1997, *94*, 2969-2974.

168. Fischetti, R. F., Rodi, D. J., Mirza, A., Irving, T. C., Kondrashkina, E., Makowski, L., *J. Synchrontron. Rad.* 2003, *10*, 398-404.

169. Glatter, O., Kratzky, O., *Small Angle X-Ray Scattering*, Academic Press, New York 1982, p. 156.

170. Fish, W. W., Reynolds, J. A., Tanford, C., *J. Biol. Chem.* 1970, *245*, 5166-5168.

171. Ogasawar, N., Yoshino, M., Asai, J. P., *J. Biochem.* 1970, *68*, 331-340.

172. Tseng, Y. C. L., Latham, K. R., *Lipids* 1984, *19*, 96-102.

173. Hardison, R., *J. Exp. Biol.* 1998, *201*, 1099-1117.

174. Davison, A. S., Green, B. N., Roberts, N. B., *Clin. Chem. Lab. Med.* 2008, *46*, 1230-1238.

175. Mandal, A. K., Bisht, S., Bhat, V. S., Krishnaswamy, P. R., Balaram, P., *Clin. Biochem.* 2008, *41*, 75-81.

176. Wild, B. J., Green, B. N., Cooper, E. K., Lalloz, M. R. A., Erten, S., Stephens, A. D., Layton, D. M., *Blood Cells Mol. Dis.* 2001, *27*, 691-704.

177. Williams, J. P., Giles, K., Green, B. N., Scrivens, J. H., Bateman, R. H., *Rapid Commun. Mass Spectrom.* 2008, *22*, 3179-3186.

178. Kang, Y., Terrier, P., Douglas, D. J., *J. Am. Soc. Mass Spectrom.* 2011, *22*, 290-299.

179. Tomoda, A., Yoneyama, Y., Tsuji, A., *Biochem. J.* 1981, *195*, 485-492.

180. Ofori-Acquah, S. F., Green, B. N., Davies, S. C., Nicolaides, K. H., Serjeant, G. R., Layton, D. M., *Anal. Biochem* 2001, *298*, 76-82.

181. Williams, R. C., Kim, H., *Biochemistry* 1976, *15*, 2207-2211.

182. Manning, L. R., Jenkins, W. T., Hess, J. R., Vandegriff, K., Winslow, R. M., Manning, J. M., *Protein Sci.* 1996, *5*, 775-781.

183. Chrisman, P. A., Newton, K. A., Reid, G. E., Wells, J. M., McLuckey, S. A., *Rapid Commun. Mass Spectrom.* 2001, *15*, 2334-2340.

184. Versluis, C., van der Staaij, A., Stokvis, E., Heck, A. J. R., de Craene, B., *J. Am. Soc. Mass Spectrom.* 2001, *12*, 329-336.

185. Jurchen, J. C., Garcia, D. E., Williams, E. R., *J. Am. Soc. Mass Spectrom.* 2004, *15*, 1408-1415.

186. Jurchen, J. C., Williams, E. R., *J. Am. Chem. Soc.* 2003, *125*, 2817-2826.

187. Wanasundara, S. N., Thachuk, M., *J. Am. Soc. Mass Spectrom.* 2007, *18*, 2242-2253.

188. Adachi, K., Zhao, Y., Yamaguchi, T., Surrey, S., *J. Biol. Chem.* 2000, *275*, 12424-12429.

189. Kang, Y., Douglas, D. J., *J. Am. Soc. Mass Spectrom.* 2011, *22*, 1187-1196.

190. Glasoe, P. K., Long, F. A., *J. Phys. Chem.* 1960, *64*, 188-190.

191. Efimova, Y. M., Haemers, S., Wierczinski, B., Norde, W., Van Well, A. A., *Biopolymers* 2007, *85*, 264-273.

192. Kang, Y., Terrier, P., Ding, C. F., Douglas, D. J., *J. Am. Soc. Mass Spectrom.* 2012, *23*, 57-67.

193. Killion, P. J., Cameron, B. F., *Biophys. J.* 1972, *12*, 528-639.

194. Mao, D. M., Douglas, D. J., *J. Am. Soc. Mass Spectrom.* 2003, *14*, 85-94.

195. White, A., Tull, D., Johns, K., Withers, S. G., Rose, D. R., *Nat. Struct. Biol.* 1996, *3*, 149-154.

196. Poon, D. K. Y., Schubert, M., Au, J., Okon, M., Withers, S. G., McIntosh, L. P., *J. Am. Chem. Soc.* 2006, *128*, 15388-15389.

197. Wright, P. J., Douglas, D. J., *54th ASMS Conference on Mass Spectrometry and Allied Topics*, Seattle, WA. 2006.